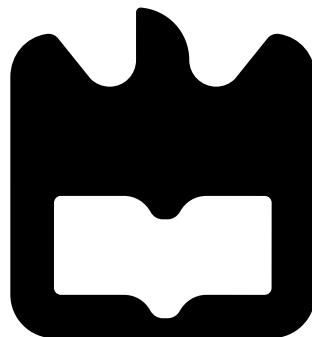




João Pedro
Dias Rodrigues

Análise fenomenológica em teorias para lá do
Modelo Padrão: os casos do B-L-SM mínimo e de
um 3HDM do tipo BGL

Phenomenological analysis in beyond the Standard
Model theories: the cases of the minimal B-L-SM
and of a BGL-like 3HDM





João Pedro
Dias Rodrigues

**Análise fenomenológica em teorias para lá do
Modelo Padrão: os casos do B-L-SM mínimo e de
um 3HDM do tipo BGL**

**Phenomenological analysis in beyond the Standard
Model theories: the cases of the minimal B-L-SM
and of a BGL-like 3HDM**

Dissertação apresentada à Universidade de Aveiro para cumprimento dos requisitos necessários à obtenção do grau de Mestre em Engenharia Física, realizada sob a orientação científica do Doutor António Morais, Investigador Doutorado do Departamento de Física da Universidade de Aveiro e sob a coorientação do Doutor Roman Pasechnik, Professor Associado do Departamento de Astronomia e Física Teórica da Universidade de Lund.

O trabalho nesta tese foi suportado pelo projeto *From Higgs Phenomenology to the Unification of Fundamental Interactions* com referência PTDC/FIS-PAR/31000/2017.



Fundação
para a Ciência
e a Tecnologia



UNIÃO EUROPEIA

Fundos Europeus
Estruturais e de Investimento

o júri / the jury

presidente

Margarida Facão

Professora Auxiliar do Departamento de Física da Universidade de Aveiro

vogais

António Morais

Investigador Nível 1 do Departamento de Física da Universidade de Aveiro

Nuno Castro

Professor Assistente da University of Minho.

agradecimentos / acknowledgements

Eu gostaria de expressar os meus mais profundos agradecimentos ao meu orientador, Professor António Morais, ele guiou-me e encorajou-me a ser profissional e a fazer as escolhas certas. Sem a sua ajuda e paciência o projeto não teria sido realizado.

Ao João Pino eu queria do fundo do meu coração agradecer todo os conselhos e apoio que me levaram a ter sucesso neste trabalho. A tua perseverança e ética de trabalho são inspiracionais.

Ao Felipe, apesar de chegares tão tarde a foi sempre um prazer falar contigo graças ao teu sentido de humor e sabedoria.

Finalmente a minha família merece um especial obrigado por todo o amor e apoio que me motivou a acabar esta etapa da minha vida.

[Add Roman](#)

I wish to express my sincere appreciation to my supervisor, Professor António Morais, he convincingly guided and encouraged me to be professional and do the right thing. Without his persistent help and endless patience, the goal of this project would not have been realized.

To João Pino it is whole-heartedly that I appreciated your great advice for my study proved monumental towards the success of this study. Also your perseverance and work ethic is with no exaggeration inspiring.

To Felipe, although you joined us so late into the project your presence was always welcome thanks to your impeccable sense of humour and down to earth wisdom. Lastly but not least I wish to acknowledge the support and great love of my family, and friends. They kept me going and this work would not have been possible without their input.

[Add Roman](#)

Resumo

O Modelo Padrão é neste momento o modelo ideal na analise de física de partículas, este une numa arquitectura autoconsistente e propriamente motivada três das quatro forças fundamentais do universo, no entanto, o consenso científico é que modelo padrão esta incompleto, visto que apesar do excelente acordo entre muitas das suas previsões e a realidade, imensas experiencias estão a mostrar fenómenos que o modelo padrão não consegue explicar na sua forma actual.

Dadas estas falhas a comunidade científica propõem novos modelos motivados pela procura de uma teoria que consiga reconciliar o modelo padrão com a incorporação de estas novas observações. Observações como a inclusão de massas de neutrinos, violação excessiva de sabor, ou a previsão de matéria escura.

Estes modelos conseguem abordar diferentes problemas do modelo padrão introduzindo novos mecanismos, como novas partículas ou diferente estrutura de interações. Logicamente estas previsões têm que ser consistentes com a realidade, e neste trabalho é exatamente esse exercício que tencionamos fazer contra um conjunto de modelos, nomeadamente dois modelos intitulados de B-L-SM e 3HDM.

A principal criação deste trabalho foi um conjunto de scipts que podessem, independentemente do modelo, simular as previsões feitas por uma teoria e comparar-las aos mais recentes limites impostos por experiencias, calculando ao mesmo tempo o impacto que as componentes de nova física poderiam ter nestas mesmas experiencias.

Neste trabalho, começamos por uma breve revisão do Modelo Padrão, seguidamente iremos introduzir os dois modelos que se classificam como para além do modelo padrão, começando com o a introdução teoricamente necessária para conseguirmos concretizar uma análise numérica sobre cada um destes. Finalizando com a apresentação de possíveis sinais de nova física que cada cenário poderá trazer.

Abstract

The standard model of particle physics is at this moment the paragon for the study of particles and their interactions. It unifies three out of the four known fundamental forces of the universe in a well motivated framework, however the current consensus among physicists is that it is incomplete. This comes from the fact that many modern experiments have discovered phenomena that the standard model cannot explain within its framework.

Motivated by these apparent flaws in the standard model, more and more models are proposed as to include possible explanations for some of these deviations. These (so far) unexplained phenomena include dark matter, neutrino mass hierarchies and excessive flavor violation.

These models include a diverse set of tools, ranging from novel particle types to new interactions mechanisms, as to account for these phenomena. Logically the predictions made by these models have to be consistent with the reality revealed by new experiments such as the Large Hadron Collider. In this work we perform a very common exercise where, we test the validity of new models against experimental bounds precisely measuring new physics contributions.

Given this goal the central construct of this work was the generation of a computational tool that would allow us to analyze several of these models with a focus on interchangeability. This would verify if the models can respect the large number of constraints imposed by the multiple international experiments and at the same serve to check how each of these fair in explaining each of the new physical phenomena.

The structure of this work begins with a general review of the Standard Model as it is the foundation for the remaining theories we present, the B-L-SM and the 3HDM. Both these theories will be first introduced theoretically and then checked against the latest constraints through our numerical scans. We finalize each section by presenting the results of this numerical analysis.

Contents

Contents	i
List of Figures	ii
List of Tables	iv
1 Introduction	1
2 The Standard Model of Particle Physics	3
2.1 Internal symmetry of the Standard Model	3
2.2 The Higgs Mechanism and the Mass Generation of the Gauge Bosons	6
2.3 Fermion Masses in the Standard Model and Quark Mixing	8
2.3.1 Charged Flavour Currents vs. Neutral Flavor Currents	10
3 B-L-SM Model	14
3.1 Formulating the Model	15
3.2 Numerical Results	19
3.2.1 The Scanning Apparatus	20
3.2.2 Numerical discussion	21
4 3HDM Model	29
4.1 The Case of the BGL-2HDM and its Relation to our Work	30
4.2 The formulation of a BGL-like 3HDM	31
4.2.1 The Scalar Sector	31
4.2.2 The Gauge Sector	33
4.2.3 The Yukawa sector	33
4.3 The BGL-like suppression of FCNCs in the 3HDM model	35
4.4 The inversion process	36
4.4.1 The CP-odd portion of the scalar sector	37
4.4.2 The CP-even portion of the Scalar Sector	40
4.5 Numerical Discussion of the 3HDM	42
4.5.1 Methodology and Constraints	42
4.5.2 Discussion of results	45
5 Conclusions	50
Bibliography	52

List of Figures

2.1	Box diagram describing $K_L^0 \rightarrow \mu^- \mu^+$, through an intermediate u quark.	9
2.2	Feynman diagrams for flavour conserving couplings of quarks to photon, Z boson, gluon and the Higgs (the first three diagrams), and the flavour changing coupling to the W (the last diagram). The 3×3 matrices are visual representations of couplings in the generation space, with couplings to γ, Z, g being flavour universal, while the couplings to the Higgs are flavour diagonal but not universal. Finally the couplings involving the W are flavour changing and hierarchical.	10
2.3	Representative tree level charged current diagram (left) and a loop induced FCNC diagram (right).	11
2.4	"Contact" interactions with loop interactions containing NP	12
2.5	A representative SM diagram for $b \rightarrow s\mu\mu$ transition (left), and representative possible loop level NP contributions (middle and right).	12
2.6	The SM diagrams for $b \rightarrow c\tau\nu$ transition (left), and the possible tree level NP contributions to $b \rightarrow c\tau\nu$ transition (middle and right). Where the LQ stands for a hypothetical Leptoquark particle that would interact with both leptons and quarks.	12
3.1	One-loop diagrams contributing to Δa_μ^{NP} in the B-L-SM.	21
3.2	B-L-SM scatter plots for EW precision observables showing the ST (left) and TU (right) planes. Accepted points lying within a 95% C.L. ellipsoid of the best fit point are represented in black whereas grey points are excluded.	22
3.3	Scatter plots showing the Z' Drell-Yan production cross section times the decay branching ratio into a pair of electrons and muons (left panel) and the new scalar mass m_{h_2} (right panel) as functions of $m_{Z'}$ and the NP contributions to the muon Δa_μ anomaly. Coloured points have survived all theoretical and experimental constraints while grey points are excluded by direct Z' searches at the LHC. The region between the two dashed lines represents the current ATLAS expected limit on the production cross section times branching ratio into a pair of leptons at 95% C.L. and is taken from the plot in Fig. 4 of Ref. [1]. The four highlighted points in both panels denote the benchmark scenarios described in detail in Tab. 3.4.	23
3.4	Scatter plots showing the Z' Drell-Yan production cross section times the decay branching ratio into a pair of electrons and muons in terms of the $m_{Z'}$ boson mass. The colour gradation represents the new scalar mass (top-left), the ratio between the EW- and $U(1)_{B-L}$ -breaking VEVs (top-right) and the scalar mixing angle (bottom). The grey points are excluded by direct Z' searches at the LHC. The four benchmark points in Tab. 3.4 are represented by the black dots (last two rows), cyan diamond (first row) and red cross (second row).	25
3.5	The same as in Fig. 3.4 but with the colour scale representing the gauge-mixing parameters g_{YB} (top-left), θ'_W (top-right), and the $U(1)_{B-L}$ gauge coupling (bottom).	26
3.6	The same as in Fig. 3.4 but with the colour scale representing the coupling of leptons to the Z' (top panels) and the coupling of W bosons to Z'	27
3.7	Barr-Zee type two-loop diagrams contributing to Δa_μ	27

4.1	Leptonic and semi-leptonic H^\pm tree-level diagrams where M stands for a generic meson. ℓ is any lepton with ν_ℓ being the corresponding neutrino.	44
4.2	Meson oscillation mediated by a neutral scalar Higgs.	44
4.3	NP contribution to the transition mediated by a charged or neutral Higgs at one-loop order as to contribute to $\mathcal{BR}(B \rightarrow \chi_s \gamma)$ trough $b \rightarrow \bar{s} \gamma$	44
4.4	3HDM scatter plots for EW precision observables showing the ST(left) and TU(right)planes. Accepted points lying within a 95% C.L. ellipsoid of the best fit point are represented in black whereas grey points are excluded.	46
4.4	Scatter plots of parameter space allowed under several cuts imposed on the BGL-like 3HDM. On the upper right side we have the plot showing the masses of the two heavier CP-even scalars H_2 and H_1 while in the right we show the relation between the lightest (non SM Higgs) of the CP-even and pseudoscalar particles. As for the bottom plots see the remaining CP-odd scalars and how they are excluded under several cuts. Right we have the pseudoscalar masses A_1 and A_2 while in the left side we have the CP- odd charged Higgs states H_1^\pm and H_2^\pm . Red points failed HS and HB tests; yellow points violate unitarity constraints; orange points only fail electroweak precision constraints, and green ones satisfy all restrictions.	47
4.5	Scatter plot of the estimated QFV observables normalized to the SM values versus the lightest scalar Higgs. The grey points in all plots represent a point that would be outside the 2σ bound for one of the observables while in a red color scale we see the second CP-even neutral scalar mass for the remaining points.	48
4.6	Scatter plot of the estimated QFV observables normalized to SM values overlaped with EW and Higgs sector just as in previous figures.	48
4.7	Relative mass and QFV observable changes with the increase of 1% in all softbreaking terms	49
4.8	50

List of Tables

2.1	Quark and Lepton charges	4
2.2	Gauge and Scalar fields in the SM	5
2.3	Fermion fields in the SM	5
2.4	FCCCs examples	10
2.5	FCNCs examples	10
3.1	Quantum fields and their respective quantum numbers in the minimal B-L-SM extension. The last two lines represent the weak and $B - L$ hypercharges	15
3.2	Possible signs of the potential parameters in Eq.(3.1). The \checkmark symbol indicates the existence of solutions for tadpole conditions Eq. (3.6), while the \times indicates unstable configurations.	16
3.3	Parameter scan ranges used in our analysis. Note that the value of λ_1 is mostly constrained by the tree-level Higgs boson mass given in Eq. (3.11).	21
3.4	A selection of four benchmark points represented in Figs. 3.3, 3.4 to 3.6. The $m_{Z'}$, m_{h_2} and x parameters are given in TeV. The first line represents a point with light h_2 while the second line shows the lightest allowed Z' boson found in our scan. The last two lines show two points that reproduce the observed value of the muon ($g - 2$) within 1σ uncertainty.	24
4.1	Table containing SM theoretical uncertainties and values along side with the QFV experimental error bars and 95% C.L central value as reference [2].	43
4.2	A selection of four benchmark points. All written masses are given in GeV. These correspond to the lightest scalars found that respect all QFV and scalar sector constraints.	49

Chapter 1

Introduction

Our current understanding of all subatomic phenomena must be understood through the Standard Model (SM) of particle physics. The SM has thus far been the best descriptor for the experimentally observed spectra of particles and their interactions at the electroweak (EW) scale. Being that, finally, in 2012 a resonance was discovered at the Large Hadron Collider (LHC) that confirms the existence of its last predicted particle, the Higgs boson, finally revealing all of the models particles and proving the existence of the Higgs mechanism [3].

The development of the SM was a arduous task, leading scientists successfully combine three of the four fundamental interactions of nature, the electromagnetic, weak and strong interactions, in a well motivated framework.

However, despite its successes the SM still lacks a strong explanation for several experimental observations. To enumerate some of these previously alluded too problems, we have: First, we have the fact that the SM can not account for one of the most important cosmological discoveries of the century, the existence of dark matter [4]. This is a fundamental flaw since the SM lacks a possible dark matter candidate, or dark particle.

Secondly, the SM does not offer any justification for the existence of baryon asymmetry in the universe, i.e. why is the observable universe primarily composed of matter rather than anti-matter [5].

Thirdly, the SM suffers from peculiar oddities in the fermion sector in the form of unjustified mass and mixing hierarchies. This is usually referred to as the flavor problem and is considered a sizable drawback of the SM. As an example, we observe the top quark mass ($\mathcal{O}(100)$ GeV) to be five order of magnitudes heavier than the up quark ($\mathcal{O}(1)$ MeV), and eleven orders of magnitude above the highest neutrino mass limit ($\mathcal{O}(1)$ eV) set by kinetic beta decay analysis [6]. These high differences are thought to be too large to be natural, so a physical property that would justify such gap is a desired characteristic of many Beyond the Standard Model (BSM) frameworks.

Fourth, neutrino masses (as alluded to) are not included in the SM. Although there are precise oscillation measurements that measure masses differences in the eV range with precise mixing in between 3 different generations of neutrinos [7].

In addition to these, there are still many other subtle flaws, like the lack of a strong phase transition, the R_κ parameter and $g - 2$ anomaly of lepton magnetic moments, etc. These are just some of the typical justifications given to explore possible BSM scenarios. The holy grail of which would be a model that solves all these problems in a properly motivated framework that addresses these and many more cosmological and phenomenological problems and is in harmony with all measurements.

For now such a model remains far out of reach, and given the large number of possible solutions, the narrowing down of theories through phenomenological studies is a very worthwhile endeavor. This work will be a review of two such studies.

The “normal” procedure for these kinds of studies consist in performing large a numerical analysis of all possible combinations of free parameters of a given model, which we call the parameter space, as to narrow it down through comparison with modern bounds set by experiments. This

allows us to predict exactly what observations this model could still allow for in experimental detection and measure if the proposed model could have a significant impact as to explain observed deviations or if it is, in a extreme case, completely excluded by modern limits.

Paradoxically, as of late these studies have become progressively harder to perform regardless of the improvement in hardware given that the available space for NP gets reduced by each successful particle experiment. Chief among them are the ATLAS, CMS experiments at the LHC, whose large amount of collect data over past years is setting ever more stringent bounds on viable parameter spaces of popular BSM scenarios. And as available space for new physics decreases, it becomes more challenging to reveal remaining space without falling within the possibility of fine tuning our model. Fine tuning consists in carefully balancing several contributions as to, cancel or magnify as to be allowed by current bounds.

Note, that the SM has shown itself consistence with most constraints that were initial believed to be a possible gateway to NP i.e. divergences from its predictions. Thus, the search continues for hints at possible directions to complete the SM. One of these is brought to use trough flavor physics, as we'll soon examine further on.

Conventionally, phenomenological simulations of BSM searches in these multi-dimensional parameter spaces have been made in large computer-clusters requiring several weeks of computational time trough simple Monte-Carlo methods. These simple methods are the basis for the work presented in this thesis although some modern studies have incorporated new methods to scan these complex problems like machine learning. Similar to done by our colleagues in [8]. These new methods promise to greatly increase the efficacy of similar studies.

Over the course of this thesis we intent to perform two of these BSM studies. However we must begin by laying down the fundamental basis for this type discussion by presenting a short overview of the SM. Afterwards we will present, first the B-L-SM (Baryon-Lepton-SM) model, a simple unitary extension of the SM - and then, move on to a more complex model with additional Higgs doublets fields as an attempt to present a framework that addresses the flavor problem via the Three Higgs Doublet Model (3HDM) with a stabilizing symmetry. We will see how each of these models addresses specific problems differently and discuss the advantages and disadvantages of a simple unitary extension versus a multiple doublet approach.

For example multiple Higgs doublets can easily offer an explanation for the observed excess of charge parity or \mathcal{CP} violation but suffer from the possible inclusion of tree-level Flavour Changing Neutral Currents (FCNCs). These FCNCs are undesirable [9], at least in large number, given current observations, so mechanisms have to be put in place to prevent them, while in the case of the simple unitary extensions such problems tend to not arise [10].

We also want to stress that, while the minimal structure of the Higgs sector postulated by the SM is not an immediate contradiction to experimental measurements it is not manifestly required by the data. In fact, an extended scalar sector is often desirable feature of BSM scenarios despite the tight bounds on Higgs boson couplings to the SM gauge bosons and heavy fermions. **Ask:Morais How do I cite <https://pdg.lbl.gov/2019/reviews/rpp2018-rev-higgs-boson.pdf> exactly instead of the whole corpus.**

These additions are partially motivated by the fact that in the SM, the single Higgs doublet is a bit "overstretched" in the SM. It takes care, simultaneously of the gauge boson masses, up and down-type quarks masses and leptons masses. N-Higgs-doublet models have multiple scalar and complex fields that can relax this, while the simpler unitary additions cannot address this observation. In fact these multiple Higgs doublet models are often engineered based on a naturalness argument, that is, the notion of generations can be brought to the Higgs sector and these might help explain mass hierarchies.

Chapter 2

The Standard Model of Particle Physics

As stated in chapter 1, it is hard to question the validity of the SM as a successful, at least approximate, framework, with whom to describe the phenomenology of particle physics up to the largest energy scales probed by collider measurements so far, although some inconsistencies remain and must be addressed. Note, what we call the SM is the conjugation of several theories, quantum chromodynamics (QCD), Higgs sector and the EW theory.

The formulation of the SM came from previous principles relating to symmetries in nature, specifically symmetry in physical laws. In fact, much in modern physics can be attributed to Emmy Noether's work. She deduced, through her first theorem, that if the action in a system is invariant under some group of transformations (symmetry), then there exist one or more conserved quantities (constants of motion) [11].

Physicists took this idea and were led to a fundamental question, is it possible that upon imposing to a given Lagrangian the invariance under a certain group of symmetries to reach a given form for its dynamics? We can quote Salam and Ward in Ref [12]:

"Our basic postulate is that it should be possible to generate strong, weak and electromagnetic interaction terms (with all their correct symmetry properties and also with clues regarding their relative strengths) by making local gauge transformations on the kinetic energy terms in the free Lagrangian for all particles."

Although we are glossing over a lot of complexity in this statement, given that for the SM to be properly formulated, additional concepts are required. As in the case of weak interactions, the presence of a massive weak gauge boson requires the concept of spontaneous breakdown of the gauge symmetry via what is known as the Higgs mechanism [13]. While the concept of asymptotic freedom played a crucial role in describing perturbatively the strong interaction at short distances [14].

2.1 Internal symmetry of the Standard Model

The SM is a gauge Quantum Field Theory (QFT), that is, manifestly invariant under a set of field transformations. The SM gauge group [15], \mathcal{G}_{SM} ,

$$\mathcal{G}_{SM} = \text{SU}(3)_C \times \text{SU}(2)_L \times \text{U}(1)_Y. \quad (2.1)$$

Where, $\text{SU}(3)_C$, with C being colour, is the group that describes the QCD sector, responsible for the strong force. This symmetry will remain unbroken by the EW Vacuum Expectation Value (VEV). Secondly, we have the $\text{SU}(2)_L \times \text{U}(1)_Y$ portion, with L being Left and Y the hypercharge, that will be broken by the Higgs mechanism into $\text{U}(1)_Q$, the electromagnetic gauge symmetry.

Each particle in the SM stems from a field that is charged in a particular manner on each of these groups. Recall that Quantum Field Theory (QFT) treats particles as excited states of their

respective quantum fields, which are more fundamental than the particles. Interactions between particles are described by interaction terms in the Lagrangian involving their corresponding quantum fields. Of which each interaction can be visually represented by a Feynman diagram according to perturbation theory. Generally speaking, an interacting QFT can not be solved analytically, requiring the use of perturbative methods. In this mindset, one employs the use of Feynman diagrams to better visualize interactions at any given order in perturbation theory.

It is important to highlight that given the invariance under the group in Eq. (2.1), it is impossible for any field, besides the scalar field, to have an explicit mass term in the bare Lagrangian. In this chapter we shall present how the mass of particles is generated via the Higgs mechanism. And offer a brief discussion of flavor physics in the SM and how flavor changing currents can point to NP.

Particle States and Fields

The particle spectrum of the SM is composed by, the gauge bosons, W^\pm and Z bosons, mediators of the weak interactions, the photon γ , the electromagnetic interaction messenger and the strong force mediators, the gluons, G . Additionally, the model is also composed by the matter particles, the fermions, composed by quarks and leptons. A spin-0 scalar also emerges known as the Higgs Boson, h .

Leptons and quarks are organized in three generations each, with 2 pairs by each generation leading to 6 different particles. For quarks we have the up and down for the first generation, charm and strange for the second as well as the top and bottom for the third one. Similarly, there are 6 types of leptons, the 3 charged leptons, electron, muon and tau, and the associated neutrinos. These are represented in different manners, being that the quarks are represented by (u, d, c, s, t, b) while leptons as $(e, \nu_e, \mu, \nu_\mu, \tau, \nu_\tau)$, where ν denotes the neutrinos.

While quarks interact via the weak, electromagnetic and strong forces, the charged leptons only feel the electromagnetic and weak forces and the neutrinos are weakly interacting. A physical fermion is composed of a left-handed and a right-handed field. The left-handed components of the fermions are doublets under $SU(2)_L$,

$$L^i = \begin{pmatrix} \nu_{e_L} \\ e_L \end{pmatrix}, \begin{pmatrix} \nu_{\mu_L} \\ \mu_L \end{pmatrix}, \begin{pmatrix} \nu_{\tau_L} \\ \tau_L \end{pmatrix} \quad \text{and} \quad Q^i = \begin{pmatrix} u_L \\ d_L \end{pmatrix}, \begin{pmatrix} c_L \\ s_L \end{pmatrix}, \begin{pmatrix} t_L \\ b_L \end{pmatrix}, \quad (2.2)$$

where the i index stands for generation, often designed as the flavour index. Conversely the right-handed components are singlets of $SU(2)_L$ and are represented as,

$$e_R^i = \{e_R, \mu_R, \tau_R\}, \quad u_R^i = \{u_R, c_R, t_R\}, \quad d_R^i = \{d_R, s_R, b_R\}. \quad (2.3)$$

Note also that the quarks form triplets of $SU(3)_C$ whereas leptons are color singlets, meaning that only quarks interact strongly. The Higgs boson also emerges from an $SU(2)_L$ doublet with the form,

$$H = \begin{pmatrix} \phi^1 + i \phi^2 \\ \phi^3 + i \phi^4 \end{pmatrix} \equiv \begin{pmatrix} \phi^+ \\ \phi^0 \end{pmatrix}, \quad (2.4)$$

where we see the four components that correspond to the respective degrees of freedom of the Higgs Field. After the process of Spontaneous Symmetry Breaking (SSB) of the $SU(2)_L \times U(1)_Y$ group, the charges read as,

Table 2.1: Quark and Lepton charges

	$SU(3)_C$	$U(1)_Q$
Up type quarks (u, c, t)	3	$2/3$
Down type quarks (d, s, b)	3	$-1/3$
Charged leptons (e, μ, τ)	1	-1
Neutrinos $(\nu_e, \nu_\mu, \nu_\tau)$	1	0

Gauge Group Numbers

The full set of SM fields and respective quantum numbers are shown in the tables 2.2 and 2.3. These show us the representations of these fields, e.g. if a field F has a quantum number of 3 under $SU(2)_L$ then it would be a triplet of $SU(2)_L$, $F^a = (F^1, F^2, F^3)$, where a is an index in the adjoint representation of the group.

Table 2.2: Gauge and Scalar fields in the SM

Fields	Spin 0 field	Spin 1 Field	$SU(3)_C \times SU(2)_L \times U(1)_Y$
Gluons	×	G^a	(8,1,0)
A bosons	×	A^a	(1,3,0)
B bosons	×	B	(1,1,0)
Higgs field	(ϕ^\pm, ϕ^0)	×	(1,2,1)

The gauge groups presented in table 2.2 are composed of 12 generators and are governed by the following algebra,

$$[M_a, M_b] = i f_{abc} M_c \quad [T_a, T_b] = i \epsilon_{abc} T_c \quad [M_a, T_b] = [M_a, Y] = [T_b, Y] = 0 \quad (2.5)$$

where for $SU(3)_C$, $M_a = \lambda_a/2$, with $(a = 1, \dots, 8)$. As for $SU(2)_L$, we have $T_i = \sigma_i/2$, $(i = 1, 2, 3)$, and for Y is the generator of $U(1)_Y$. The symbols λ_a and σ_i represent the Gell-Mann and Pauli matrices respectively.

Table 2.3: Fermion fields in the SM

Fields	Spin $\frac{1}{2}$ Field	$SU(3)_C \times SU(2)_L \times U(1)_Y$
Quarks (3 gen.)	$Q = (u_L, d_L)$	(3, 2, 1/3)
	u_R	(3, 1, 4/3)
	d_R	(3, 1, -2/3)
Leptons (3 gen.)	$L = (\nu_{e_L}, e_L)$	(1, 2, -1)
	e_R	(1, 1, -2)

From here, given the gauge group in, Eq. (2.1) and accounting for the charges and fields, we can derive the form of the SM's Lagrangian.

Lagrangian Formulation

Given the SM gauge groups seen in Eq. (2.1), the charges seen in Tables 2.2 and 2.3 and their algebra, the covariant derivative, D_μ , can be shown to read as,

$$D_\mu = \partial_\mu - ig_s M^a G_\mu^a - ig T^i A_\mu^i - \frac{1}{2} ig' Y B_\mu , \quad (2.6)$$

We can expect 3 different type of couplings, g_s related to the $SU(3)_C$ subgroup, g to the $SU(2)_L$ and g' to $U(1)_Y$. The associated canonical field strength tensors would be,

$$G_a^{\mu\nu} = \partial^\mu G_a^\nu - \partial^\nu G_a^\mu - g_s f_{abc} G_a^\mu G_b^\nu \quad (2.7)$$

$$A_a^{\mu\nu} = \partial^\mu A_a^\nu - \partial^\nu A_a^\mu - g \epsilon_{abc} A_b^\mu A_c^\nu \quad (2.8)$$

$$B^{\mu\nu} = \partial^\mu B^\nu - \partial^\nu B^\mu \quad (2.9)$$

Given these we can now present the SM Lagrangian. It is often convenient to do so in portions, usually divided in three ¹ sections,

$$\mathcal{L}_{SM} = \mathcal{L}_{kin} + \mathcal{L}_{Yuk} + \mathcal{L}_\phi \quad (2.10)$$

¹There is also the need for the introduction of gauge fixing terms and ghosts. However, this is merely a formal requirement and does not imply addition of new physical states.

Where we have the kinetic portion of the SM terms, \mathcal{L}_{kin} , responsible for free propagation of particles, the Yukawa portion, \mathcal{L}_{Yuk} , corresponding to interactions of particles with the Higgs Boson, and finally the \mathcal{L}_ϕ scalar potential. The full kinetic portion of the SM read,

$$\begin{aligned}\mathcal{L}_{kin} = & -\frac{1}{4}G_a^{\mu\nu}G_{a\mu\nu} - \frac{1}{4}A_a^{\mu\nu}A_{a\mu\nu} - \frac{1}{4}B^{\mu\nu}B_{\mu\nu} \\ & - i\bar{Q}_{L_i}\not{D}Q_{L_i} - i\bar{u}_{R_i}\not{D}u_{R_i} - i\bar{d}_{R_i}\not{D}d_{R_i} - i\bar{L}_{L_i}\not{D}L_{L_i} - i\bar{e}_{R_i}\not{D}e_{R_i} \\ & - (D_\mu H)^\dagger(D^\mu H),\end{aligned}\quad (2.11)$$

where \not{D} is the Dirac covariant derivative, $\gamma^\mu D_\mu$ where γ^μ being the gamma matrices. From the last line of Eq. (2.11) and with Eq. (2.6) we will present how the fields A_μ^a and B_μ give rise to the weakly interacting vector bosons W^\pm and Z^0 and the electromagnetic vector boson γ . Contrary to the colour sector, where the eight generators G_μ^a simply correspond to eight gluons G mediating the strong interactions. The scalar potential part is written as,

$$\mathcal{L}_\phi = -\mu^2 HH^\dagger - \lambda(HH^\dagger)^2. \quad (2.12)$$

Finally the Yukawa portion of the Lagrangian is,

$$\mathcal{L}_{Yuk} = Y_{ij}^u \bar{Q}_{L_i} u_{R_j} \tilde{H} + Y_{ij}^d \bar{Q}_{L_i} d_{R_j} H + Y_i^e j \bar{L}_{L_i} e_{R_i} H + \text{H.c.}, \quad (2.13)$$

where, $\tilde{H} = i\sigma_2 H$ and H.c. stands for Hermitian conjugate, also the terms $Y^{e,u,d}$ stands for the Yukawa matrices, these are generic 3×3 with complex and adimensional matrix elements. Note that all indices seen in Eqs. (2.11), (2.12) and (2.13), (j, i) are summed over.

2.2 The Higgs Mechanism and the Mass Generation of the Gauge Bosons

From what was defined above, we can now study the process SSB by which,

$$\text{SU}(2)_L \times \text{U}(1)_Y \rightarrow \text{U}(1)_Q. \quad (2.14)$$

Enabling us to find the real physical states of the gauge bosons and the origin of their mass. Let us consider the part of the Lagrangian containing the scalar covariant derivatives, the scalar potential and the gauge-kinetic terms:

$$\mathcal{L}_{Gauge} \supset (D_\mu H)(D^\mu H)^\dagger - \mu^2 H^\dagger H - \lambda(H^\dagger H)^2 - \frac{1}{4}W_a^{\mu\nu}W_{a\mu\nu} - \frac{1}{4}B^{\mu\nu}B_{\mu\nu}. \quad (2.15)$$

We expect a phase shift to occur, namely one that ensures $\mu^2 < 0$ while at the same ensuring that the field now explicitly breaks the $\text{SU}(2)_L \times \text{U}(1)_Y$. For this to happen we expect the shifted squared value of the Higgs field to be,

$$(H^\dagger H)^2 = \frac{-\mu^2}{2\lambda} \equiv v^2, \quad (2.16)$$

called the EW-Vacuum expectation value (EW-VEV), its value is experimentally measured to be $v \approx 246$ GeV. The choice of vacuum can be aligned in such a way that we have,

$$H_{min} = \frac{1}{\sqrt{2}} \begin{pmatrix} 0 \\ v \end{pmatrix}. \quad (2.17)$$

Given that now the $\text{SU}(2)_L \times \text{U}(1)_Y$ symmetry is broken down to $\text{U}(1)_Q$ we jump from a scenario where there were four generators, which are $T^{1,2,3}$ and Y , to, after the breaking, having solely one unbroken combination that is $Q = (T^3 + Y/2)$ associated to the electric charge. This

means that in total we will have three broken generators, thus, from the Goldstone theorem, there would have to be created three massless particles.

These Goldstones modes however can be parameterized as phases in field space and can be absorbed into the physical basis fields, leaving us with a single physical massive scalar, the Higgs boson. Note that, with this transformation we are removing three scalar degrees of freedom and transferring them to the gauge bosons. So, while before the breaking of the EW symmetry we have four massless gauge bosons, after the breaking we are left with three massive ones. Therefore, without loss of generality, we can rewrite the Higgs doublet as

$$\begin{pmatrix} \phi_1 + i\phi_2 \\ v + h + i\phi_3 \end{pmatrix} = H \rightarrow H = \frac{1}{\sqrt{2}} \begin{pmatrix} 0 \\ v + h \end{pmatrix}. \quad (2.18)$$

Once the Higgs doublet shifts to the EW-VEV, the Lagrangian (2.15) can be recast as:

$$\begin{aligned} \mathcal{L}' = & \frac{1}{2} \partial_\mu h \partial^\mu h - \frac{1}{2} (2v^2 \lambda) h^2 - \frac{1}{4} W_a^{\mu\nu} W_{a\mu\nu} - \frac{1}{4} B^{\mu\nu} B_{\mu\nu} \\ & + \frac{1}{8} v^2 g^2 (A_\mu^1 A^{1,\mu} + A_\mu^2 A^{2,\mu}) + \frac{1}{8} v^2 (g^2 A_\mu^3 A^{3,\mu} + g'^2 B_\mu B^\mu - 2g^2 g'^2 A_\mu^3 B^\mu), \end{aligned} \quad (2.19)$$

A few things become obvious. First, we have a lot of mass terms stemming from the squared gauge fields and a lonesome mass term belonging to the real scalar field we know to be the Higgs field. This makes the Higgs boson mass to be given by,

$$M_h = (2v^2 \lambda). \quad (2.20)$$

To obtain masses for the gauge bosons we need to rotate the gauge fields to a basis where the mass terms are diagonal. First, it is straightforward to see that the electrically charged eigenstates are given by

$$W_\mu^\pm = \frac{1}{\sqrt{2}} (A_\mu^1 \pm iA_\mu^2), \quad (2.21)$$

meaning that the mass of the W bosons is,

$$M_{W^\pm} = \frac{1}{2} v g. \quad (2.22)$$

The situation becomes a bit more complicated for the second term in (2.19) due to a mixing between A_μ^3 and B_μ . In the gauge eigenbasis the mass terms read

$$\begin{pmatrix} A_\mu^3 & B_\mu \end{pmatrix} \cdot \frac{1}{2} v^2 \begin{pmatrix} g^2 & -gg' \\ -gg' & g'^2 \end{pmatrix} \cdot \begin{pmatrix} A^{\mu,3} \\ B^\mu \end{pmatrix}, \quad (2.23)$$

which can be diagonalized to obtain,

$$\begin{pmatrix} A_\mu & Z_\mu \end{pmatrix} \begin{pmatrix} 0 & 0 \\ 0 & \frac{1}{2} v \sqrt{g^2 + g'^2} \end{pmatrix} \begin{pmatrix} A^\mu \\ Z^\mu \end{pmatrix}, \quad (2.24)$$

we identify the eigenvector associated with the null eigenvalue to be the photon and the massive one, $M_Z = \frac{1}{2} v \sqrt{g^2 + g'^2}$, to be the Z boson. Such eigenvectors can be written as

$$A_\mu = \cos(\theta_W) B_\mu + \sin(\theta_W) A_\mu^3, \quad (2.25)$$

$$Z_\mu = -\sin(\theta_W) B_\mu + \cos(\theta_W) A_\mu^3, \quad (2.26)$$

where θ_W is the so called Weinberg mixing angle and is defined as,

$$\cos(\theta_W) = \frac{g}{\sqrt{g^2 + g'^2}}. \quad (2.27)$$

So we conclude our exploration of the electroweak sector with all the correct massive spectrum observed and its origin discussed.

2.3 Fermion Masses in the Standard Model and Quark Mixing

As referenced previously, given the charges of the fermion and lepton fields we cannot construct a gauge invariant theory with explicit mass terms for fermions. The mass of these particles are generated through the Higgs mechanism, via Yukawa terms between the fermions and the scalar field. These interactions can be seen in Eq (2.28),

$$\mathcal{L}_{Yuk} = Y_{ij}^u \bar{Q}_{L_i} u_{R_j} \tilde{H} + Y_{ij}^d \bar{Q}_{L_i} d_{R_j} H + Y_{ij}^e \bar{L}_{L_i} e_{R_j} H + \text{H.c.} \quad (2.28)$$

as the Higgs field settles into the EW VEV (see Eq. (2.18)) mass terms for the quarks and leptons are generated. The Higgs mechanism generates the mass for all the fermionic and leptonic particles except for neutrinos, this is due to the SM not containing right handed neutrinos, i.e it is impossible build terms that would lead to neutrino masses without explicitly breaking the SM symmetry group. The addition of right handed neutrino fields is very commonly made in BSM scenarios.

To reach the physical states from the weak eigenbasis we must diagonalize the Yukawa matrices. This is done through bi-unitary transformations. We can write these transformation under the form,

$$M_{\text{diag.}}^{u,d,e} = U_L^{u,d} Y^{u,d} U_R^{u,d} \frac{v}{\sqrt{2}}, \quad (2.29)$$

where $U_L^{u,d}$ and $U_R^{u,d}$ are the required 4 unitary matrices.

For simplicity sake we assume that the leptonic Yukawa couplings matrix Y^e is flavour diagonal i.e. a diagonal matrix needing not to be transformed. This makes only the quarks to be relevant to our discussion.

Naturally, we can invert Eq. (2.29), returning,

$$Y_{ij}^u = \frac{\sqrt{2}}{v} (U_L^u M_{\text{diag.}}^u U_R^u)_{ij}, \quad Y_{ij}^d = \frac{\sqrt{2}}{v} (U_L^d M_{\text{diag.}}^d U_R^d)_{ij}. \quad (2.30)$$

Considering the Higgs mechanism, we can see this change creates mass terms for physical quark fields by replacing the result of Eq. (2.30) in the Yukawa portion of the Lagrangian (Eq. (2.13)).

$$\begin{aligned} \mathcal{L}_{Yuk} &\supset -\frac{v}{\sqrt{2}} Y_{ij}^d (\bar{u}_{L_i} \bar{d}_{L_i}) d_{R_j} \tilde{H} - \frac{v}{\sqrt{2}} Y_{ij}^u (\bar{u}_{L_i} \bar{d}_{L_i}) u_{R_j} + \text{H.c.} \\ &\quad \Downarrow \\ &- (U_L^d M_{\text{diag.}}^d U_R^d)_{ij} d_{L_i} d_{R_j} - (U_L^u M_{\text{diag.}}^u U_R^u)_{ij} u_{L_i} u_{R_j} + (\text{Interactions with } h) + \text{H.c.} \quad (2.31) \\ &\quad \Downarrow \\ &- M_{\text{diag.}_j}^d d'_{L_i} d'_{R_j} - M_{\text{diag.}_j}^u u'_{L_i} u'_{R_j} + (\text{Interactions with } h) + \text{H.c.} \end{aligned}$$

where the primed fields are the quark fields in the mass basis, defined as,

$$\begin{aligned} d'_{L,R} &= U_{L,R}^d d_{L,R}, \\ u'_{L,R} &= U_{L,R}^u u_{L,R}. \end{aligned} \quad (2.32)$$

Note that the increasing masses seen in each generation depend directly on the hierarchy of the Yukawa terms. This means that the mass of all particles directly relates to how strongly they each interact with the Higgs boson. If you then take into account the real masses e.g. for the leptons, the tau mass is in the GeV range while the electron's is in the 0.1 MeV range. This translates to very different couplings for each flavour. This hierarchy is unjustified in the SM.

As a result of this redefinition we can now look at the gauge interactions to see that charged currents appear where W^\pm couples to the physical u'_{L_j} and d'_{L_j} quarks. The coupling of the fermions to the gauge fields changes by virtue of the fact that only left handed quarks are $SU(2)_L$ doublets. If we expand the up and down quark fields on the kinetic portion of the Lagrangian,

$$\begin{aligned} \mathcal{L}_{ferm} \supset & \frac{1}{2} \bar{u}'_L \gamma^\mu (g' Y B_\mu + g Z_\mu) \left(U_L^u U_L^{u\dagger} \right) u'_L - \frac{1}{\sqrt{2}} g \bar{u}'_L \gamma^\mu \left(U_L^u U_L^{d\dagger} \right) d'_L W_\mu^+ \\ & - \frac{1}{\sqrt{2}} g \bar{d}'_L \gamma^\mu \left(U_L^u U_L^{d\dagger} \right) u'_L W_\mu^- + \frac{1}{2} \bar{d}'_L \gamma^\mu (g' Y B_\mu - g Z_\mu) \left(U_L^d U_L^{d\dagger} \right) d'_L \end{aligned} \quad (2.33)$$

By employing properties of unitary matrices, namely, $U_{L,R}^{u,d} U_{L,R}^{u,d\dagger} = 1$, we note that the interactions with the neutral bosons remain the same in the mass basis. However the charged currents are affected by this change. Therefore, we define the Cabibbo-Kobayashi-Maskawa (CKM) matrix, as $V_{CKM} = U_L^u U_R^{u\dagger}$ and write the sensitive terms,

$$\mathcal{L}_{kin} \supset \frac{1}{\sqrt{2}} g \bar{u}'_L \gamma^\mu V_{CKM} d'_L W_\mu^+ + \text{H.c.} \quad (2.34)$$

The CKM matrix, is a 3×3 unitary matrix. It is a parametrization of the three mixing angles and a CP-violating KM (Kobayashi-Maskawa) phase. The mixing angles refer to those between the up and down quark families. We can see their hierarchy in Fig. 2.2.

It is through this complex phase in the CKM matrix that the SM can account for the phenomena of \mathcal{CP} violation. First observed in the famous K^0 decay into $\mu^+ \mu^-$ ($CP = +1$ and $CP = -1$ respectively) [16], that won the 1980 Nobel Prize [17]. The discovery opened the door to questions still at the core of particle physics and of cosmology today. Not just the lack of an exact CP-symmetry, but also the fact that it is so close to a symmetry.

Figure 2.1: Box diagram describing $K_L^0 \rightarrow \mu^- \mu^+$, through an intermediate u quark.

We avoided discussing leptons since in the SM their mass eigenstates can be easily shown to have no real consequence besides a change of basis. We might also note a very interesting feature of the Standard Model, by consequence of the $SU(2)_L \times U(1)_Y$ symmetry we can see that in Eq.(2.33) there are no interactions of the right handed unitary matrices and thus no mixing, coupling, or charged currents of right handed quarks, making them theoretically invisible. The nature of CKM elements and how the quarks behavior differs when interacting weakly through neutral currents can be seen in the following figure,

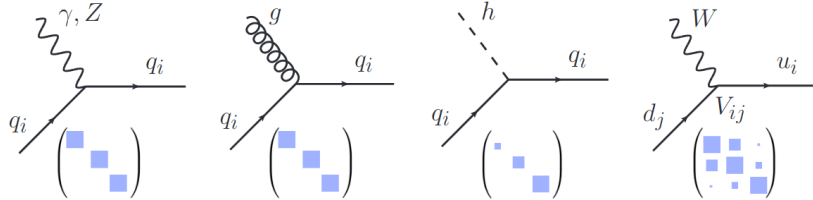


Figure 2.2: Feynman diagrams for flavour conserving couplings of quarks to photon, Z boson, gluon and the Higgs (the first three diagrams), and the flavour changing coupling to the W (the last diagram). The 3×3 matrices are visual representations of couplings in the generation space, with couplings to γ, Z, g being flavour universal, while the couplings to the Higgs are flavour diagonal but not universal. Finally the couplings involving the W are flavour changing and hierarchical.

Note, the CKM matrix elements are fundamental parameters of the particle physics and their precise determination a important landmark for experimental particle physics. It follows then that reproducing the quark mixing parameters is fundamental for BSM searches that include changes to how the quarks interact with possible new Higgs bosons.

2.3.1 Charged Flavour Currents vs. Neutral Flavor Currents

It is very noteworthy to highlight a important distinction between flavor changing neutral and charged currents. FCNCs are processes in which the quark flavor changes, while the quark charge stays the same. The Flavour Changing Charged Currents (FCCCs) change both the flavour and the charge of the quark. Extracting some representative probabilities from [18] reveals that the two types of processes are strikingly statistically different. The charged currents lead to the dominant weak decays, while the FCNCs induce decays that are extremely suppressed. Rounding the experimental results, and not showing the errors, a few representative decays are,

Table 2.4: FCCCs examples

$$\begin{aligned} s \rightarrow u\mu^-\nu_\mu &: \mathcal{BR}(K^+ \rightarrow \mu^-\nu) = 64\% \\ b \rightarrow cl^-\nu_l &: \mathcal{BR}(B^- \rightarrow D^0 l \bar{\nu}_l) = 2.3\% \\ c \rightarrow u\mu^-\nu_\mu &: \mathcal{BR}(D^\pm \rightarrow K^0 \mu^\pm \nu) = 9\% \end{aligned}$$

Table 2.5: FCNCs examples

$$\begin{aligned} s \rightarrow d\mu^+\mu^- &: \mathcal{BR}(K_L \rightarrow \mu^+\mu^-) = 7 \times 10^{-9} \\ b \rightarrow d\mu^+\mu^- &: \mathcal{BR}(B^- \rightarrow K^{*-} l^+ l^-) = 5 \times 10^{-7} \\ c \rightarrow ul^+l^- &: \mathcal{BR}(D^0 \rightarrow \pi l^+ l^-) = 1.8 \times 10^{-4} \end{aligned}$$

The reason for such a striking difference is that in the SM the charged currents occur at tree level, while FCNCs are forbidden at tree level and only arise starting at one loop order. Note the lack of neutral couplings (involving the Z boson) between the up and down families in Eq 2.33. The relative complexity of these processes can be easily seen in Fig 2.3,

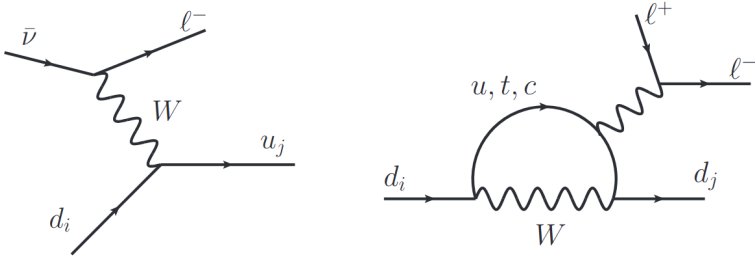


Figure 2.3: Representative tree level charged current diagram (left) and a loop induced FCNC diagram (right).

Furthermore, the FCNCs come suppressed by the difference of the masses of the quarks running in the loop, $m_j^2 - m_i^2$. This so called Glashow-Iliopoulos-Maiani (GIM) mechanism [19]. Given the differences between the masses of the up and down sectors this has a significant impact.

Flavour as a Probe into New Physics

Now that we have introduced a small portion of flavor physics we can briefly touch on why collider experiments have been sold as a pathway to discovering new physics i.e. how deviation in rare decays could pin point exactly what is missing in the SM.

Thanks to these large experiments we have many new observables in flavor physics, e.g. the branching ratios not coinciding with the SM prediction [20], observed Lepton Flavor Violation in tree and loop levels [21]. As well as providing limits on processes that are prohibited in the SM but that could happen with different models, such as lepton flavor violation in Higgs decays [22] in models without Lepton flavour universality.

However, one of the favored ways to search for NP is through FCNCs this is because as mentioned there are no FCNCs at tree-level in the SM i.e. the gluon, Z and Higgs are strictly flavor conserving as we see in Fig. 2.2 at tree-level. Thus given FCNC processes are heavily suppressed in the SM through the aforementioned GIM mechanism and loop order, and that FCNCs processes can be easily modified by NP, either through new tree level or loop level NP contributions these can serve as a good tool to search for exotic signatures. Note, these signatures could show themselves through virtual NP particles and thus also provide evidence of high mass (Possibly TeV range) at a lower beam energy than the required energy to for one to be freely produced. This is if we assume NP can couple between generations and flavors of quarks.

The recipe then, seems simple, identify processes that are rare in the SM and then search for deviations from the SM predictions. However, thus far all but a few processes are within 2σ experimental and theoretical bounds given by the SM. Some of the most radical being the quark level transitions, $b \rightarrow s\mu\mu$ [23] and $b \rightarrow c\tau\nu$ [24] channels. They are, so far, showing over 4σ deviations from their expected value.

Without going into too much depth onto the NP searches, we can examine the scale at which these processes are "integrated away". This is the energy scale at which a NP vector-axial operator would allow these processes to exist only at high energies. These energies are naturally high given the terms in Eq. (2.35).

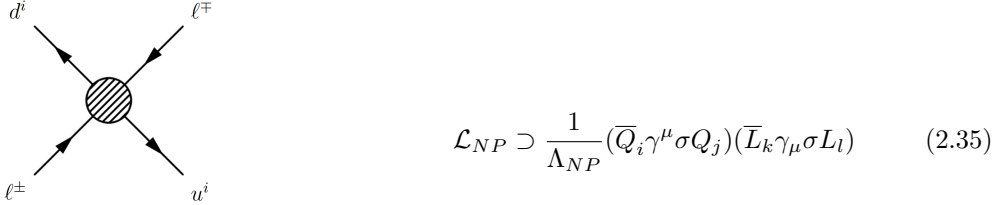


Figure 2.4: "Contact" interactions with loop interactions containing NP

To explain $b \rightarrow s\mu\mu$ transitions you would need a $\Lambda_{NP} \approx 3$ TeV while for $b \rightarrow c\tau\nu$ you would need a $\Lambda_{NP} \approx 30$ TeV. This is a strong indicator that some components are missing in our formulation like a new mediator for gauge interactions. The advantage of this scale is it lies almost certainly in most BSM scenarios, avoiding most experimental constraints.

As for the FCNC diagram, the $b \rightarrow s\mu\mu$ channel can be seen in Fig 2.5,

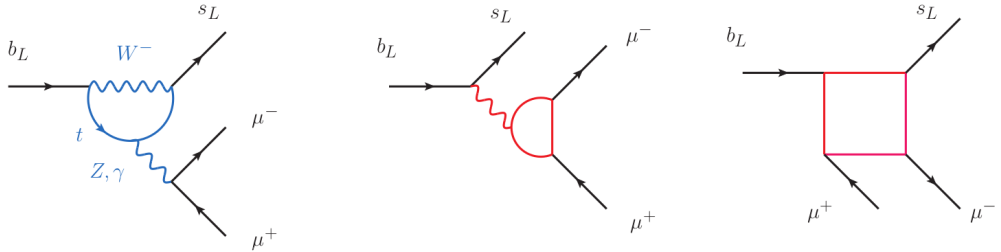


Figure 2.5: A representative SM diagram for $b \rightarrow s\mu\mu$ transition (left), and representative possible loop level NP contributions (middle and right).

The $b \rightarrow c\tau\nu$ flavour anomaly is similarly very clean theoretically [25]. However, the NP effect in these diagrams is large ($\mathcal{O}(20\%)$) compared to the SM. This means that the scale of NP needs to be lower or happen at tree-level. Consequently the NP interpretations here are often in conflict with experimental constraints, such as this decay. The theoretical bias here would have been that the new charged currents are either due to a charged Higgs, H^+ , or a new vector boson, W' , see Fig. 2.6. However these would have too large a effect in the B^- lifetime to fully explain the anomaly according to Ref. [26].

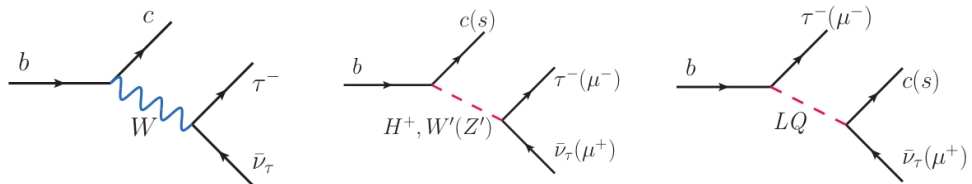


Figure 2.6: The SM diagrams for $b \rightarrow c\tau\nu$ transition (left), and the possible tree level NP contributions to $b \rightarrow c\tau\nu$ transition (middle and right). Where the LQ stands for a hypothetical Leptoquark particle that would interact with both leptons and quarks.

Another prediction of the SM is that the rates for the $b \rightarrow se^+e^-$ and $b \rightarrow s\mu^-\mu^+$ transitions should be equal to each other. The SM prediction of Lepton Flavour Universality (LFU) is deeply engrained in the structure of the theory, since it is a consequence of the fact that the electroweak gauge group is the same for all three generations. The prediction of LFU can be tested experimentally, also through flavour physics, by theoretically clean observables such as the ratios of these flavour observables,

$$R_{K^*} = \frac{\text{Br}(B \rightarrow K^* \mu^-\mu^+)}{\text{Br}(B \rightarrow K^* e^-e^+)} \quad (2.36)$$

Another strong indicator of new physics is the fact the experimental value for this ratio is $R_{K^*} \approx 0.7$, violating LFU by $2.2 - 2.6\sigma$ [27].

Chapter 3

B-L-SM Model

In this chapter we introduce the minimal $U(1)_{B-L}$ gauge extension of the SM named, the B-L-SM Model [28, 29, 30]. In this model, we are capable of explaining the generation of neutrinos masses generation via a simple see-saw mechanism. Additionally, by virtue of two new physical states, specifically a new Higgs like boson H' and a Z' gauge boson we can also address other phenomenology, such as deviations in EW measurements, namely the $(g - 2)_\mu$ anomaly [31].

The additional bosons acquire mass primarily through the spontaneous breaking of the $U(1)_{B-L}$ symmetry that gives its name to the model. This unitary group originates from the promotion of an accidental symmetry present in the SM, the Baryon number (B) minus the Lepton number (L) to a fundamental Abelian symmetry group. This origin for the mass of the referenced bosons means the model is already very heavily constrained due to long-standing direct searches at the LHC.

Through this model we can address the metastability of the EW vacuum in the SM through the new scalar. Allowing for Higgs stabilization up to the Plank scale with a new Higgs starting from a few hundred GeVs [32, 33, 34].

The B-L-SM framework is particularly interesting in the context of the study of Grand Unified Theories (GUT) as it easily embeds into higher order symmetry groups like the $SO(10)$ [35, 36, 37, 38, 39] or E_6 [40, 41, 42] Lie groups. The presence of a new complex singlet field, χ , with a Higgs doublet typically results in enhanced strength of the EW phase transition potentially converting it into a strong first-order one. This would be could be detectable in the form of a gravitational wave background [43]. Such a analysis is of utmost importance given that it could provide a way to detect NP or exclude models without the need for a larger particle collider.

However, a family-universal symmetry such as $U(1)_{B-L}$, being introduced without changing the SM fermion content would lead to chiral anomalies. This translates to a non-conservative charged current on some channels involving the $U(1)_{B-L}$. These are not completely undesired by themselves, as they would allow for the presence of extra sources of \mathcal{CP} violation, but this inclusion at tree-level without a suppression mechanism would lead to far too much \mathcal{CP} violation.

The model also benefits from the presence of three generations of right-handed heavy Majorana neutrinos that through the new field additions are possible in a framework free of anomalies while also allowing for a minimal see-saw mechanism that generates light neutrino masses unlike the SM. [44, 45, 46]. The mass scale of such neutrinos is established once the $U(1)_{B-L}$ symmetry is broken. These neutrinos are of cosmological significance given their presence could imply the existence of a sterile state that can play the role of Dark Matter [47]. The relatively small alteration of a, \mathbb{Z}_2 , symmetry in the neutrino sector can make these fully sterile, as seen in [48, 49]. These neutrinos can, in such case, be used to help explain the baryon asymmetry via the leptogenesis mechanism, this scenario is discussed in depth in the following Refs. [50, 51, 52].

With this in mind, we structure this chapter in the following way. First, we present the fundamental theoretical background on the model with a strong focus on the basic details of the scalar and the gauge boson mass spectra and mixing. Followed by a modern precise study of the phenomenological status of the B-L-SM model through a layered algorithm that will be discussed

preceding the results. With this algorithm we provide a numerical analysis that tests the relevant phenomenological constraints in direct and EW observables. We table off this chapter with a few representative benchmark points.

3.1 Formulating the Model

Essentially, the minimal B-L-SM is a BSM framework containing only three new ingredients, a new gauge interaction given the new symmetry group, three generations of right handed neutrinos, and a complex scalar field χ .

The first of these is well motivated by the aformentioned GUT scenarios, While a new sector of additional three $U(1)_{B-L}$ charged Majorana neutrinos is essential for anomaly cancellation.

Finally, the SM-like Higgs doublet, H , does not carry neither baryon nor lepton number, this way it does not participate in the breaking of $U(1)_{B-L}$. It is then necessary to introduce a new scalar singlet field, χ , solely charged under $U(1)_{B-L}$, to perform the breaking of the $B - L$ symmetry.

The particle content and related charges of the minimal $U(1)_{B-L}$ extension of the SM are shown in Tab 3.1. Note these are similar to the SM as to be expected.

	q_L	u_R	d_R	l_L	e_R	ν_R	H	χ
$SU(3)_C$	3	3	3	1	1	1	1	1
$SU(2)_L$	2	1	1	2	1	1	2	1
$U(1)_Y$	1/6	2/3	-1/3	-1/2	-1	0	1/2	0
$U(1)_{B-L}$	1/3	1/3	1/3	-1	-1	-1	0	2

Table 3.1: Quantum fields and their respective quantum numbers in the minimal B-L-SM extension. The last two lines represent the weak and $B - L$ hypercharges

Scalar sector

With the information from Tab 3.1, we can begin examining the new Lagrangian terms. Starting by the scalar potential, which now depends on two fields,

$$V(H, \chi) = \mu_1^2 H^\dagger H + \mu_2^2 \chi^* \chi + \lambda_1 (H^\dagger H)^2 + \lambda_2 (\chi^* \chi)^2 + \lambda_3 \chi^* \chi H^\dagger H, \quad (3.1)$$

where, λ_i , the scalar couplings and $\mu_{1,2}^2$ the quadratic terms for H and χ respectively. This potential must lead to a stable vacuum state, which means that the scalar potential must be bounded from below (BFB), as to ensure a global minima. Studying the potential on Eq. (3.1) we deduce the conditions,

$$4\lambda_1\lambda_2 - \lambda_3^2 > 0 \quad , \quad \lambda_1, \lambda_2 > 0 \quad (3.2)$$

Where the full components of the scalar fields H and χ are given by,

$$H = \frac{1}{\sqrt{2}} \begin{pmatrix} -i(\omega_1 - i\omega_2) \\ v + (h + iz) \end{pmatrix} \quad \chi = \frac{1}{\sqrt{2}} (x + (h' + iz')) \quad (3.3)$$

where we note that the parameters v and x are VEV's associated with the H field and the χ field, respectively. In these equations we can see that h and h' represent the radial quantum fluctuations around the minimum of the potential. These will constitute the physical degrees of freedom associated with H and H' . There are also four Goldstone directions denoted as ω_1, ω_2, z and z' which are absorbed into longitudinal modes of the W^\pm, Z and Z' gauge bosons once SSB takes place. After SSB the associated VEVs take the form,

$$\langle H \rangle = \frac{1}{\sqrt{2}} \begin{pmatrix} 0 \\ v \end{pmatrix} \quad \langle \chi \rangle = \frac{x}{\sqrt{2}} \quad (3.4)$$

From here we can solve the tadpole equations in relation to each of the VEVs as to ensure non-zero VEV. We arrive at,

$$v^2 = \frac{-\lambda_2\mu_1^2 + \frac{\lambda_3}{2}\mu_2^2}{\lambda_1\lambda_2 - \frac{1}{4}\lambda_3^2} > 0 \quad \text{and} \quad x^2 = \frac{-\lambda_1\mu_2^2 + \frac{\lambda_3}{2}\mu_1^2}{\lambda_1\lambda_2 - \frac{1}{4}\lambda_3^2} > 0 \quad (3.5)$$

which, when simplified with the BFB conditions yield a simpler set of equations,

$$\lambda_2\mu_1^2 < \frac{\lambda_3}{2}\mu_2^2 \quad \text{and} \quad \lambda_1\mu_2^2 < \frac{\lambda_3}{2}\mu_1^2 \quad (3.6)$$

Note that although λ_1 and λ_2 must be positive to ensure the correct conical shape of the potential, no such conditions exist for the sign of λ_3 , μ_1 , and μ_2 . However observing Eq(3.6) we can infer that only some combinations of signs are impossible,

$\mu_2^2 > 0$	$\mu_2^2 > 0$	$\mu_2^2 < 0$	$\mu_2^2 < 0$	
$\mu_1^2 > 0$	$\mu_1^2 < 0$	$\mu_1^2 > 0$	$\mu_1^2 < 0$	
$\lambda_3 < 0$	\times	\checkmark	\checkmark	\checkmark
$\lambda_3 > 0$	\times	\times	\times	\checkmark

Table 3.2: Possible signs of the potential parameters in Eq(3.1). The \checkmark symbol indicates the existence of solutions for tadpole conditions Eq. (3.6), while the \times indicates unstable configurations.

For our numerical analysis we decided to leave the sign of λ_3 positive, choosing a configuration where both μ parameters are negative. This does not directly translate to any real physical consequence. With these conditions now established we proceed to investigate the physical states of the B-L-SM scalar sector. At the vacuum, we evaluate the Hessian matrix as,

$$\mathbf{M}^2 = \begin{pmatrix} 4\lambda_2x^2 & \lambda_3vx \\ \lambda_3vx & 4\lambda_1v^2 \end{pmatrix}, \quad (3.7)$$

Moving this matrix to its physical mass eigen-base, we obtain the following eigenvalues,

$$m_{h_{1,2}}^2 = \lambda_1v^2 + \lambda_2x^2 \mp \sqrt{(\lambda_1v^2 - \lambda_2x^2)^2 + (\lambda_3vx)^2}. \quad (3.8)$$

The physical basis vectors h_1 and h_2 can then be related to the original fields of gauge eigen-basis h and h' trough a simple rotation matrix:

$$\begin{pmatrix} h_1 \\ h_2 \end{pmatrix} = \mathbf{O} \begin{pmatrix} h \\ h' \end{pmatrix}, \quad (3.9)$$

where \mathbf{O} can be parameterized by a single mixing angle α_h ,

$$\mathbf{O} = \begin{pmatrix} \cos \alpha_h & -\sin \alpha_h \\ \sin \alpha_h & \cos \alpha_h \end{pmatrix}. \quad (3.10)$$

It is particularly interesting to analyse the scenario where the scalar fields approximately decouple, that is, in the limit, $v/x \ll 1$. In these circumstances, the scalar masses and the mixing angle become rather simple,

$$\sin \alpha_h \approx \frac{1}{2} \frac{\lambda_3}{\lambda_2} \frac{v}{x} \quad m_{h_1}^2 \approx 2\lambda_1v^2 \quad m_{h_2}^2 \approx 2\lambda_2x^2 \quad (3.11)$$

We will see in the context of our numerical results that for a phenomenologically consistent mass scale these equations serve as a valid approximation for most of the points.

Gauge Sector

Moving onto the gauge boson and Higgs kinetic terms in the B-L-SM, consider the following portion of the Lagrangian,

$$\mathcal{L}_{U(1)'s} = |D_\mu H|^2 + |D_\mu \chi|^2 - \frac{1}{4} F_{\mu\nu} F^{\mu\nu} - \frac{1}{4} F'_{\mu\nu} F'^{\mu\nu} - \frac{1}{2} \kappa F_{\mu\nu} F'^{\mu\nu} \quad (3.12)$$

where $F^{\mu\nu}$ and $F'^{\mu\nu}$ are the standard field strength tensors, respectively for the $U(1)_Y$ and $U(1)_{B-L}$ Abelian groups,

$$F_{\mu\nu} = \partial_\mu A_\nu - \partial_\nu A_\mu \quad \text{and} \quad F'_{\mu\nu} = \partial_\mu A'_\nu - \partial_\nu A'_\mu. \quad (3.13)$$

written in terms of the gauge fields A_μ and A'_μ , respectively. Given that this is a model with two Unitary groups, without a parity symmetry (\mathbb{Z}_2) to prevent it, we must consider the possible mixing in between them. In this work we parameterized this mixing through a parameter κ .

The Abelian part of the covariant derivative in Eq. (3.12) is given by,

$$D_\mu \supset i g_1 Y A_\mu + i g'_1 Y_{B-L} A'_\mu, \quad (3.14)$$

with g_1 and g'_1 the $U(1)_Y$ and $U(1)_{B-L}$ the gauge couplings with the Y and $B-L$ charges are specified in Tab.tab:BLSM`Charges. It is convenient to rewrite the gauge kinetic terms in the canonical form, i.e.

$$F_{\mu\nu} F^{\mu\nu} + F'_{\mu\nu} F'^{\mu\nu} + 2\kappa F_{\mu\nu} F'^{\mu\nu} \rightarrow B_{\mu\nu} B^{\mu\nu} + B'_{\mu\nu} B'^{\mu\nu}. \quad (3.15)$$

A generic orthogonal transformation in the field space does not eliminate the kinetic mixing term. So, in order to satisfy Eq. (3.15) an extra non-orthogonal transformation should be imposed such that Eq. (3.15) is realized. Taking $\kappa = \sin \alpha$, a suitable redefinition of fields $\{A_\mu, A'_\mu\}$ into $\{B_\mu, B'_\mu\}$ that eliminates κ -term according to Eq. (3.12) can be cast as

$$\begin{pmatrix} A_\mu \\ A'_\mu \end{pmatrix} = \begin{pmatrix} 1 & -\tan \alpha \\ 0 & \sec \alpha \end{pmatrix} \begin{pmatrix} B_\mu \\ B'_\mu \end{pmatrix}, \quad (3.16)$$

Note there is a limit without kinetic mixing where $\alpha = 0$. Note that this transformation is generic and valid for any basis in the field space. The transformation (3.16) results in a modification of the covariant derivative that acquires two additional terms encoding the details of the kinetic mixing, i.e.

$$D_\mu \supset \partial_\mu + i(g_Y Y + g_{B-L} Y_{B-L}) B_\mu + i(g_{B-L} Y_{B-L} + g_{YB} Y) B'_\mu, \quad (3.17)$$

where the gauge couplings take the form

$$g_Y = g_1 g_{B-L} = g'_1 \sec \alpha g_{YB} = -g_1 \tan \alpha g_{BY} = 0, \quad (3.18)$$

which is the standard convention in the literature. Note that this definition is merely to simplify the equations and has no physical impact. We will later see that this kinetic mixing is a desired feature and why stabilizing it with a \mathbb{Z}_2 symmetry would be detrimental in terms of depth. The resulting mixing between the neutral gauge fields including Z' can be represented as follows

$$\begin{pmatrix} \gamma_\mu \\ Z_\mu \\ Z'_\mu \end{pmatrix} = \begin{pmatrix} \cos \theta_W & \sin \theta_W & 0 \\ -\sin \theta_W \cos \theta'_W & \cos \theta_W \cos \theta'_W & \sin \theta'_W \\ \sin \theta_W \sin \theta'_W & -\cos \theta'_W \sin \theta'_W & \cos \theta'_W \end{pmatrix} \begin{pmatrix} B_\mu \\ A_\mu^3 \\ B'_\mu \end{pmatrix} \quad (3.19)$$

where θ_W is the weak mixing angle and θ'_W is defined as

$$\sin(2\theta'_W) = \frac{2g_{YB}\sqrt{g^2 + g_Y^2}}{\sqrt{(g_{YB}^2 + 16(\frac{x}{v})^2 g_{B-L}^2 - g^2 - g_Y^2)^2 + 4g_{YB}^2(g^2 + g_Y^2)}}, \quad (3.20)$$

in terms of g and g_Y being the $SU(2)_L$ and U_Y gauge couplings, respectively. In the physically relevant limit, $v/x \ll 1$, the above expression greatly simplifies leading to

$$\sin \theta'_W \approx \frac{1}{16} \frac{g_{YB}}{g_{B-L}} \left(\frac{v}{x} \right)^2 \sqrt{g^2 + g_Y^2}, \quad (3.21)$$

up to $(v/x)^3$ corrections. In the limit of no kinetic mixing, i.e. $g_{YB} \rightarrow 0$, there is no mixture of Z' and SM gauge bosons.

Note, that the kinetic mixing parameter θ'_W has rather stringent constraints from Z pole experiments both at the Large Electron-Positron Collider (LEP) and the Stanford Linear Collider (SLC), restricting its value to be smaller than 10^{-3} approximately [53], which we set as an upper bound in our numerical analysis. Expanding the kinetic terms $|D_\mu H|^2 + |D_\mu \chi|^2$ around the vacuum one can extract the following mass matrix for the vector bosons

$$m_V^2 = \frac{v^2}{4} \begin{pmatrix} g^2 & 0 & 0 & 0 & 0 \\ 0 & g^2 & 0 & 0 & 0 \\ 0 & 0 & g^2 & -gg_Y & -gg_{YB} \\ 0 & 0 & -gg_Y & g_Y^2 & g_Y g_{YB} \\ 0 & 0 & -gg_{YB} & g_Y g_{YB} & g_{YB}^2 + 16 \left(\frac{x}{v} \right)^2 g_{B-L}^2 \end{pmatrix} \quad (3.22)$$

whose, first set of eigenvalues read,

$$m_A = 0, \quad m_W = \frac{1}{2} v g \quad (3.23)$$

corresponding to the expected physical photon and W^\pm bosons. While the following set,

$$m_{Z,Z'} = \sqrt{g^2 + g_Y^2} \cdot \frac{v}{2} \sqrt{\frac{1}{2} \left(\frac{g_{YB}^2 + 16(\frac{x}{v})^2 g_{BL}^2}{g^2 + g_Y^2} + 1 \right) \mp \frac{g_{YB}}{\sin(2\theta'_W) \sqrt{g^2 + g_Y^2}}}. \quad (3.24)$$

correspond to two neutral massive vector bosons, with one of them, not necessarily the lightest, representing the SM-like Z boson. It follows from LEP and SLC constraints on θ'_W , that Eq. (3.21) also implies that either g_{YB} or the ratio v/x are small. In this limit, Eq. (3.24) simplifies to

$$m_Z \approx \frac{1}{2} v \sqrt{g^2 + g_Y^2} \quad \text{and} \quad m_{Z'} \approx 2 g_{B-L} x, \quad (3.25)$$

where the $m_{Z'}$ depends only on the SM-singlet VEV x and on the $U(1)_{B-L}$ gauge coupling and will be attributed to a heavy Z' state, while the light Z -boson mass corresponds to its SM value.

The Yukawa Sector

One of the key features of the B-L-SM model is the presence of non-zero neutrino masses. In its minimal version, such masses are generated via a type-I seesaw mechanism, thus producing a very light neutrino for each of the three known neutrino flavours, and a corresponding heavy neutrino one for each, which has yet to be observed. In the type-I seesaw mechanism the mixing of neutrinos fields is written with similar shape to,

$$\begin{pmatrix} 0 & A \\ \hline A & B \end{pmatrix} \quad (3.26)$$

This system would have a set eigenvalues written as,

$$\lambda_\pm = \frac{B \pm \sqrt{B^2 + 4A}}{2} \quad (3.27)$$

Investigating the nature of this set of eigenvalues allows us to understand the see-saw process. The mean of these values being always equal to $|B|$, if one value goes up, another goes down, like a see-saw. B is set to be proportional to Majorana mass terms, orders of magnitude higher than the cross-terms A . Given this, the smaller eigenvalue, is,

$$\lambda_- \approx \frac{A^2}{B} \quad (3.28)$$

This mechanism serves to explain why the neutrino masses are so small.

The total Yukawa Lagrangian of the model reads,

$$\mathcal{L}_f = -Y_u^{ij} \bar{q}_{Li} u_{Rj} \tilde{H} - Y_d^{ij} \bar{q}_{Li} d_{Rj} H - Y_e^{ij} \bar{\ell}_{Li} e_{Rj} H - Y_\nu^{ij} \bar{\ell}_{Li} \nu_{Rj} \tilde{H} - \frac{1}{2} Y_\chi^{ij} \bar{\nu}_{Ri}^c \nu_{Rj} \chi + \text{H.c.} \quad (3.29)$$

Notice the explicit lack of Majorana neutrino mass terms of the form $M \bar{\nu}_R^c \nu_R$. These explicitly violate the $U(1)_{B-L}$ symmetry and are therefore not present. In Eq. (3.29), Y_u , Y_d and Y_e are the 3×3 Yukawa matrices that reproduce the quark and charged lepton sector exactly the same way as in the SM, while Y_ν and Y_χ are the new Yukawa matrices responsible for the generation of right handed neutrino masses and mixing with left handed fields. In particular, one can write,

$$\mathbf{m}_{\nu_l}^{Type-I} = \frac{1}{\sqrt{2}} \frac{v^2}{x} \mathbf{Y}_\nu^t \mathbf{Y}_\chi^{-1} \mathbf{Y}_\nu, \quad (3.30)$$

for light ν_l neutrino masses, whereas the heavy ν_h ones are given by

$$\mathbf{m}_{\nu_h}^{Type-I} \approx \frac{1}{\sqrt{2}} \mathbf{Y}_\chi x, \quad (3.31)$$

where we have assumed a flavour diagonal basis.

Note that the smallness of light neutrino masses imply that either the x VEV is very large or (if we fix it to be at the $\mathcal{O}(\text{TeV})$ scale and $\mathbf{Y}_\chi \sim \mathcal{O}(1)$) the corresponding Yukawa coupling should be tiny, $\mathbf{Y}_\nu < 10^{-6}$. It is clear that the low scale character of the type-I seesaw mechanism in the minimal B-L-SM is *faked* by small Yukawa couplings to the Higgs boson. A more elegant description was proposed in Ref. [54] where small SM neutrino masses naturally result from an inverse seesaw mechanism. In this work, however, we will not study the neutrino sector and thus, for an improved efficiency of our numerical analysis of Z' observables, it will be sufficient to fix the Yukawa couplings to $\mathbf{Y}_\chi = 10^{-1}$ and $\mathbf{Y}_\nu = 10^{-7}$ values such that the three lightest neutrinos lie in the sub-eV domain.

3.2 Numerical Results

Before we begin this section, we would like to point-out recent work done by our colleagues where a comprehensive study for the Z' at the LHC is performed [55]. In particular from 0.2 GeV to 200 GeV. As for slightly heavier Z' masses beyond $m_{Z'} \gtrsim 100$ GeV, the combined effect of the EW precision observables and the ATLAS searches for Drell-Yan Z' production decaying into di-leptons, i.e. $pp \rightarrow Z' \rightarrow ee, \mu\mu$ [1], is also finely investigated. We then endeavoured to achieve a complementary study where we investigated the case of very heavy Z' bosons.

Our goal is to see if the case of an heavy Z' , whose kinetic mixing is highly constrained by LHC experimental results, can provide additional phenomenological implications besides the addition of a new unobserved vector boson. This was chiefly done by the investigation of the $(g-2)_\mu$ anomaly. We examine the relations that this anomaly has with the parameter space, such as gauge couplings, as well as the extra scalar mass. The $(g-2)_\mu$ anomaly refers to the discrepancy between the measured anomalous magnetic moment of the muon, $a_\mu^{\text{exp}} \equiv \frac{1}{2} (g-2)_\mu^{\text{exp}}$, and its theoretical prediction, $a_\mu^{\text{SM}} \equiv \frac{1}{2} (g-2)_\mu^{\text{SM}}$, which reads [31]

$$\Delta a_\mu = a_\mu^{\text{exp}} - a_\mu^{\text{SM}} = 268(63)(43) \times 10^{-11} \quad (3.32)$$

with numbers in brackets denoting experimental and theoretical errors, respectively. This represents a deviations of 3.5 standard deviations from the combined 1σ error and is calling for new physics effects beyond the SM theory.

There is a strong possibility that through radiative corrections a new gauge bosons could explain this deviation [56]. In fact a version of this study has already been performed in the supersymmetrical version of the B-L-SM [57, 58].

3.2.1 The Scanning Apparatus

The numerical data presented in this section was generated via a large chain of nested scripts. These were created as a possible first generation of a scanning framework for generic phenomenological models. This machinery was adapted to the 3HDM numerical scan so this introduction will be glossed over in the 3HDM section, as much remained the same.

The underlying code is a mixture of Linux bash and Python 3 scripts, and utilizes **SPheno** 4.0.3 [59, 60], **SARAH** 4.13.0 [61, 62], **HiggsBounds** 4.3.1 [63], **HiggsSignals** 1.4.0 [64] and **MadGraph5_aMC@NLO** 2.6.2 [65] programs/packages.

These scripts generate a Monte-Carlo type scan through a desired parameter space. Unless introduced, all non-relevant physical constants and parameters are defined in a way as to keep the observed gauge, lepton and quark structure consistent with the SM. Skipping a bit ahead, as an example, for the B-L-SM scan our scanning routine randomly samples parameter space points according to the ranges in Tab. 3.3 while keeping things like Higgs doublet VEV and Weinberg angle to reproduce the correct W and Z structure.

Given the randomness in our scan, we can reach unphysical, or nonsensical regions, that contain objects like tachyonic scalar masses un-renormalizable quantities, divergent radiative corrections etc. These points must be rejected before even considering experimental constraints. This is done by **SPheno**, rejecting any point generated with unphysical parameters.

We could consider this our first layered check. While a second layer of tests include the phenomenological studies we shall perform. This is the region where we confront the surviving scenarios with experimental data. Such as precision measurements from the oblique S, T, U parameters and constraining the Higgs Sector to reproduce the observed signal seen in the LHC in 2012. The latter is made automatically through the package **HiggsBounds** 4.3.1 that shall be used to apply a 95% C.L. exclusion limit cut on a new scalar particle, h_2 , while **HiggsSignals** 1.4.0 is used to calculate and later check, through a χ^2 distribution, the probability for consistency with the observed Higgs boson signal data. To calculate these variables **HiggsBounds** 4.3.1 and **HiggsSignals** 1.4.0 are provided all scalar masses, total decay widths, Higgs decay branching ratios as well as the SM-normalized effective Higgs couplings to fermions and bosons squared (that are needed for analysis of the Higgs boson production cross sections).

After setting a random set of parameters **SPheno** will generate all relevant data for our analysis if possible. **SPheno** is a particle spectrum generator code written in Fortran 90. Its emphasis on easy generalisability and speed made it a natural part of our numerical analysis. It takes information about our models Lagrangian, such as fields, charges and fundamental symmetries, and creates a executable file capable of quickly generating a spectrum file with all details regarding mass, decay and flavour observables information in the standardized SUSY Les-Houches accord format. All generated spectrums are processed and stored. This Lagrangian information is fed to **SPheno** also in standardized format automatically generated by a Mathematica packaged designed for such purposes called **SARAH**.

On a third and final layer of phenomenological tests we have studied the viability of the surviving scenarios from the perspective of direct collider searches for a new Z' gauge boson. We have used, the popular **MadGraph5_aMC@NLO**, to compute the Z' Drell-Yan production cross section and subsequent decay into the first and second-generation leptons, i.e. $\sigma(pp \rightarrow Z') \times B(Z' \rightarrow \ell\ell)$ with $\ell = e, \mu$, and then compare our results to the most recent ATLAS exclusion bounds from the LHC runs at the center-of-mass energy $\sqrt{s} = 13$ TeV [1]. The **SPheno** SLHA output files were used as parameter cards for **MadGraph5_aMC@NLO**, where the information required to calculate $\sigma(pp \rightarrow Z') \times B(Z' \rightarrow \ell\ell)$, such as the Z' boson mass, its total width and decay branching ratios

into lepton pairs, is provided. The lepton anomalous magnetic moments $(g - 2)_\ell / 2 \equiv a_\ell$ are calculated in **SPheno** at one-loop order. In the B-L-SM, NP contributions to a_μ , denoted as Δa_μ^{NP} in what follows, can emerge from the diagrams containing Z' or h_2 propagators. New physics contributions Δa_μ^{NP} to the muon anomalous magnetic moment are given at one-loop order by the Feynman diagrams depicted in Fig. 3.1.

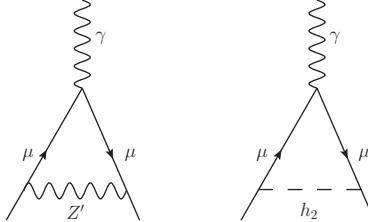


Figure 3.1: One-loop diagrams contributing to Δa_μ^{NP} in the B-L-SM.

3.2.2 Numerical discussion

For the B-L-SM scan our routine randomly samples parameter space points according to the ranges in Tab. 3.3.

λ_1	$\lambda_{2,3}$	$g_{\text{B-L}}$	g_{YB}	x [TeV]
$[10^{-2}, 10^{0.5}]$	$[10^{-8}, 10]$	$[10^{-8}, 10]$	$[10^{-8}, 10]$	$[0.5, 20.5]$

Table 3.3: Parameter scan ranges used in our analysis. Note that the value of λ_1 is mostly constrained by the tree-level Higgs boson mass given in Eq. (3.11).

Electroweak Precision Observables

Typically, the most stringent constraints of the scalar sector emerge from the oblique S, T, U parameters, which are also calculated by **SPheno**. This concept was first introduced by Peskin and T. Takeuchi in Ref [66]. Current precision measurements provide the allowed regions,

$$S = 0.02 \pm 0.10, \quad T = 0.07 \pm 0.12, \quad U = 0.00 \pm 0.09 \quad (3.33)$$

where $S-T$ are 92% correlated, while $S-U$ and $T-U$ are -66% and -86% anti-correlated, respectively. We compare our results with the EW fit in Eq. (3.33) and require consistency with the best fit point within a 95% C.L. ellipsoid (see Ref. [67] for further details about this method). In short we require that the contributions coming from new physics respect the EW precision tests within a 95% C.L. ellipsoid by imposing,

$$\Delta\chi \equiv \sum_{ij} \left(\Delta\mathcal{O}_i^{\text{NP}} - \mathcal{O}_i^{(0)} \right) [(\sigma^2)^{-1}]_{ij} \left(\mathcal{O}_j^{\text{NP}} - \mathcal{O}_j^{(0)} \right) < 7.815 \quad (3.34)$$

Where $\Delta\mathcal{O}_i^{\text{NP}} \equiv \mathcal{O}_i - \mathcal{O}_i^{\text{SM}} \rightarrow (\Delta S, \Delta T, \Delta U)$ being that, $\mathcal{O}_i^{(0)}$ is the deviation generated by the Higgs doublet in the SM if his mass is 125.09. And where the covariance matrix expressed in terms of correlation matrix and started deviations can be seen in,

$$[\sigma^2]^{-1} \equiv \begin{pmatrix} 867.49 & -904.30 & -360.66 \\ -904.30 & 1154.65 & 584.55 \\ -360.66 & 584.55 & 455.19 \end{pmatrix} \quad (3.35)$$

These values are taken from [68].

We show in Fig. 3.2 our results in the ST (left) and TU (right) planes where black points are consistent with EW precision observables at 95% C.L. whereas grey ones lie outside the corresponding ellipsoid of the best fit point and, thus, the first points to be excluded in our analysis.

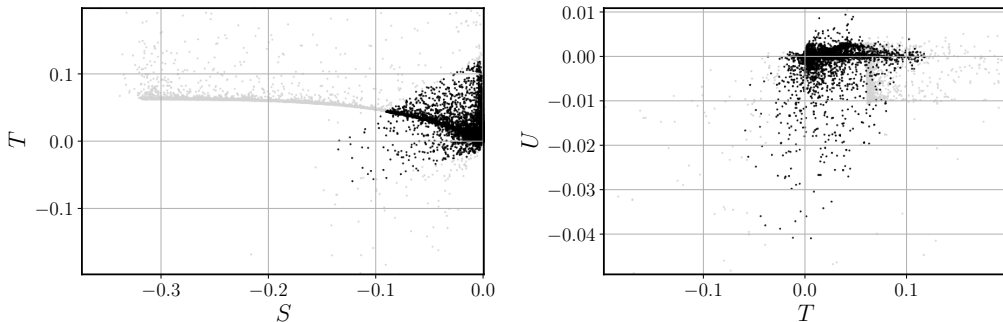


Figure 3.2: B-L-SM scatter plots for EW precision observables showing the ST (left) and TU (right) planes. Accepted points lying within a 95% C.L. ellipsoid of the best fit point are represented in black whereas grey points are excluded.

Higgs Constraints

As stated before, we confront the surviving scenarios, black points in Fig. 3.2, with collider bounds. In particular the 95% Confidence Level (C.L.) exclusion limits on a new scalar particle and check for consistency with the observed Higgs boson at 3σ . These Bounds are checked by `HiggsBounds/HiggsSignals`, which is a set of packages that test the theoretical predictions of our Model from against the exclusion bounds that have been set from Higgs searches at the LHC, LEP and the Tevatron. We have accepted points whose fit to the data replicates the observed signal at 95% C.L. while the measured value for its mass, $m_{h_1} = 125.10 \pm 0.14$ GeV [31]. The information required for this check is the the number of neutral and charged Higgs bosons and the information generated by the `SPheno` output in the format of a SUSY Les Houches Accord (SLHA) [69] file. Specifically, `SPheno` provides scalar masses, total decay widths, Higgs decay branching ratios as well as the SM-normalized effective Higgs couplings to fermions and bosons squared (that are needed for analysis of the Higgs boson production cross sections). For details about this calculation, see Ref. [63].

The basic value calculated by `HiggsSignals` is the signal strength modifier μ_x which parameterizes the signal rate of a particular final state x normalized to the SM expectation through a peak-centered χ^2 statistical method.

The combined implementation of `HiggsBounds/HiggsSignals`, looks at the properties of the discovered Higgs and searches for additional Higgs states, which are then either excluded or allowed in the particle spectra of our model.

Z' Constraints

From here we move onto the third layer of phenomenological tests where we look at the viability of the surviving points from the perspective of direct collider searches for a new Z' gauge boson at the most recent collider experiments. We have used `MadGraph5_aMC@NLO 2.6.2` [65], to compute the Z' Drell-Yan production cross section and subsequent decay into the first and second-generation leptons, i.e. $\sigma(pp \rightarrow Z') \times B(Z' \rightarrow \ell\ell)$ with $\ell = e, \mu$, and then compared our results to the most recent ATLAS exclusion bounds from the LHC runs at the center-of-mass energy $\sqrt{s} = 13$ TeV [1].

The `SPheno` SLHA output files were used as parameter cards for `MadGraph5_aMC@NLO`, where the information required to calculate $\sigma(pp \rightarrow Z') \times B(Z' \rightarrow \ell\ell)$, such as the Z' boson mass, its total width and decay branching ratios into lepton pairs, is provided. Let us now discuss

the phenomenological properties of the B-L-SM model. First, we focus on the current colider constraints and study their impact on both the scalar and gauge sectors.

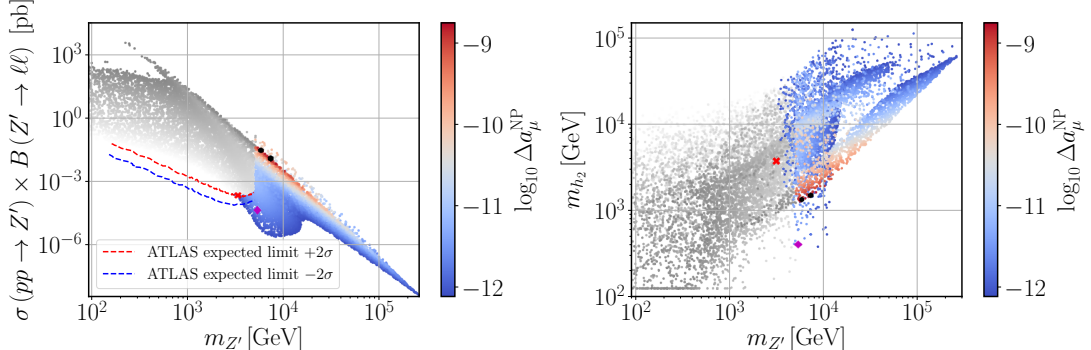


Figure 3.3: Scatter plots showing the Z' Drell-Yan production cross section times the decay branching ratio into a pair of electrons and muons (left panel) and the new scalar mass m_{h_2} (right panel) as functions of $m_{Z'}$ and the NP contributions to the muon Δa_μ anomaly. Coloured points have survived all theoretical and experimental constraints while grey points are excluded by direct Z' searches at the LHC. The region between the two dashed lines represents the current ATLAS expected limit on the production cross section times branching ratio into a pair of leptons at 95% C.L. and is taken from the plot in Fig. 4 of Ref. [1]. The four highlighted points in both panels denote the benchmark scenarios described in detail in Tab. 3.4.

We show in Fig. 3.3 the scenarios generated in our parameter space scan (see Tab. 3.3) that have passed all theoretical constraints such as boundedness from below, unitarity and EW precision tests, and experimental restrictions, such as the compatibility with the SM Higgs data and where a new visible scalar h_2 is unconstrained by the direct collider searches. On the left panel, we show the Z' production cross section times its branching ratio to the first- and second-generation leptons, $\sigma B \equiv \sigma(pp \rightarrow Z') \times B(Z' \rightarrow \ell\ell)$ with $\ell = e, \mu$, as a function of the new vector boson mass and the new physics contribution to the muon anomalous magnetic moment Δa_μ^{NP} (colour scale). On the right panel, we show the new scalar mass as a function of the Z' Mass. All points above the red dashed line are excluded at 95% C.L. by the upper expected limit on Z' direct searches at the LHC by the ATLAS experiment and are represented in grey shades. Darker shades denote *would-be-scenarios* with larger values of Δa_μ^{NP} while the smaller contributions to the muon $(g-2)_\mu/2$ anomaly are represented with the lighter shades. The region between the two dashed lines corresponds to the Z' ATLAS limit with a 2σ uncertainty represented by the yellow band in Fig. 4 of [1]. Provided that the observed limit by the ATLAS detector lies within this region we have taken a conservative approach and accepted all points whose σB value lies below the red dashed line (upper limit) in Fig. 3.3. The blue dashed line, which corresponds to the stricter 2σ lower bound, is only shown for completeness of information. The red cross in our figures signals the lightest Z' found in our scan which we regard as a possible early-discovery (or early-exclusion) benchmark point in the forthcoming LHC runs. Such a benchmark point is shown in the first line of Tab. 3.4. On the right panel, we notice that the new scalar bosons can become as light as 380 – 400 GeV, but with Z' masses in the range of 5 – 9 TeV. We highlight with a magenta diamond the benchmark point with the lightest Z' boson within this range. This point is shown in the second line of Tab. 3.4.

$m_{Z'}$	m_{h_2}	x	$\log_{10} \Delta a_\mu^{\text{NP}}$	σB	θ'_W	α_h	$g_{\text{B-L}} \simeq g^{\ell\ell Z'}$
3.13	3.72	15.7	-12.1	2.22×10^{-4}	≈ 0	5.67×10^{-5}	0.0976
5.37	0.396	9.10	-11.7	4.23×10^{-5}	2.55×10^{-7}	9.44×10^{-7}	0.302
7.35	1.49	0.321	-8.75	0.0115	1.83×10^{-7}	1.20×10^{-6}	3.15
5.91	1.32	0.335	-8.78	0.0285	1.30×10^{-4}	1.04×10^{-5}	2.94

Table 3.4: A selection of four benchmark points represented in Figs. 3.3, 3.4 to 3.6. The $m_{Z'}$, m_{h_2} and x parameters are given in TeV. The first line represents a point with light h_2 while the second line shows the lightest allowed Z' boson found in our scan. The last two lines show two points that reproduce the observed value of the muon ($g - 2$) within 1σ uncertainty.

Implications of direct Z' searches at the LHC for the $(g - 2)_\mu$ anomaly

Looking again to Fig. 3.3 (left panel), we see that there is a thin dark-red stripe where Δa_μ^{NP} explains the observed anomaly shown in Eq. (3.32) for a range of $m_{Z'}$ boson masses approximately between 5 TeV and 20 TeV. This region is particularly interesting as it can be partially probed by the forthcoming LHC runs or at future colliders. If a Z' boson discovery remains elusive for such a mass range, it can exclude a possibility of explaining the muon $(g - 2)_\mu$ anomaly in the context of the B-L-SM. It is also worth noticing that such preferred Δa_μ^{NP} values represent a small island in the right plot of Fig. 3.3 where the new scalar boson mass is restricted to the range of $1 \text{ TeV} < m_{h_2} < 4 \text{ TeV}$.

Since the couplings of a new scalar h_2 to the SM fermions are suppressed by a factor of $\sin \alpha_h$, which we find to be always smaller than 0.08 as can be seen in the bottom panel of Fig. 3.4, the right diagram in Fig. 3.1, which scales as $\Delta a_\mu^{h_2} \propto m_\mu^2/m_{h_2}^2 (y_\mu \sin \alpha_h)^2$ with $\sin^2 \alpha_h < 0.0064$ and $y_\mu = Y_e^{22}$, providing sub-leading contributions to Δa_μ . Furthermore, as we show in the top-left panel of Fig. 3.4 the new scalar boson mass, which we have found to satisfy $m_{h_2} \gtrsim 380 \text{ GeV}$, is not light enough to compensate the smallness of the scalar mixing angle. Conversely, the new Z' boson can have sizeable couplings to fermions via gauge interactions proportional to $g_{\text{B-L}}$. Therefore, the left diagram in Fig. 3.1 provides the leading contribution to the $(g - 2)_\mu$ in the model under consideration. In particular, $\Delta a_\mu^{Z'}$ is given by [70]

$$\Delta a_\mu^{Z'} = \frac{1}{12\pi^2} \frac{m_\mu^2}{m_{Z'}^2} \left(3g_L^{\mu\mu Z'} g_R^{\mu\mu Z'} - g_L^{\mu\mu Z'}{}^2 - g_R^{\mu\mu Z'}{}^2 \right) \quad (3.36)$$

where the left- and right-chiral projections of the charged lepton couplings to the Z' boson, $g_L^{\ell\ell Z'}$ and $g_R^{\ell\ell Z'}$, respectively, can be approximated as follows

$$\begin{aligned} g_L^{\ell\ell Z'} &\simeq g_{\text{B-L}} + \frac{1}{32} \left(\frac{v}{x} \right)^2 \frac{g_{\text{YB}}}{g_{\text{B-L}}} [g_Y^2 - g^2 + 2g_Y g_{\text{YB}}] , \\ g_R^{\ell\ell Z'} &\simeq g_{\text{B-L}} + \frac{1}{16} \left(\frac{v}{x} \right)^2 \frac{g_{\text{YB}}}{g_{\text{B-L}}} [g_Y^2 + g_Y g_{\text{YB}}] , \end{aligned} \quad (3.37)$$

to second order in v/x -expansion. If $v/x \ll 1$, corresponding to the darker shades of the color scale in the top-right panel of Fig. 3.4, we can further approximate

$$g_L^{\ell\ell Z'} \simeq g_R^{\ell\ell Z'} \simeq g_{\text{B-L}} , \quad (3.38)$$

such that the muon anomalous magnetic moment gets significantly simplified to

$$\Delta a_\mu^{Z'} \simeq \frac{g_{\text{B-L}}^2}{12\pi^2} \frac{m_\mu^2}{m_{Z'}^2} . \quad (3.39)$$

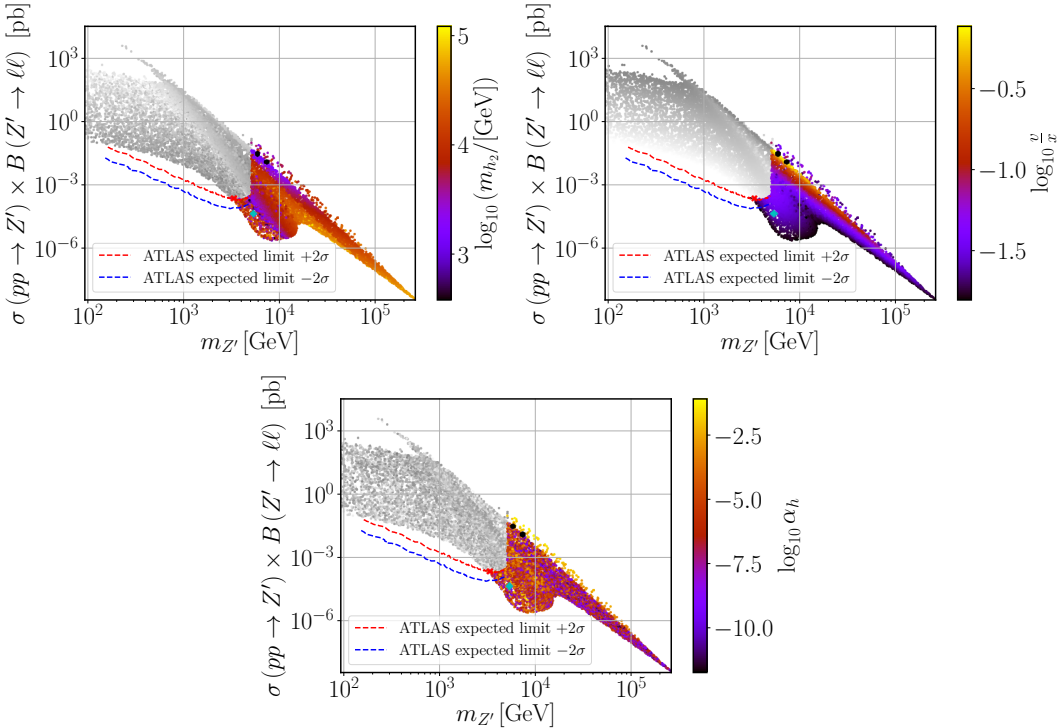


Figure 3.4: Scatter plots showing the Z' Drell-Yan production cross section times the decay branching ratio into a pair of electrons and muons in terms of the $m_{Z'}$ boson mass. The colour gradation represents the new scalar mass (top-left), the ratio between the EW- and $U(1)_{B-L}$ -breaking VEVs (top-right) and the scalar mixing angle (bottom). The grey points are excluded by direct Z' searches at the LHC. The four benchmark points in Tab. 3.4 are represented by the black dots (last two rows), cyan diamond (first row) and red cross (second row).

Similarly, for the yellow band in the bottom of Fig. 3.5, which corresponds to the region where Δa_μ^{NP} is maximized (see top-left panel of Fig. 3.3), a large value of the $U(1)_{B-L}$ gauge coupling also allows one to simplify Eq. (3.36) reducing it to the form of Eq. (3.39). This is in fact what we have observed and, for the yellow band region, we see in the bottom panel of Fig. 3.5 that $g_{B-L} \simeq 3$. A sizeable value of g_{B-L} is indeed what is contributing to the enhancement of Δa_μ^{NP} , in particular, for the red region in both panels of Fig. 3.3. We show in the third and fourth lines of Tab. 3.4 the two benchmark points that better reproduce the muon anomalous magnetic moment represented by two black dots in Figs. 3.3, 3.4 to 3.6.

In fact, a close inspection of Fig. 3.3 (left panel) and Fig. 3.4 (top-right panel) reveals an almost one-to-one correspondence between the colour shades. This suggests that $\Delta a_\mu^{Z'}$ must somehow be related to the VEV ratio v/x . To understand this behaviour, let us also look to Fig. 3.5 (top-left panel) where we see that the kinetic-mixing gauge coupling g_{YB} is typically very small apart from two green bands where it can become of order $\mathcal{O}(1)$. Interestingly, whenever g_{YB} becomes sizeable, $v/x \ll 1$ is realised, which means that Eq. (3.25) is indeed a good approximation as was argued above. It is then possible to eliminate g_{B-L} from Eq. (3.39) and rewrite it as

$$\Delta a_\mu^{Z'} \simeq \frac{y_\mu^2}{96\pi^2} \left(\frac{v}{x}\right)^2, \quad (3.40)$$

which explains the observed correlation between both Fig. 3.3 (left panel) and Fig. 3.4 (top-right panel) and, for instance, the thin red stripe of points is compatible with a full description of the muon $(g-2)_\mu/2$ anomaly. Note that this simple and illuminating relation becomes valid as a consequence of the heavy Z' mass regime, in combination with the smallness of the θ'_W mixing

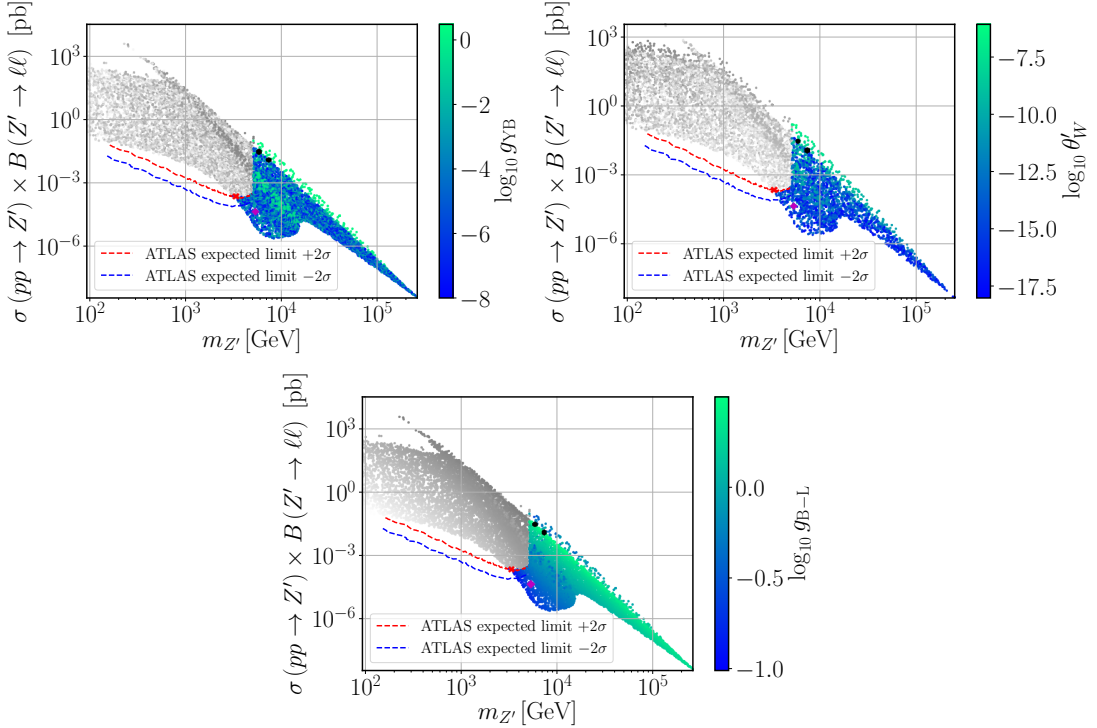


Figure 3.5: The same as in Fig. 3.4 but with the colour scale representing the gauge-mixing parameters g_{YB} (top-left), θ'_W (top-right), and the $U(1)_{B-L}$ gauge coupling (bottom).

angle required by LEP constraints. Indeed, while we have not imposed any strong restriction on the input parameters of our scan (see Tab. 3.3), Eq. (3.21) necessarily implies that both g_{YB} and v/x cannot be simultaneously sizeable in agreement with what is seen in Fig. 3.5 (top-left panel) and Fig. 3.4 (top-right panel). The values of θ'_W obtained in our scan are shown in the top-right panel of Fig. 3.5.

For completeness, we show in Fig. 3.6 the physical couplings of Z' to muons (top panels) and to W^\pm bosons (bottom panel). Note that, for the considered scenarios, the latter can be written as

$$g^{WWZ'} \simeq \frac{1}{16} \frac{g_{YB}}{g_{B-L}} \left(\frac{v}{x}\right)^2. \quad (3.41)$$

While both g_{B-L} and the ratio v/x provide a smooth continuous contribution in the $\sigma B - m_{Z'}$ projection of the parameter space, the observed blurry region in $g^{WWZ'}$ is correlated with the one in the top-left panel of Fig. 3.5 as expected from Eq. (3.41). On the other hand, the couplings to leptons $g_{L,R}^{\ell\ell Z'}$ exhibit a strong correlation with g_{B-L} in Fig. 3.5, in agreement with our discussion above and with Eq. (3.38).

Barr-Zee type contributions

To conclude our analysis, one should note that the two-loop Barr-Zee type diagrams [71] are always sub-dominant in our case. To see this, let us consider the four diagrams shown in Fig. 3.7. The same reason that suppresses the one-loop h_2 contribution in Fig. 3.1 is also responsible for the suppression of both the top-right and bottom-right diagrams in Fig. 3.7 (for details see e.g. Ref. [72]). Recall that the coupling of h_2 to the SM particles is proportional to the scalar mixing angle α_h , which is always small (or very small) as we can see in Fig. 3.4. An analogous effect is present in the diagram involving a W -loop, where a vertex proportional to $g^{WWZ'}$ suppresses such a contribution. The only diagram that might play a sizeable role is the top-left one where

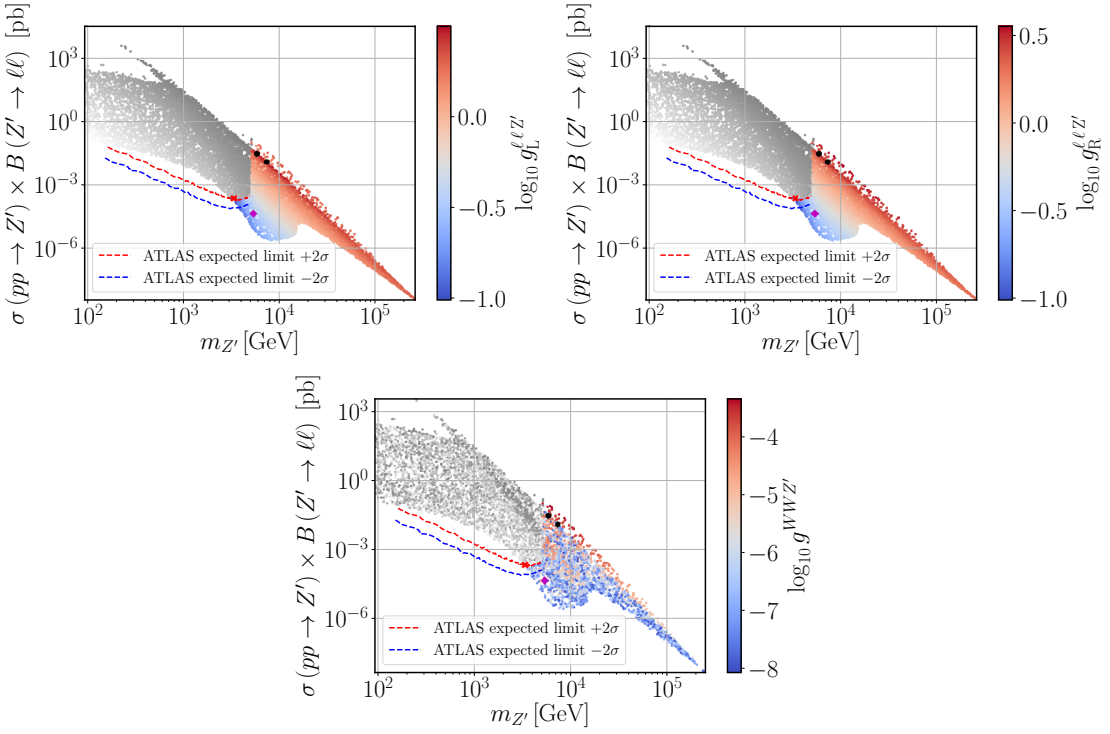


Figure 3.6: The same as in Fig. 3.4 but with the colour scale representing the coupling of leptons to the Z' (top panels) and the coupling of W bosons to Z' .

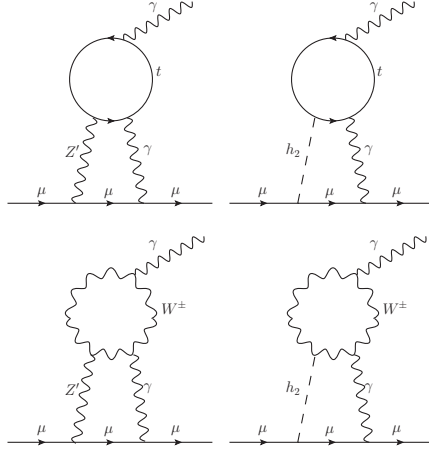


Figure 3.7: Barr-Zee type two-loop diagrams contributing to Δa_μ .

the couplings of Z' to both muons and top quarks are not negligible.

Let us then estimate the size of the first diagram in Fig. 3.7. This type of diagrams were already calculated in Ref. [73] but for the case of a SM Z -boson. Since the same topology holds for the considered case of B-L-SM too, if we trade Z by the new Z' boson, the contribution to the muon $(g-2)_\mu$ anomaly can be rewritten as

$$\Delta a_\mu^{\gamma Z'} = -\frac{g^2 g_{B-L}^2 m_\mu^2 \tan^2 \theta_W}{1536 \pi^4} \left(g_L^{ttZ'} - g_R^{ttZ'} \right) T_7(m_{Z'}^2, m_t^2, m_t^2), \quad (3.42)$$

where T_7 is a loop integral. The parameters $g_{\text{L,R}}^{ttZ'}$, calculated in **SARAH**, are the left- and right-chirality projections of the Z' coupling to top-quarks, given by

$$\begin{aligned} g_{\text{L}}^{ttZ'} &= -\frac{g_{\text{B-L}}}{3} \cos \theta'_W + \frac{g}{2} \cos \theta_W \sin \theta'_W - \frac{g_Y}{6} \sin \theta_W \sin \theta'_W - \frac{g_{\text{YB}}}{3} \sin \theta_W \sin \theta'_W, \\ g_{\text{R}}^{ttZ'} &= -\frac{g_{\text{B-L}}}{3} \cos \theta'_W - \frac{2g_Y}{3} \sin \theta_W \sin \theta'_W - \frac{g_{\text{YB}}}{3} \sin \theta_W \sin \theta'_W. \end{aligned} \quad (3.43)$$

The loop integral $T_7(m_{Z'}^2, m_t^2, m_t^2)$ was determined in Ref. [73] and, in the limit $m_{Z'} \gg m_t$, it can be shown to be simplifiable to,

$$T_7(m_{Z'}^2, m_t^2, m_t^2) \simeq \frac{2}{m_{Z'}^2}, \quad (3.44)$$

up to a small truncation error. For the parameter space region under consideration the difference $g_{\text{L}}^{ttZ'} - g_{\text{R}}^{ttZ'}$ can be cast in a simplified form as follows

$$(g_{\text{L}}^{ttZ'} - g_{\text{R}}^{ttZ'}) \simeq \frac{(g^2 + g_Y^2) g_{\text{YB}}}{32 g_{\text{B-L}}} \left(\frac{v}{x}\right)^2. \quad (3.45)$$

Using this result and the approximate value of the loop factor, we can calculate the ratio between the two- and one-loop contributions to the muon $(g-2)_\mu$,

$$\frac{\Delta a_\mu^{\gamma Z'}}{\Delta a_\mu^{Z'}} \simeq -\frac{g^2 g_{\text{YB}}}{2048 \pi^2} \frac{g_{\text{YB}}}{g_{\text{B-L}}} \left(\frac{v}{x}\right)^2 \ll 1, \quad (3.46)$$

which shows that $\Delta a_\mu^{\gamma Z'}$ does indeed play a subdominant role in our analysis and can be safely neglected.

Chapter 4

3HDM Model

Having concluded our discussion of the B-L-SM we can move onward to more complex model. This chapter will introduce all the required theoretical background to the analysis of a three Higgs Doublet Model (3HDM), specifically a minimal BGL (Branco-Grimus-Lavoura) like 3HDM, such as presented in Refs. [74, 75] with a stabilizing flavour symmetry. Specifically this model contains the addition of a $U(1) \times Z_2$ flavour symmetry. The theoretical background will include a discussion on the inversion process included in our simulations. Note that the basis for a BGL like treatment of the 3HDM will be the inclusion of this flavour symmetry, as to attempt to constrain the otherwise dangerous tree-level flavour violating decays that as mentioned in Chapter 2 surge in these kind of frameworks.

Once properly introduced we continue to present phenomenological conclusions from a performed simulation in a similar fashion as before. This simulation used a newer version of the previously discussed code containing the addition of a flavour calculation process based on `python3` package entitled `flavio` [76] and the inclusion of the Higgs alignment limit as to improve the scanning apparatus capabilities and ensure proper gauge couplings to a SM-like Higgs boson. This Higgs alignment process consists in forcing a CP-even eigenstate to serve as the observed Higgs Boson and give it precisely 125.09 GeV mass. We are able to perform the Higgs alignment through the aforementioned inversion process of the scalar potential. This inversion process consists in translating all Lagrangian terms in the gauge basis into physical parameters.

Note, a key change from the B-L-SM case is that the respective masses will all be calculated at tree-level instead of at 2-loop level. This is done for multiple reasons most of which reflect computational shortcomings and time constraints. Note that radiative processes are still calculated correctly just using tree-level masses, e.g. the value of $(g - 2)_\mu$ is still calculated by SPheno but for a tree-level set of masses.

Note a feature of these additional Higgs doublets is that they do not alter the tree-level EW ρ parameter. Although, this value can vary by around 20% from its SM prediction leaving some room for somewhat more exotically manufactured models.

Our results show that light scalars are still within the reach of future collider experiments in our models framework while having FCNCs concurrent with observations and respecting many more theoretical and experimental bounds, such as in our previous analysis.

Given these conclusions we also performed a additional simulation after all data was collected, the goal of which was to check if accidental fine-tuning was present in our results due to a random synchronicity. To do this we varied all the soft breaking terms for the collected data by 1% of their original value disregarding the effects this will have for the alignment of the Higgs. In the validated parameter space by all other constraints we found no significant sensitivity to mass variation. Furthermore for completeness we also implemented a `MadGraph5_aMC@NLO 2.6.2` routine as to probe future detection of these light scalars in newer collider experiments and discovered there is

still regions that are far from discovery.

4.1 The Case of the BGL-2HDM and its Relation to our Work

Any 3HDM can be thought as part of a larger family of multiple Higgs Doublet Models, or NHDMs, the first iteration of which was the Two Higgs Doublet Model (2HDM) proposed by T.D. Lee [77]. At the time, Lee was motivated by the search for a spontaneous breaking of the CP symmetry which was included in his model. As the name indicates, in these types of models in parallel with the standard SM Higgs doublet some additional replicas of that same doublet (or slightly modified) are introduced. In the NHDM these form a sort of family in the scalar sector in analogy to the fermion sector. In which the 3HDM boasts to be the most similar given its number of elements. This idea is far from original and was first discussed first by Weinberg in, [78].

However, it was the 2HDM that quickly became a very popular model after its proposal. Thus a great deal of interest was invested in 2HDMs over the years, given the possibility for dark matter candidates, as well as providing a large particle spectrum, including charged and additional neutral scalars who enable FCNC deviations. With this work we try to challenge the popular 2HDM BGL hegemony. This endeavour is justified through phenomenological comparison of the 3HDM to the 2HDM model rather than the "naturalist" family argument proposed by Weinberg. For example, vacuum stability in the 2HDM model can only accommodate one instance of spontaneous CP or charge symmetry breaking [79, 80, 81]. However in NHDMs, such as the 3HDM, charge breaking minima were found to be stable while at the same time coexisting with charge-preserving ones, for more information see, [82]. Also, for the 2HDM a full list of all possible incorporations of symmetries consistent with $SU(2) \times U(1)$ has been achieved [83, 84], while for the 3HDM no work has thus far been completed, see, [85, 86]. Further motivating generic unitarity constraints have been found for the 2HDM [87] but not for 3HDMs. Not to mention these models provide a richer playground for experimental detection and testing than the 2HDM given its extended scalar sector.

As noted, most 2HDM structures often allow for the possibility of tree-level scalar mediated FCNCs. These tree-level FCNCs are, in most cases, in direct opposition to experimental results, as discussed in chapter 2, section 2.3. In fact, consulting the literature, as in, [88], we see that this forces the extra scalars in the minimal 2HDM case to have masses above 1 TeV as to suppress these FCNCs. These heavy scalars are far from ideal, since there is no indication such heavy scalars exist nor do they provide us with interesting physics. Therefore several mechanisms have been proposed to deal with suppression of these tree-level FCNCs as to allow for richer physics and lighter scalars.

First, in, [89, 90, 91], it is proposed a framework in which we have the balancing of CP-odd and CP-even contribution to FCNCs, however, this requires some fine-tuning, making it very unappealing based on a "naturalist" argument. Another possibility is to assume alignment between different Yukawa matrices such that no FCNCs are present, see [92, 93, 94] for more information. Finally we could also use the approach presented in the BGL version of the 2HDM [95, 96], here the authors impose a flavour-violating symmetry naturally keeping the FCNCs under control through the CKM matrix. The phenomenology of the model has been studied quite thoroughly in previous works, see Refs. [97, 98], and it remains a possible scenario for BSM physics. This approach offers a better motivation to the lack of FCNCs than the SM by virtue being processes that are forbidden under this symmetry.

Inspired by this BGL model our studies will try to reproduce a similar mechanism on a 3HDM Model. And in fact similar studies have been done in 3HDMs that include different flavour symmetries, such as Ref. [99].

Given this background it is no surprise that we will focus in particular in the measuring Quark Flavour Violation (QFV) observables. In our analysis these will consist of meson decays or oscillations that include the changing of quark flavour within the meson. These QFV observables will be compared to measured amplitudes in collider experiments as to offer a novel exclusion to

our model.

Note, the additional flavour symmetry constrains the terms that can appear in the Yukawa sector of the Lagrangian resulting in very specific structures (or textures) of the Yukawa couplings. These shapes generate a suppression mechanism through the CKM matrix off-diagonal terms restricting the values of FCNCs in our model.

4.2 The formulation of a BGL-like 3HDM

In a sense this model is an extension of the SM as it still includes all the same fields with same charges under the \mathcal{G}_{SM} as we saw in chapter 2. Making the field content of the model the same as the SM with the addition of new scalars, therefore all fields are seen in,

$$Q_{L_i} = \begin{pmatrix} u_{L_i} \\ d_{L_i} \end{pmatrix}, \quad \Psi_{L_i} = \begin{pmatrix} \nu_{L_i} \\ e_{L_i} \end{pmatrix},$$

$$p_R, \quad n_R, \quad e_{R_i} \quad i = \{1, 2, 3\},$$

$$\phi_k = \begin{pmatrix} W_k^\pm + i W_k^\mp \\ \frac{1}{\sqrt{2}}(v_k + h_k + i Z_k) \end{pmatrix}, \quad k = \{1, 2, 3\}.$$
(4.1)

where Q_{L_i} , ϕ_k and Ψ_{L_i} are $SU(2)_L$ doublets while, p and n (these are analogous to u_{R_i} , d_{R_i} in the SM respectively), and e_{R_i} are $SU(2)_L$ singlets where the i and k generation stand for their respective generation indexes. Where the new charges under $U(1) \times \mathbb{Z}_2$ can be seen in the transformations that these fields undergo,

U(1) :	\mathbb{Z}_2 :
$Q_{L_3} \rightarrow e^{i\alpha} Q_{L_3}$	$Q_{L_3} \rightarrow -Q_{L_3}$
$p_{R_3} \rightarrow e^{2i\alpha} p_{R_3}$	$p_{R_3} \rightarrow -p_{R_3}$
$\phi_1 \rightarrow e^{i\alpha} \phi_1$	$\phi_1 \rightarrow -\phi_1$
$\Psi_{L_1} \rightarrow e^{i\alpha} \Psi_{L_1}$	$\Psi_{L_1} \rightarrow -\Psi_{L_1}$
$\phi_3 \rightarrow e^{i\alpha} \phi_3$	$\phi_3 \rightarrow -\phi_3$

(4.2)

All remaining fields not shown in Eq. 4.2 remain unchanged under transformations of the $U(1) \times \mathbb{Z}_2$ global symmetry i.e. are not charged under these symmetries. Note there is no right handed neutrino fields in this model making it so that no neutrino mass terms appear.

4.2.1 The Scalar Sector

Let us then start our proper introduction to the workings of the model by presenting the scalar sector where the new spin-0 $SU(2)$ doublets, ϕ_k , $k = \{1, 2, 3\}$ reside. Note the scalar potential is \mathcal{CP} -invariant, this means,

$$\phi_1 = \phi_1^*, \quad \phi_2 = \phi_2^*, \quad \phi_3 = \phi_3^*$$
(4.3)

The generic scalar potential is extensively written in,

$$V(\phi_i) = -\mu_1^2 (\phi_1^\dagger \phi_1) - \mu_2^2 (\phi_2^\dagger \phi_2) - \mu_3^2 (\phi_3^\dagger \phi_3)$$

$$- \mu_{21}^2 (\phi_2^\dagger \phi_1) - \mu_{23}^2 (\phi_2^\dagger \phi_3) - \mu_{13}^2 (\phi_1^\dagger \phi_3) + \text{H.c.}$$

$$+ \lambda_1 (\phi_1^\dagger \phi_1) + \lambda_2 (\phi_2^\dagger \phi_2) + \lambda_3 (\phi_3^\dagger \phi_3)$$

$$+ \lambda_4 (\phi_1^\dagger \phi_1) (\phi_2^\dagger \phi_2) + \lambda_5 (\phi_1^\dagger \phi_1) (\phi_3^\dagger \phi_3) + \lambda_6 (\phi_2^\dagger \phi_2) (\phi_3^\dagger \phi_3)$$

$$+ \lambda_7 (\phi_1^\dagger \phi_2) (\phi_1^\dagger \phi_2) + \lambda_8 (\phi_1^\dagger \phi_3) (\phi_3^\dagger \phi_1) + \lambda_9 (\phi_2^\dagger \phi_3) (\phi_3^\dagger \phi_2)$$

$$+ \lambda_{10} \left\{ (\phi_1^\dagger \phi_3)^2 + \text{H.c.} \right\}$$
(4.4)

Due to the \mathcal{CP} symmetry imposed on this potential all parameters, $(\lambda_i, i = \{1, \dots, 10\})$ and soft-breaking terms, here are real. The most generic version of this soft breaking is given by the second line, where the soft-breaking terms μ_{23}^2 , μ_{13}^2 and μ_{21}^2 are seen. The parameter μ_{23}^2 , is necessarily added as to impede the formation of a massless axion and is the only term that respect the \mathbb{Z}_2 symmetry while the others explicitly break it. Note the U(1) portion is broken explicitly by all these terms.

After the process of SBB, all Higgs doublets, ϕ_k , take a VEV shape similar to that of the SM Higgs, written as,

$$\phi_k = \begin{pmatrix} W_k^\pm + iW_k^\mp \\ \frac{1}{\sqrt{2}}(v_k + h_k + iZ_k) \end{pmatrix} \rightarrow \langle \phi_k \rangle = \begin{pmatrix} 0 \\ \frac{v_k}{\sqrt{2}} \end{pmatrix}, \quad k = \{1, 2, 3\} \quad (4.5)$$

Here we see the charged portion of the field, W_k^\pm , the CP-odd portion, Z_k , and finally the CP-even, h_k .

Recall that, for the given scalar potential V as seen in Eq. (4.4) to have a stable vacuum it needs to satisfy the tadpole equations i.e. a unchanging potential ensuring that there is a absolute minimum of energy. To solve these one must write the derivatives of the potential with respect to the fields and then observe their values once the process of SBB occurs, this process yields the following equations,

$$\begin{aligned} \frac{\partial V}{\partial \phi_1} &= \frac{1}{2}v_1(-2\mu_1^2 + (\lambda_4 + \lambda_7)v_1^2 + (\lambda_5 + \lambda_8 + 2\lambda_{10})v_7^2) + \lambda_1v_1^3 - \mu_{13}^2v_3 - \mu_{21}^2v_2 \\ \frac{\partial V}{\partial \phi_2} &= \frac{1}{2}v_2^2(-2\mu_2^2 + (\lambda_6 + \lambda_9)v_3^2 + (\lambda_4 + \lambda_7)v_1) + \lambda_2v_2^3 - \mu_{21}^2v_1 - \mu_{23}^2v_3 \\ \frac{\partial V}{\partial \phi_3} &= \frac{1}{2}(2\lambda_3v_3^3 + (\lambda_6 + \lambda_9)v_2^2v_3 + (\lambda_5 + \lambda_8 + 2\lambda_{10})v_1^2v_3 - 2\mu_3^2v_3 - 2\mu_{13}^2v_1 - 2\mu_{23}^2v_2) \end{aligned} \quad (4.6)$$

The Higgs Basis

It is convenient for the remainder of our study to now introduce the basis changing matrix to what we will call the Higgs Basis. In our analysis of the 3HDM we did not perform the conventional direct diagonalisation of the scalar and Yukawa bi-linear terms expressed in the scalar potential (Eq. (4.4)) expanded around the vacuum state. Instead we use a intermediate basis in between the process of expressing the mass eigenstates as to significantly simplifies the analysis of the scalar, pseudoscalar, charged scalar and quark physical terms e.g this base change will allow us to express the charge and pseudoscalar states in such a way as to become apparent that a Goldstone emerges in each case. These Goldstones will account for the longitudinal polarization of W and Z bosons.

The transformation from the gauge to the Higgs basis reads,

$$\mathcal{O} = \begin{pmatrix} \frac{v}{v_1} & \frac{v}{v_2} & \frac{v}{v_3} \\ \frac{v_3}{v_{13}} & 0 & \frac{-v_1}{v_{13}} \\ \frac{v_2v_1}{vv_{13}} & \frac{v_{13}}{v} & \frac{v_2v_3}{vv_{13}} \end{pmatrix} \quad (4.7)$$

where $v_{13} = \sqrt{v_1^2 + v_3^2}$. This basis transformation explicitly relate the fields in the following manner,

$$\begin{pmatrix} \phi_1 \\ \phi_2 \\ \phi_3 \end{pmatrix} = \mathcal{O} \begin{pmatrix} h' \\ H'_1 \\ H'_2 \end{pmatrix}, \quad \begin{pmatrix} Z_1 \\ Z_2 \\ Z_3 \end{pmatrix} = \mathcal{O} \begin{pmatrix} z \\ A'_1 \\ A'_2 \end{pmatrix}, \quad \begin{pmatrix} W_1^\pm \\ W_2^\pm \\ W_3^\pm \end{pmatrix} = \mathcal{O} \begin{pmatrix} \omega^\pm \\ H_1^{\pm'} \\ H_2^{\pm'} \end{pmatrix} \quad (4.8)$$

Without accounting for the quark fields. It is convenient to further parameterize the choice of VEVs trough mixing angles and its fixed total magnitude, $v = \sqrt{v_1^2 + v_2^2 + v_3^2}$,

$$v_1 = v \cos(\psi_1) \cos(\psi_2), \quad v_2 = v \sin(\psi_1) \cos(\psi_2), \quad v_3 = v \sin(\psi_2) \quad (4.9)$$

where the two mixing angles ψ_1 and ψ_2 . Through this parameterization we can re-write the orthogonal mixing matrix,

$$\mathcal{O} = \begin{pmatrix} \cos(\psi_1) \cos(\psi_2) & \cos(\psi_2) \sin(\psi_1) & \sin(\psi_2) \\ -\sin(\psi_1) & \cos(\psi_1) & 0 \\ -\cos(\psi_1) \sin(\psi_2) & \sin(\psi_1) \sin(\psi_2) & \cos(\psi_2) \end{pmatrix} \quad (4.10)$$

4.2.2 The Gauge Sector

Before beginning our study of the inversion process of the scalar sector it is prudent to first consider and discuss the remaining portions of the 3HDM Lagrangian. We begin this by present first the Gauge sector. Note, after the Higgs Doublets shift to their VEVs we have the following mass terms,

$$\mathcal{L}_{\text{gauge}} \supset \frac{1}{4} (v_1^2 + v_2^2 + v_3^2) g^2 W_\mu^+ W^{-\mu} + \frac{1}{8} (v_1^2 + v_2^2 + v_3^2) (g'^2 + g^2) Z_\mu Z^\mu \quad (4.11)$$

We can clearly see that to reproduce the correct gauge boson masses we must ensure that,

$$\sum_{k=1}^3 v_k^2 \approx 246^2 (\text{GeV})^2 . \quad (4.12)$$

This is a very important condition as it will reflect what range of values that are available for our Higgs Doublets to take.

Recall that additional gauge couplings to the Higgs bosons have also been precisely measured meaning the only way to achieve the correct Higgs kinetic constraints and weak interactions is to have h state that corresponds to the observed Higgs state with the measured 125.09 GeV mass. This is why we impose the previously mentioned Higgs alignment limit as otherwise different tree-level couplings to the gauge bosons would show themselves. This is explicitly demonstrated in Ref. [100].

This alignment then consists in a particular configuration of the 3HDM parameter space making so that one of the Higgs states in the gauge basis completely overlaps with a physical state i.e completely aligned with the CP-even physical Higgs boson (h).

In the 3HDM this alignment is also conveniently used to reproduce the same SM-like Leptonic Yukawa sector, as couplings and structure remain the same given the leptons couple exclusively to this SM-like Higgs. This means the 3HDM is lepton flavour universal just like the SM.

Note that strict alignment is not manifestly required by the data and in fact there are ways we could deviate as much as $\mathcal{O}(10\%)$ (see Ref. [101]) from the SM predicted gauge coupling value through light mixing.

This means we are ignoring some of the parameter space by imposing precise Higgs Alignment. However given our random methodology allowing for mixing would decrease by several orders of magnitude our scans efficiency. Given time investment, a future version of the presented algorithm (possibly made "smarter" through new techniques applied in the field such as machine learning) could efficiently observe and constrict EW effects coming from a more complex mixture of scalars and find more viable regions of the parameter space.

4.2.3 The Yukawa sector

Now having dealt with the scalar and gauge sector we can continue to study the Yukawa sector. The Yukawa portion of the Lagrangian is seen in,

$$\begin{aligned} \mathcal{L}_Y = & - \sum_{k=1}^3 \left[\bar{Q}_{L_a} (\Gamma_k)_{ab} \sigma_k n_{R_b} + \bar{Q}_{L_a} (\Delta_k)_{ab} \tilde{\phi}_k p_{R_b} + \text{H.c.} \right] \\ & + (\Psi_{L_a} (Y_1^e)_{ab} \phi_1 e_{R_b} + \text{H.c.}) \end{aligned} \quad (4.13)$$

Here we see the quark and lepton interactions, note that Γ_k and Δ_k are the down and up Yukawa matrices in the 3HDM model respectively, one for each, k , generation. Notice how the leptons couple only to the first generation Higgs Doublet. This translates into the lepton Yukawa matrix being diagonal as in the SM, allowing leptons to couple exclusively to the lightest doublet, ϕ_1 and preserving lepton flavour universality,

$$Y_1^e = \frac{\sqrt{2}}{v_1} M_{\text{diag.}}(m_e, m_\mu, m_\tau) \quad (4.14)$$

Note that there are no neutrino right handed fields, just like in the SM in Eq. 4.13. Furthermore, examining the effects the imposed symmetry, $U(1) \times \mathbb{Z}_2$, had on the shape of the Yukawa matrices leads us to discover their texture.

$$\begin{aligned} \Gamma_1 &= \begin{pmatrix} 0 & 0 & 0 \\ 0 & 0 & 0 \\ \times & \times & 0 \end{pmatrix}, & \Gamma_2 &= \begin{pmatrix} \times & \times & 0 \\ \times & \times & 0 \\ 0 & 0 & 0 \end{pmatrix}, & \Gamma_3 &= \begin{pmatrix} 0 & 0 & 0 \\ 0 & 0 & 0 \\ 0 & 0 & \times \end{pmatrix}, \\ \Delta_1 &= \begin{pmatrix} 0 & 0 & 0 \\ 0 & 0 & 0 \\ 0 & 0 & 0 \end{pmatrix}, & \Delta_2 &= \begin{pmatrix} \times & \times & 0 \\ \times & \times & 0 \\ 0 & 0 & 0 \end{pmatrix}, & \Delta_3 &= \begin{pmatrix} 0 & 0 & 0 \\ 0 & 0 & 0 \\ 0 & 0 & \times \end{pmatrix}. \end{aligned} \quad (4.15)$$

Note, here the \times represent a complex non-zero value in the respective matrix. We can immediately see the treatment of the first generation of quarks differ between bottom and up types. These textures of the Yukawa matrices and the size of their components will determine the strength of FCNCs at tree and loop-levels. The quadratic terms that spawn in the Lagrangian after SBB have the following relations to the Yukawa matrices,

$$\begin{aligned} M_n &= \frac{v_1}{\sqrt{2}} \Gamma_1 + \frac{v_2}{\sqrt{2}} \Gamma_2 + \frac{v_3}{\sqrt{2}} \Gamma_3 , \\ M_p &= \frac{v_1}{\sqrt{2}} \Delta_1 + \frac{v_2}{\sqrt{2}} \Delta_2 + \frac{v_3}{\sqrt{2}} \Delta_3 . \end{aligned} \quad (4.16)$$

Here we begin to see for the first time the origin of the tree-level FCNCs in 3HDMs given the Yukawa textures. We observe the following mass terms in the gauge basis,

$$M_n = \begin{pmatrix} \times & \times & 0 \\ \times & \times & 0 \\ 0 & 0 & \times \end{pmatrix} \quad M_p = \begin{pmatrix} \times & \times & 0 \\ \times & \times & 0 \\ \times & \times & \times \end{pmatrix} \quad (4.17)$$

Note that there is no overlap between matrix elements inside the up or down sectors, e.g for the case of the $(m_p)_{31}$ and $(m_p)_{32}$ only the first matrix, Γ_1 contributes for its value,

$$(M_p)_{31} = \frac{1}{\sqrt{2}} v_1 (\Gamma_1)_{31} , \quad (M_p)_{32} = \frac{1}{\sqrt{2}} v_1 (\Gamma_1)_{32} \quad (4.18)$$

However, to properly examine this sector we must be able to transform the Lagrangian n and p into their proper quark fields d and u respectively. This, like in the SM, is achieved by a set of bi-unitarity transformations, $V_{L,R}$ and $U_{L,R}$, that will relate the Gauge basis and the mass basis. Where naturally the CKM matrix will be $V_{\text{CKM}} = V_L^\dagger U_R$. These matrices are defined such,

$$M^u = V_L^n M_n V_R^n \approx V_L^n \begin{pmatrix} \times & \times & 0 \\ \times & \times & 0 \\ 0 & 0 & \times \end{pmatrix} V_R^n , \quad m^d = U_L^p M_p U_R^p \approx U_L^p \begin{pmatrix} \times & \times & 0 \\ \times & \times & 0 \\ \times & \times & \times \end{pmatrix} U_R^p . \quad (4.19)$$

This then imposes certain shapes to the unitary transformations we apply,

$$V_L^p = \begin{pmatrix} \times & \times & 0 \\ \times & \times & 0 \\ 0 & 0 & 1 \end{pmatrix}, \quad V_R^p = \begin{pmatrix} \times & \times & 0 \\ \times & \times & 0 \\ 0 & 0 & e^{i\alpha} \end{pmatrix}, \quad U_{L,R}^n = \begin{pmatrix} \times & \times & \times \\ \times & \times & \times \\ \times & \times & \times \end{pmatrix}. \quad (4.20)$$

We introduce a complex phase in $V_{L,R}^p$ so that these matrices can be parametrized with two angles. While the parametrization of $U_{L,R}^n$ will require 3. We know these to be the physical degrees of freedom that will be included in the CKM matrix. The CKM matrix elements can then be expressed as,

$$\begin{pmatrix} V_{ud} & V_{us} & V_{ub} \\ V_{cd} & V_{cs} & V_{cb} \\ V_{td} & V_{ts} & V_{tb} \end{pmatrix} = \begin{pmatrix} V_{L,11}^p & V_{L,12}^p & 0 \\ V_{L,21}^p & V_{L,22}^p & 0 \\ 0 & 0 & e^{i\alpha} \end{pmatrix} \begin{pmatrix} U_{R,11}^n & U_{R,12}^n & U_{R,13}^n \\ U_{R,21}^n & U_{R,22}^n & U_{R,23}^n \\ U_{R,31}^n & U_{R,32}^n & U_{R,33}^n \end{pmatrix}^\dagger \quad (4.21)$$

While by moving to the mass basis, We can write that $U_L^\dagger = V_{CKM}^\dagger V_L^\dagger$, which together with,

$$M_u^{\text{diag}} = U_L M_p U_R, \quad M_d^{\text{diag}} = V_{CKM}^\dagger U_L^\dagger M_n U_R. \quad (4.22)$$

These equations allow for a system of coupled linear equations that can be solved with respect to the Yukawa textures and return their values for a given set of Unitary matrices, CKM matrix and quark masses. This portion of the inversion is also performed as we expect to have proper quark masses and to respect the CKM matrix in all our parameter space.

4.3 The BGL-like suppression of FCNCs in the 3HDM model

Given that we now know how quark and lepton masses are generated in the model and how to express their physical fields let us now analyse carefully the Yukawa couplings between the scalar eigenstates and the physical quarks, with particular attention to any FCNC couplings which may arise as to discuss it's suppression. First by performing the discussed shift to the Higgs basis, where $\{\phi_1, \phi_2, \phi_3\}$ become $\{h', H'_1, H'_2\}$

In terms of quark field interactions with these states in the gauge basis we have,

$$\mathcal{L}_Y^{\text{CP-even}} = -\frac{1}{\sqrt{2}} \left[\bar{n}_L \left(\sum_{k=1}^3 \Gamma_k \phi_k \right) n_R + \bar{p}_L \left(\sum_{k=1}^3 \Delta_k \phi_k \right) p_R + \text{H.c.} \right]. \quad (4.23)$$

This can be represented in terms of the field h' as,

$$\mathcal{L}_Y^{H_0} = -\frac{h'}{v} \left[\bar{n}_L \left(\sum_{k=1}^3 \Gamma_k v_k \right) n_R + \bar{p}_L \left(\sum_{k=1}^3 \Delta_k v_k \right) p_R + \text{h.c.} \right]. \quad (4.24)$$

Where we can replace the result seen in, Eq. (4.16),

$$\mathcal{L}_Y^{h'} = \frac{h'}{v} \bar{n}_L M_n n_R + \bar{p}_L M_p p_R. \quad (4.25)$$

Showing that the SM like Higgs in our model has the same type of tree-level coupling as in the SM. Meanwhile for the, generally, heavier states $H'_{2,3}$ we can write their coupling to down quarks as,

$$\mathcal{L}_Y^{H'_1, H'_2} = \frac{H'_1}{v} \bar{n}_L N_{d1} n_R + \frac{H'_2}{v} \bar{n}_L N_{d2} n_R + \text{H.c.} . \quad (4.26)$$

where the matrix terms N_{d1} and N_{d2} can be shown to be,

$$\begin{aligned} N_{d1} &= \frac{v}{\sqrt{2}v_{13}} U_L^\dagger (\Gamma_1 v_3 - \Gamma_3 v_1) \\ N_{d2} &= U_L^\dagger \left[\frac{v_2}{v_{13}} \frac{1}{\sqrt{2}} (\gamma_1 v_1 + \gamma_3 v_3) - \frac{v_{13}}{v_2} \frac{1}{\sqrt{2}} \Gamma_2 v_2 \right] U_R \end{aligned} \quad (4.27)$$

To simply the expression of these interaction terms we go back to the textures of the Yukawas, from the block structures presented, and by virtue of our choice to keep the third row of U_L the same as the CKM matrix, $(U_L)_{3j} = V_{3j}$. Therefor by defining the simple projection operator, P as,

$$P = \begin{pmatrix} 0 & 0 & 0 \\ 0 & 0 & 0 \\ 0 & 0 & 1 \end{pmatrix}. \quad (4.28)$$

We can in the down sector Yukawa matrices write,

$$\Gamma_3 = (\Gamma_3)_{33} P \quad , \quad \frac{1}{\sqrt{2}} (\Gamma_1 v_3 - \Gamma_3 v_1) = PM_d. \quad (4.29)$$

Hence,

$$\begin{aligned} (N_{d1})_{ij} &= \frac{vv_3}{v_1 v_{13}} V_{3i}^* V_{3j} (M_d)_{jj} - \frac{1}{\sqrt{2}} \frac{vv_{13}}{v_1} (\Gamma_3)_{33} V_{3i}^* (U_R)_{3B}, \\ (N_{d2})_{ij} &= \frac{v_{13}}{v_2} (M_d)_{jj} \delta_{ij} + \left(\frac{v_{13}}{v_2} + \frac{v_2}{v_{13}} \right) V_{3i}^* V_{3j} (M_d)_{jj}. \end{aligned} \quad (4.30)$$

We can see through the proper expansion of these terms that all non diagonal terms, (where $j \neq i$) of N_{d2} , contain one CKM matrix term. While for N_{d1} we have two CKM matrix elements. Even given these terms we must suppress the size of the elements in Γ_1 .

A similar procedure in the up quark sector would reveal that there are no scalar mediated FCNCs at tree level in the up sector. This is due to the special structures of the up type Yukawa matrices, we can see Δ_1 is a empty matrix and this prevents FCNCs.

Thus given the magnitude of these CKM matrix terms we can expect our values to naturally be controlled.

4.4 The inversion process

Over the course of this introduction we alluded to the Higgs alignment and how we expect one of our scalar states must completely overlap with a possible SM like Higgs. To ensure this we mentioned we must apply the inversion process to our Lagrangian. To clarify what we mean by inversion process, it should be possible to write all Lagrangian terms with respect to the physical characteristics of the model, such as mixing angles and physical state masses to their Lagrangian terms in the gauge basis.

We can begin the inversion process by revisiting the tad pole equations, recall that we must ensure the derivatives of the potential, seen in Eqs. (4.6), vanish for some value of the spin-0 fields ϕ_i , leads us to the so-called tadpole equations of the model. This enables us to express the μ_1 , μ_2 and μ_3 as follows,

$$\begin{aligned} \mu_1^2 &= \frac{1}{2} \left(2\lambda_1 v_1^2 + (\lambda_4 + \lambda_7) v_2^2 + (\lambda_5 + \lambda_8 + 2\lambda_{10}) v_3^2 - \frac{2(\mu_{13}^2 v_3 + \mu_{21}^2 v_2)}{v_1} \right), \\ \mu_2^2 &= \frac{1}{2} \left((\lambda_4 + \lambda_7) v_1^2 + 2\lambda_2 v_2^2 + (\lambda_6 + \lambda_9) v_3^2 - \frac{2(\mu_{21}^2 v_1 + \mu_{23}^2 v_3)}{v_2} \right), \\ \mu_3^2 &= \frac{2\lambda_3 v_3^3 + (\lambda_6 + \lambda_9) v_2^2 v_3 + (\lambda_5 + \lambda_8 + 2\lambda_{10}) v_1^2 v_3 - 2\mu_{13}^2 v_1 - 2\mu_{23}^2 v_2}{2v_3}. \end{aligned} \quad (4.31)$$

4.4.1 The CP-odd portion of the scalar sector

We can now turn our attention now to the physical scalar spectrum of the model. This potential is explicitly CP invariant given all parameters are real. In fact in this model we expect to find no more sources of CP-violation than in the SM.

Pseudoscalar Eigenstates

Returning to the CP-odd portion of the scalar sector (related to the Z_k degrees of freedom) contains quadratic terms after the process of SBB. These are easily extracted from the scalar potential in the form,

$$V_{\text{shifted}} \supset \begin{pmatrix} z_1 & z_2 & z_3 \end{pmatrix} \frac{M_P^2}{2} \begin{pmatrix} z^1 \\ z^2 \\ z^3 \end{pmatrix}, \quad (4.32)$$

where M_P^2 is the 3×3 pseudoscalar mass matrix in a non diagonal form, i.e. in the unphysical gauge basis. It can however be expressed in a block diagonal matrix through the rotation matrix we introduced in Eq. (4.10), thus in the Higgs basis our mass matrix would take the shape of,

$$B_P^2 = \mathcal{O} M_P^2 \mathcal{O}^T = \begin{pmatrix} 0 & 0 & 0 \\ 0 & (B_P^2)_{22} & (B_P^2)_{23} \\ 0 & (B_P^2)_{32} & (B_P^2)_{33} \end{pmatrix}, \quad (4.33)$$

The line and column of zeroes in this matrix tells us that it has a zero eigenvalue. This eigenstate, as previously alluded to, will provide a Goldstone. This is clearly the Goldstone that will become the longitudinal polarization of the Z . The elements of the B_P^2 matrix are given by,

$$\begin{aligned} (B_P^2)_{22} &= \frac{-2\lambda_{10}v_2^3v_3^2v_1 + \mu_{21}^2v_1^4 + \mu_{23}^2v_3v_1^3 + 2\mu_{21}^2v_2^2v_1^2 + v_2^3(\mu_{13}^2v_3 + \mu_{21}^2v_2)}{v_1v_2(v_1^2 + v_2^2)}, \\ (B_P^2)_{32} &= \frac{v(v_1(\mu_{23}^2 + 2\lambda_{10}v_2v_3) - \mu_{13}^2v_2)}{v_1^2 + v_2^2}, \\ (B_P^2)_{33} &= \frac{v^2(2\lambda_{10}v_3v_1^2 - \mu_{13}^2v_1 - \mu_{23}^2v_2)}{(v_1^2 + v_2^2)v_3}. \end{aligned} \quad (4.34)$$

From the above equations we notice that, apart from the three VEVs, only two parameters, λ_{10} and μ_{23} , enter in the pseudoscalar mass eigensystem. From this intermediate basis we can clearly see that in the Higgs basis the pseudoscalar masses mix in such a way that this mixing could easily be parametrized by an angle, γ_1 , like so,

$$\mathcal{O}_{\gamma_1} = \begin{pmatrix} 1 & 0 & 0 \\ 0 & \cos(\gamma_1) & -\sin(\gamma_1) \\ 0 & \sin(\gamma_1) & \cos(\gamma_1) \end{pmatrix}, \quad (4.35)$$

Therefor the mass eigenstates of the pseudoscalars in the mass basis can be related to the gauge basis by the equation,

$$\mathcal{O}_{\gamma_1} (B_P^2) \mathcal{O}_{\gamma_1}^T = \begin{pmatrix} 0 & 0 & 0 \\ 0 & m_{A_1} & 0 \\ 0 & 0 & m_{A_2} \end{pmatrix}, \quad (4.36)$$

Expanding the system seen in Eq. (4.36), we can deduce the equations for the mass terms in terms of the original Lagrangian parameters,

$$\begin{aligned} m_{A_1}^2 \cos^2(\gamma_1) + m_{A_2}^2 \sin^2(\gamma_1) &= (B_P^2)_{22}, \\ m_{A_1}^2 \sin(\gamma_1) \cos(\gamma_1) + m_{A_2}^2 \sin(\gamma_1) \cos(\gamma_1) &= (B_P^2)_{32}, \\ m_{A_1}^2 \sin^2(\gamma_1) + m_{A_2}^2 \cos^2(\gamma_1) &= (B_P^2)_{33}. \end{aligned} \quad (4.37)$$

From these two sets of equations (Eq (4.37) and Eq. (4.34)) we can show that,

$$\begin{aligned} m_{A_1} = \frac{1}{v_1 v_2 (v_1^2 + v_2^2)} &\left[v v_2 v_1 \tan(\gamma_1) (v_1 (\mu_{23}^2 + 2\lambda_{10} v_2 v_3) - \mu_{13}^2 v_2) - 2\lambda_{10} v_2^3 v_3^2 v_1 \right. \\ &\left. + \mu_{21}^2 v_1^4 + \mu_{23}^2 v_3 v_1^3 + 2\mu_{21}^2 v_2^2 v_1^2 + v_2^3 (\mu_{13}^2 v_3 + \mu_{21}^2 v_2) \right], \end{aligned} \quad (4.38)$$

and

$$\begin{aligned} m_{A_2} = \frac{1}{v_1 v_2 (v_1^2 + v_2^2)} &\left[v v_2 v_1 \cot(\gamma_1) (\mu_{13}^2 v_2 - v_1 (\mu_{23}^2 + 2\lambda_{10} v_2 v_3)) - 2\lambda_{10} v_2^3 v_3^2 v_1 \right. \\ &\left. + \mu_{21}^2 v_1^4 + \mu_{23}^2 v_3 v_1^3 + 2\mu_{21}^2 v_2^2 v_1^2 + v_2^3 (\mu_{13}^2 v_3 + \mu_{21}^2 v_2) \right]. \end{aligned} \quad (4.39)$$

Through the inversion of these equations we can obtain a parametrization of, λ_{10} , v , through the mixing angles $\psi_{1,2}$ VEV magnitude, v , and the new pseudoscalar mixing angles $\gamma_{1,2}$, as seen in,

$$\begin{aligned} \lambda_{10} = -\frac{1}{2v_1 v_2^3 v_3^2} &\left[v_1^3 (\mu_{21}^2 v_1 + \mu_{23}^2 v_3) + 2\mu_{21}^2 v_1^2 v_2^2 + \mu_{21}^2 v_2^4 + \mu_{13}^2 v_2^3 v_3 \right. \\ &\left. - v_1 v_2 (v_1^2 + v_2^2) (m_{A_1}^2 \cos^2(\gamma_1) + m_{A_2}^2 \sin^2(\gamma_1)) \right] \end{aligned} \quad (4.40)$$

$$\begin{aligned} \mu_{23} = -\frac{1}{v^2 v_3 (v_1^2 - v_2^2)} &\left[-v^2 v_1^2 v_2 m_{A_1}^2 \cos^2(\gamma_1) + v_2^3 v_3^2 m_{A_1}^2 \sin^2(\gamma_1) \right. \\ &- v^2 v_1^2 v_2 m_{A_2}^2 \sin^2(\gamma_1) + v_2^3 v_3^2 m_{A_2}^2 \cos^2(\gamma_1) + \mu_{21}^2 v_1^2 v_3^3 \\ &\left. + \mu_{21}^2 v_1^2 v_2^2 \right] \end{aligned} \quad (4.41)$$

Through these two equations we can also express and the final line of Eq. (4.37) the μ_{21}^2 soft-breaking term as,

$$\begin{aligned} \mu_{21} = \frac{1}{2v^2 (v_1^2 + v_2^2)} &\left[v_1 v_2 (v^2 + v_3^2) \cos(2\gamma_1) (m_{A_1}^2 - m_{A_2}^2) \right. \\ &- v (v_1 - v_2) (v_1 + v_2) v_3 \sin(2\gamma_1) (m_{A_1}^2 - m_{A_2}^2) \\ &\left. + v_1 v_2 (v - v_3) (v + v_3) (m_{A_1}^2 + m_{A_2}^2) \right] \end{aligned} \quad (4.42)$$

This process must be repeated for all the scalar states of the 3HDM as to properly conduct the inversion.

Charged Scalar Eigenstates

Through a similar process, we can endeavour to isolate the quadratic terms relating to the charged degrees of freedom. From the charged portion of the Higgs doublets, the W_μ fields, we express in matrix form the bi-linear terms forming a M_C^2 matrix as,

$$V \supset \begin{pmatrix} W_1 & W_2 & W_3 \end{pmatrix} \frac{M_C^2}{2} \begin{pmatrix} W_1 \\ W_2 \\ W_3 \end{pmatrix} \quad (4.43)$$

Through the same rotation to the Higgs basis we produce a similar structure to the mass matrix of the pseudoscalar fields as seen in,

$$B_C^2 = \mathcal{O} M_C^2 \mathcal{O}^T = \begin{pmatrix} 0 & 0 & 0 \\ 0 & (B_C^2)_{22} & (B_C^2)_{23} \\ 0 & (B_C^2)_{32} & (B_C^2)_{33} \end{pmatrix} \quad (4.44)$$

Here we observe again that a line and column of zeros ensures that we have a Goldstone boson. Like in the previous example this will be incorporated in the W^\pm Gauge Boson. The terms in this matrix are written as,

$$\begin{aligned} (B_C^2)_{22} &= -\frac{1}{2v_1 v_2 (v_1^2 + v_2^2)} \left[v_1^3 (2\lambda_7 v_2^3 + \lambda_9 v_3^2 v_2 - 2\mu_{23}^2 v_3) + \lambda_7 v_2 v_1^5 + \lambda_7 v_2^5 v_1 \right. \\ &\quad \left. + (\lambda_8 + 2\lambda_{10}) v_2^3 v_3^2 v_1 - 2\mu_{21}^2 v_1^4 - 4\mu_{21}^2 v_2^2 v_1^2 - 2v_2^3 (\mu_{13}^2 v_3 + \mu_{21}^2 v_2) \right] \\ (B_C^2)_{32} &= -\frac{v ((\lambda_8 - \lambda_9 + 2\lambda_{10}) v_1 v_2 v_3 - 2\mu_{13}^2 v_2 + 2\mu_{23}^2 v_1)}{2(v_1^2 + v_2^2)} \\ (B_C^2)_{33} &= \frac{v^2 (v_2 (\lambda_9 v_2 v_3 - 2\mu_{23}^2) + (\lambda_8 + 2\lambda_{10}) v_3 v_1^2 - 2\mu_{13}^2 v_1)}{2(v_1^2 + v_2^2) v_3} \end{aligned} \quad (4.45)$$

Again we note that given the two final massive eigenstates we can introduce another mixing angle, γ_2 ,

$$\mathcal{O}_{\gamma_2} = \begin{pmatrix} 1 & 0 & 0 \\ 0 & \cos(\gamma_2) & -\sin(\gamma_2) \\ 0 & \sin(\gamma_2) & \cos(\gamma_2) \end{pmatrix} \quad (4.46)$$

Relating to the massive states as,

$$\mathcal{O}_{\gamma_1} (B_C)^2 \mathcal{O}_{\gamma_1}^T = \begin{pmatrix} 0 & 0 & 0 \\ 0 & M_{H_1^\pm} & 0 \\ 0 & 0 & M_{H_2^\pm} \end{pmatrix} \quad (4.47)$$

Where we see the explicit mass eigenstates of the charged scalars H_1^\pm and H_2^\pm . Simple expansion of the equation seen above leads us to the same relations as in the pseudoscalar states but now for the charged Higgs states.

$$\begin{aligned} m_{H_1^\pm} \cos^2(\gamma_2) + m_{H_2^\pm} \sin^2(\gamma_2) &= (B_C^2)_{22} \\ \cos(\gamma_2) \sin(\gamma_2) (m_{H_2^\pm}^2 - m_{H_1^\pm}^2) &= (B_C^2)_{23} \\ m_{H_1^\pm} \sin^2(\gamma_2) + m_{H_2^\pm} \cos^2(\gamma_2) &= (B_C^2)_{33} \end{aligned} \quad (4.48)$$

Notice how the charged eigenstates are dependent only of 3 Lagrangian parameters. For brevity we do not show the mass terms explicitly but given we have three equations we can parameterize another 3 three parameters of the Lagrangian, λ_{7-9} in terms of physical masses, VEVs and a mixing angle, as seen,

$$\begin{aligned} \lambda_7 &= \frac{1}{v^2 v_1 v_2 (v_1^2 + v_2^2)} \left[-v_1 v_2 (v^2 + v_3^2) \cos(2\gamma_2) (m_{H_1^\pm}^2 - m_{H_2^\pm}^2) \right. \\ &\quad + (v_1 - v_2) (v_1 + v_2) v_3 v \sin(2\gamma_2) (m_{H_1^\pm}^2 - m_{H_2^\pm}^2) \\ &\quad - v_1 v_2 (v - v_3) (v + v_3) (m_{H_1^\pm}^2 + m_{H_2^\pm}^2) \\ &\quad + 2\mu_{21}^2 (v_1^2 + v_2^2) v^2 (m_{H_1^\pm}^2 - m_{H_2^\pm}^2) \\ &\quad - v_1 v_2 (v - v_3) (v + v_3) (m_{H_1^\pm}^2 + m_{H_2^\pm}^2) \\ &\quad \left. + 2\mu_{21}^2 (v_1^2 + v_2^2) v^2 \right] \end{aligned} \quad (4.49)$$

$$\begin{aligned} \lambda_8 = & \frac{1}{v^2 v_1 v_3} \left[2 \left(\sin(\gamma_2) m_{C1}^2 (v_1 v_3 \sin(\gamma_2) - v v_2 \cos(\gamma_2)) \right. \right. \\ & \left. \left. + \cos(\gamma_2) m_{C2}^2 (v v_2 \sin(\gamma_2) + v_1 v_3 \cos(\gamma_2)) + v^2 (\lambda_{10} v_1 v_3 - \mu_{13}^2) \right) \right] \end{aligned} \quad (4.50)$$

$$\begin{aligned} \lambda_9 = & \frac{1}{v^2 v_2 v_3} \left[2 \left(-\sin(\gamma_2) m_{C1}^2 (v_2 v_3 \sin(\gamma_2) + v v_1 \cos(\gamma_2)) + \right. \right. \\ & \left. \left. \cos(\gamma_2) m_{C2}^2 (v v_1 \sin(\gamma_2) - v_2 v_3 \cos(\gamma_2)) + \mu_{23}^2 v^2 \right) \right] \end{aligned} \quad (4.51)$$

4.4.2 The CP-even portion of the Scalar Sector

Finally we can perform the same procedure one final time for the CP-even neutral scalars. Again we begin by rotating the quadratic terms, however this time we require a more complex mixing. In the gauge basis we have,

$$V \supset \begin{pmatrix} h_1 & h_2 & h_3 \end{pmatrix} \frac{M_S^2}{2} \begin{pmatrix} h_1 \\ h_2 \\ h_3 \end{pmatrix} \quad (4.52)$$

The elements of this matrix are written as,

$$M_S^2 = \begin{pmatrix} \frac{2\lambda_1 v_1^3 + \mu_{21}^2 v_2 + \mu_{13}^2 v_3}{v_1} & v_1 v_2 (\lambda_4 + \lambda_7) - \mu_{21}^2 & v_1 v_3 (2\lambda_{10} + \lambda_5 + \lambda_8) - \mu_{13}^2 \\ v_1 v_2 (\lambda_4 + \lambda_7) - \mu_{21}^2 & \frac{\mu_{21}^2 v_1 + 2\lambda_2 v_2^3 + \mu_{23}^2 v_3}{v_2} & v_2 v_3 (\lambda_6 + \lambda_9) - \mu_{23}^2 \\ v_1 v_3 (2\lambda_{10} + \lambda_5 + \lambda_8) - \mu_{13}^2 & v_2 v_3 (\lambda_6 + \lambda_9) - \mu_{23}^2 & \frac{\mu_{13}^2 v_1 + \mu_{23}^2 v_2 + 2\lambda_3 v_3^3}{v_3} \end{pmatrix} \quad (4.53)$$

We must perform a orthogonal rotation such that we reach the scalar mass equations, which is written as,

$$\begin{pmatrix} h & 0 & 0 \\ 0 & H_1 & 0 \\ 0 & 0 & H_2 \end{pmatrix} = \mathcal{O}_\alpha \mathcal{O} (M_S^2) \mathcal{O}_\alpha^T \mathcal{O}^T \quad (4.54)$$

However given the non-trivial mixing between these states we define 3 mixing angles $\alpha_{1,2,3}$. Making \mathcal{O}_α ,

$$\mathcal{O}_\alpha = R_1 \cdot R_2 \cdot R_3 \quad , \quad (4.55)$$

which are each written as,

$$R_1 = \begin{pmatrix} \cos(\alpha_1) & \sin(\alpha_1) & 0 \\ -\sin(\alpha_1) & \cos(\alpha_1) & 0 \\ 0 & 0 & 1 \end{pmatrix} \quad , \quad R_2 = \begin{pmatrix} \cos(\alpha_2) & 0 & \sin(\alpha_2) \\ 0 & 1 & 0 \\ -\sin(\alpha_2) & 0 & \cos(\alpha_2) \end{pmatrix} \quad , \quad (4.56)$$

$$R_3 = \begin{pmatrix} 1 & 0 & 0 \\ 0 & \cos(\alpha_3) & \sin(\alpha_3) \\ 0 & -\sin(\alpha_3) & \cos(\alpha_3) \end{pmatrix} \quad . \quad (4.57)$$

Through this \mathcal{O}_α we can diagonalize scalar massive eigenstates.

$$\mathcal{O}_\alpha \underbrace{\mathcal{O} M_S^2 \mathcal{O}^T}_{B_S^2} \mathcal{O}_\alpha^T \equiv \text{diag}(m_h, m_{H_1}, m_{H_2}) \quad (4.59)$$

Here we can perform another inversion, allowing us to reach a parametrization of the six remaining couplings again through a laborious expansion,

$$\begin{aligned}\lambda_1 = \frac{1}{2v^2 v_1^3 (v_1^2 + v_2^2)} & \left[(v_1^2 + v_2^2) v_1^3 m_h^2 + v_1 m_{H_1}^2 (v_1 v_3 \sin(\alpha_3) + v v_2 \cos(\alpha_3))^2 \right. \\ & + v_1 m_{H_2}^2 (v v_2 \sin(\alpha_3) - v_1 v_3 \cos(\alpha_3))^2 \\ & \left. - v^2 (v_1^2 + v_2^2) (\mu_{13}^2 v_3 + \mu_{21}^2 v_2) \right] \end{aligned}\quad (4.60)$$

$$\begin{aligned}\lambda_2 = \frac{1}{2v^2 v_2^3 (v_1^2 + v_2^2)} & \left[(v_1^2 + v_2^2) v_2^3 m_h^2 + v_2 m_{H_1}^2 (v v_1 \cos(\alpha_3) - v_2 v_3 \sin(\alpha_3))^2 \right. \\ & + v_2 m_{H_2}^2 (v v_1 \sin(\alpha_3) + v_2 v_3 \cos(\alpha_3))^2 \\ & \left. - v^2 (v_1^2 + v_2^2) (\mu_{21}^2 v_1 + \mu_{23}^2 v_3) \right] \end{aligned}\quad (4.61)$$

$$\begin{aligned}\lambda_3 = \frac{1}{2v^2 v_2^3 (v_1^2 + v_2^2)} & \left[(v_1^2 + v_2^2) v_2^3 m_h^2 + v_2 m_{H_1}^2 (v v_1 \cos(\alpha_3) - v_2 v_3 \sin(\alpha_3))^2 \right. \\ & + v_2 m_{H_2}^2 (v v_1 \sin(\alpha_3) + v_2 v_3 \cos(\alpha_3))^2 \\ & \left. - v^2 (v_1^2 + v_2^2) (\mu_{21}^2 v_1 + \mu_{23}^2 v_3) \right] \end{aligned}\quad (4.62)$$

$$\begin{aligned}\lambda_4 = \frac{1}{v^2 v_1 v_2 (v_1^2 + v_2^2)} & \left[v_1 v_2 (v_1^2 + v_2^2) m_h^2 + (v_1^2 + v_2^2) v^2 (\mu_{21}^2 - \lambda_7 v_1 v_2) \right. \\ & - m_{H_1}^2 (v_1 v_3 \sin(\alpha_3) + v v_2 \cos(\alpha_3)) (v v_1 \cos(\alpha_3) - v_2 v_3 \sin(\alpha_3)) \\ & \left. + m_{H_2}^2 (v_1 v_3 \cos(\alpha_3) - v v_2 \sin(\alpha_3)) (v v_1 \sin(\alpha_3) + v_2 v_3 \cos(\alpha_3)) \right] \end{aligned}\quad (4.63)$$

$$\begin{aligned}\lambda_5 = \frac{1}{v^2 v_1 v_2 (v_1^2 + v_2^2)} & \left[-m_{H_1}^2 (v_1 v_3 \sin(\alpha_3) + v v_2 \cos(\alpha_3)) (v v_1 \cos(\alpha_3) - v_2 v_3 \sin(\alpha_3)) \right. \\ & + m_{H_2}^2 (v_1 v_3 \cos(\alpha_3) - v v_2 \sin(\alpha_3)) (v v_1 \sin(\alpha_3) + v_2 v_3 \cos(\alpha_3)) \\ & \left. + (v_1^2 + v_2^2) v^2 (\mu_{21}^2 - \lambda_7 v_1 v_2) + v_1 v_2 (v_1^2 + v_2^2) m_h^2 \right] \end{aligned}\quad (4.64)$$

$$\begin{aligned}\lambda_6 = \frac{1}{v^2 v_1 v_2 (v_1^2 + v_2^2)} & \left[-m_{H_1}^2 (v_1 v_3 \sin(\alpha_3) + v v_2 \cos(\alpha_3)) (v v_1 \cos(\alpha_3) - v_2 v_3 \sin(\alpha_3)) \right. \\ & + m_{H_2}^2 (v_1 v_3 \cos(\alpha_3) - v v_2 \sin(\alpha_3)) (v v_1 \sin(\alpha_3) + v_2 v_3 \cos(\alpha_3)) \\ & \left. + (v_1^2 + v_2^2) v^2 (\mu_{21}^2 - \lambda_7 v_1 v_2) + v_1 v_2 (v_1^2 + v_2^2) m_h^2 \right] \end{aligned}\quad (4.65)$$

The final μ_{13} soft-breaking term is calculated with the Higgs alignment condition.

To recapitulate, we can now express the 15 out of 16 Lagrangian terms through constants. First using tadpole equations to reach μ_1^2 , μ_2^2 and μ_3^2 in relation to the three VEVs. Secondly μ_{23}^2 , μ_{21}^2 and λ_{10} , can be exchanged for m_{A_1} , m_{A_2} and γ_1 . The remaining nine quartic couplings can be expressed by the five physical masses (three CP-even scalars, and two charged scalars) and four mixing angles (three in the CP-even sector and one in the charged scalar sector).

In all these relations will impose the strict alignment limit condition. This translates in the lightest scalar state m_h equal to 125.09 GeV.

Through this parameterization we can *a priori* ensure a positively defined set scalar states i.e. no tachyonic states as well as account for unboundness from below in our numerical scans.

Likewise, in the quark sector, it is possible to for a set of VEVs determine before hand the tree-level physical masses for quarks and their proper mixing parameters as to respect the CKM

matrix. This inversion will also be key as to ensure we have points in our scans that are all in accordance with quark physics.

4.5 Numerical Discussion of the 3HDM

Finally we move to discuss the results of our study of the 3HDM parameter space. As stated, at the starting point of our numerical scans we must ensure a positively defined spectrum i.e. no tachyonic solutions and a stable vacuum (at least at tree-level) through tadpole equations. Then to obtain relevant data in a timely fashion we performed a inversion process as to scan over physical parameters instead of Lagrangian terms. This is a fundamental component of our numerical scan and is performed by solving analytical solutions of the equations we discussed previously. Note, again that we calculate all masses at the inversion stage and SPheno level at tree-level.

Never the less we must take into account the real radiatively corrected bounds during our analysis. Although SPheno utilizes tree-level masses for all radiative processes (like EW observables) and calculates them correctly just with tree-level masses replaced for loop-level masses, it is still relevant to admit that we must consider that the radiative corrections are subdominant as for our results to have any significant validity. Furthermore, considering the amount of data we gathered, even if we make the assumption that a small portion of our results would be discarded given one-loop or higher order corrections to the mass spectrum our conclusions should still hold since there is room to account for deviations in the mass ranges found. The exercise of proper inversion for higher orders is left for future work.

The ranges of accepted values within our scans are seen in,

$$\begin{array}{c} \psi_{1,2} ; \beta_{1,2} ; \alpha_{1,2,3} \quad \|\mu_{23}\| , \|\mu_{21}\| , \|\mu_{13}\| \quad m_{A_{1,2}}, m_{H_{1,2}^\pm}, m_{H_{1,2}} \\ \hline 0 - 2\pi \qquad \qquad \qquad 1 \text{ GeV} - 10 \text{ TeV} \qquad \qquad \qquad 1 \text{ GeV} - 11 \text{ TeV} \end{array}$$

Recall that we included a inversion process in the Yukawa sector as to reproduce the proper fermion masses. This required another set of linear equations to be solved, within experimental error bars of all quark and lepton masses. This also respects the additional constraint that in the particular case of quark mixing we must ensure the proper values of the CKM mixing matrix. Only once a point is found to be within the desired Lagrangian space while also respecting the conditions for the quark masses, CKM matrix and bound from below is it then fed into SPheno and stored.

4.5.1 Methodology and Constraints

The methodology used in this analysis of the 3HDM is very similar to the one introduced in the B-L-SM discussion, with two new additions - first the discussed inversion as to assure Higgs alignment - secondly the use of the python3 package called `flavio` [76]. Introduced to enable our simulations to use the existence of quark flavour violation (QFV) processes to constrict our parameter space through the Wilson coefficients calculated by SPheno.

These QFV observables will be represented as fractions between the expected SM value and the calculated value for the point that includes the novel NP contributions. We calculated a large number of flavour violating processes in this fashion, in fact, 31 fractions between expected QFV processes in the 3HDM and the expected theoretical value of the SM were calculated.

We will avoid a in-depth discussion of how these QFV processes are calculated seeing that for our purposes knowing that their integrated through functions dependent on Wilson coefficients will suffice.

We will however, make the observations that given the additional scalars, in particular the charged scalars, allows for additional Feynman diagram one must consider in addition to the normal loop-level sources of FCNCs and FCCCs in the SM.

QFV Observables

In this work we tested the following B, D and K meson channels, being that for the B meson we tested, $\mathcal{BR}(B \rightarrow \chi_s \gamma)$, $\mathcal{BR}(B_0 \rightarrow \ell\bar{\ell})$, $\mathcal{BR}(B_s \rightarrow \ell\bar{\ell})$, ΔM_{B_s} , ΔM_{B_0} , $\mathcal{BR}(B^+ \rightarrow K^+ \nu\bar{\nu})$, $\mathcal{BR}(B^+ \rightarrow \pi^+ \nu\bar{\nu})$, $\mathcal{BR}(B^0 \rightarrow K^0 \nu\bar{\nu})$, $\mathcal{BR}(B^0 \rightarrow \pi^0 \nu\bar{\nu})$, $\mathcal{BR}(B^+ \rightarrow \pi^+ \nu\bar{\nu})$, $\mathcal{BR}(B^+ \rightarrow \ell\nu)$ and $\mathcal{BR}(B^+ \rightarrow D\bar{\ell}\bar{\nu})$. As for the K meson channels we looked into the $\mathcal{BR}(K_L \rightarrow \mu\bar{\mu})$, $\mathcal{BR}(K_L \rightarrow e\bar{e})$, $\mathcal{BR}(K^+ \rightarrow \pi^+ \bar{\nu}\nu)$, $\mathcal{BR}(K_L \rightarrow \pi^0 \bar{\nu}\nu)$, ϵ_K and ϵ'/ϵ . Finally for the D meson we tested only $\mathcal{BR}(D^+ \rightarrow \bar{\ell}\nu)$.

Note that many of these decays are present at tree-level (mediated by the W^\pm e.g. as $B \rightarrow \tau\nu$) and in loop-order (mediated by the Higgs) in the SM. In fact what we expected to find is a light enhancement of processes already included in the SM through the exotic additions of scalars along side the suppression mechanisms we discussed above.

From this large set of QFV observables we present only the ones that show interesting correlations with the parameters of our model and deviate from SM values in any significant way. Specifically these are, $B \rightarrow \chi_s \gamma$, $B_s \rightarrow \mu\mu$, ΔM_s , ΔM_d and $\Delta \varepsilon_K$. Here ΔM_s and ΔM_d represent the frequencies for $B_{0s} - B_{0s}$ and $B_{0d} - B_{0s}$ oscillations respectively.

Given that we present these results in the form Experimental versus SM fractions we can define 1 and 2 sigma error bars for each channel through the relation,

$$E_r = \frac{\text{Exp}_{BR}}{\text{SM}_{BR}} \times \left(\sqrt{\frac{\text{SM}_{error}}{\text{SM}_{BR}}} \right)^2 + \left(\frac{\text{Exp}_{error}}{\text{Exp}_{BR}} \right)^2 \quad (4.66)$$

where Exp_{BR} and Exp_{error} stand for the experimentally measured central value for a given QFV observable and its experimental error respectively, while the SM_{BR} and SM_{error} stands for the QFV predicted theoretical value for the SM and its theoretical uncertainty respectively.

For the most relevant observables the following table shows experimental values and error bars along with SM predicted values and theoretical uncertainties,

Channel	SM_{BR}	SM_{error}	Exp_{BR}	Exp_{error}
$\mathcal{BR}(B \rightarrow \chi_s \gamma)$	3.29e-4	1.87e-05	3.32e-4	0.16e-4
$\mathcal{BR}(B_s \rightarrow \mu\mu)$	3.66e-09	1.66e-10	2.8e-9	0.06e-9
$\mathcal{BR}(B_0 \rightarrow \mu\mu)$	1.14e-10	1.186e-11	0.39e-9	0.14e-9
ΔM_s	3.97e-13	5.07e-14	3.334e-13	0.013e-13
ΔM_d	1.24e-11	7.08e-13	1.1688e-11	0.0014e-11
$\mathcal{BR}(\Delta \varepsilon_K)$	1.81e-3	2.00e-4	2.228e-3	0.011e-3

Table 4.1: Table containing SM theoretical uncertainties and values along side with the QFV experimental error bars and 95% C.L central value as reference [2].

To briefly introduce how these QFV observables relate to NP we show some representative diagrams, as shown in Figs. 4.1, 4.2 and 4.3. Tree-level processes that include $H_{1,2}^\pm$ lead to leptonic and semileptonic (a decay in which one lepton and the corresponding neutrino is produced in addition to one or more hadrons) processes,

Figure 4.1: Leptonic and semi-leptonic H^\pm tree-level diagrams where M stands for a generic meson. ℓ is any lepton with ν_ℓ being the corresponding neutrino.

Again, note that our model is lepton flavour universal, meaning that all generations are included in these diagrams and the neutrino always corresponds to the same lepton generation. In Fig 4.1 we see how a virtual H^\pm leads to meson decay into leptons. These processes are present in tree-level at the SM. As for the new neutral Higgs $H_{1,2}$ and pseudoscalars $A_{1,2}$ their processes compete with loop-level processes at the SM. The most relevant include oscillations and rare neutral meson to lepton decays.

Figure 4.2: Meson oscillation mediated by a neutral scalar Higgs.

Still at loop-level, we have the final channel, $\chi_s \gamma$. The quark level transition occurring here is, $b \rightarrow s\gamma$ through the annihilation of a quark and anti-quark. We show the Feynman diagrams where this process happens in Fig. 4.3,

Figure 4.3: NP contribution to the transition mediated by a charged or neutral Higgs at one-loop order as to contribute to $\mathcal{BR}(B \rightarrow \chi_s \gamma)$ through $b \rightarrow \bar{s}\gamma$

Bounded from below

As in the B-L-SM or any other multiscalar BSM theory, special attention must be given to the to a large set of bounds imposed by the scalar content of the Model. In the 3HDM, looking at Eq. (4.4), we can see that it is not a simple process. This check begins by ensuring the couplings seen in Eq. (4.67) are positive so that the potential does not tend towards $-\infty$ when the fields become large.

$$\lambda_1 > 0 \quad , \quad \lambda_2 > 0 \quad , \quad \lambda_3 > 0 \quad , \quad (4.67)$$

To further find the proper conditions we must follow a procedure similar to the one used in the 2HDM [95]. By taking two doublets pairs at a time (i, j) to infinity but such that ensuring that $\phi_i^\dagger \phi_j = 0$ (which is easily accomplishable, if for one doublet the upper components are zero and for the other one the lower components vanish) one obtains a positive value of the potential for any value of the fields if,

$$\lambda_4 > -2\sqrt{\lambda_1 \lambda_2} \quad , \quad \lambda_5 > -2\sqrt{\lambda_1 \lambda_3} \quad , \quad \lambda_6 > -2\sqrt{\lambda_2 \lambda_3} \quad (4.68)$$

We can also adapt the bounded-from-below necessary conditions from ref. [102] (their expressions 21–24), while considering the fact that the potential of that work is different from ours and making the necessary adjustments. This translates into a generalisation of the above conditions, which become

$$\begin{aligned} \lambda_4 &> -2\sqrt{\lambda_1 \lambda_2} - \min(0, \lambda_7) \quad , \quad \lambda_5 > -2\sqrt{\lambda_1 \lambda_3} - \min(0, \lambda_8 - 2\|\lambda_{10}\|) \\ \lambda_6 &> -2\sqrt{\lambda_2 \lambda_3} - \min(0, \lambda_9) \quad . \end{aligned} \quad (4.69)$$

These conditions eliminate a great deal of parameter space, and though they are not sufficient ones, they should cover most of the parameter space leading to an unbounded-from-below potential. Additionally the upper perturbatively bound must be enforced, ensuring all scalar couplings $\lambda_{1,10}$ are maintained below 4π .

Unitarity

As for constraining the unitarity, we again leave the calculation of the scattering amplitudes of scalar-scalar elastic interactions to SPheno. In multiple Higgs models this is done by the diagonalization of the S-matrix (S for scattering), comprised of all these amplitudes. Once diagonalized, it can be checked for unitarity, and ensure that at high energies we respect the optical theorem. This could be done manually by following a process like seen in Ref[102], however it is far more convenient to leave this job for SPheno.

4.5.2 Discussion of results

The main objective of our work was to design a tool with whom we can probe large and complicated parameter spaces of BSM models as discussed previously. A more advanced version of the previously implemented process was implemented in this 3HDM model. With it we tried to scan over all relevant free parameter space and would like to present the results of said scan in this chapter. With it we find the parameter space that not only respects all scalar and EW analysis as implemented on the B-L-SM model, but also keeps all examined QFV observables within the 2σ deviation limit and ensures the proper inversion process.

We already touched on how Higgs physics can be detected on large collider experiments and how flavour can also limit our searches as strong interactions of quarks through the exotic Higgs could lead to excess quark violation.

Electroweak precision observables

The process we undertook here was exactly the same as we performed on the B-L-SM discussed in section 3.2.2. We can see the S, T and U variables for our parameter space in the Figs 4.4,

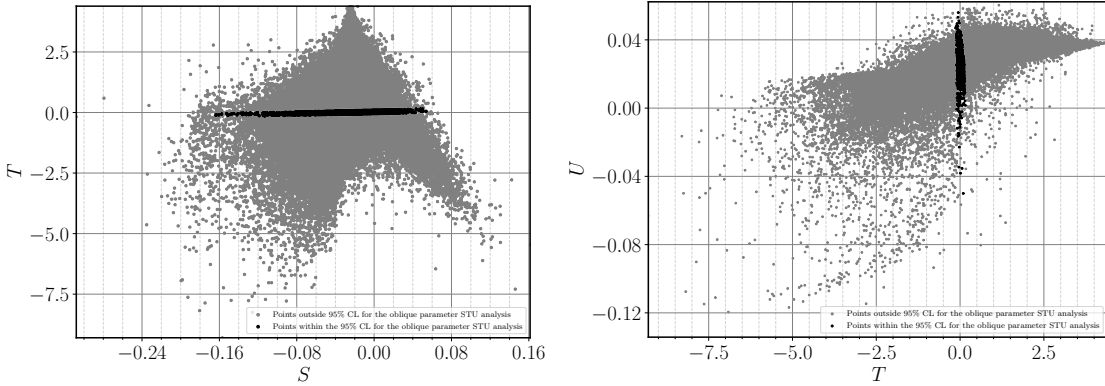


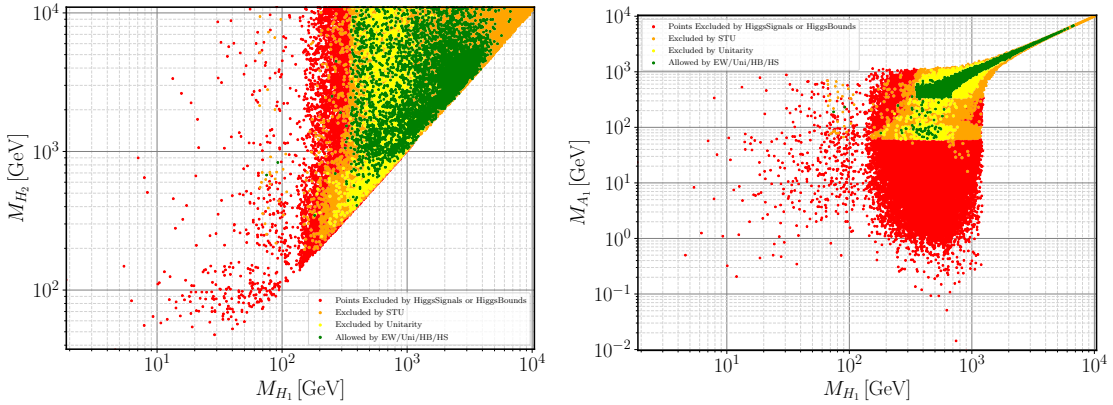
Figure 4.4: 3HDM scatter plots for EW precision observables showing the ST(left) and TU(right)planes. Accepted points lying within a 95% C.L. ellipsoid of the best fit point are represented inblack whereas grey points are excluded.

We can clearly see that NP can have a very strong effect on some of these observables, most notably in the deviation in the T variable. Note that this wide variation makes the ellipsoid seen previously look like a narrow region. As in the B-L-SM the values for $(\Delta S, \Delta T, \Delta U)$ are taken from [68].

Higgs Constraints

The STU results discussed we can continue our work by showing the available corresponding physical parameter space. Recall that our inversion process logarithmic scanned over the 16 real parameters in this space, the scalar masses, soft breaking terms and all mixing angles.

It is important to mention that the labeling of the scalars is arbitrary, we just ensure that the scalars are labeled in growing mass order e.g. $m_{H_2^\pm} > m_{H_1^\pm}$. This change does not have any real physical significance but it leaves our graphs with a linear cut where $m_i = m_j$.



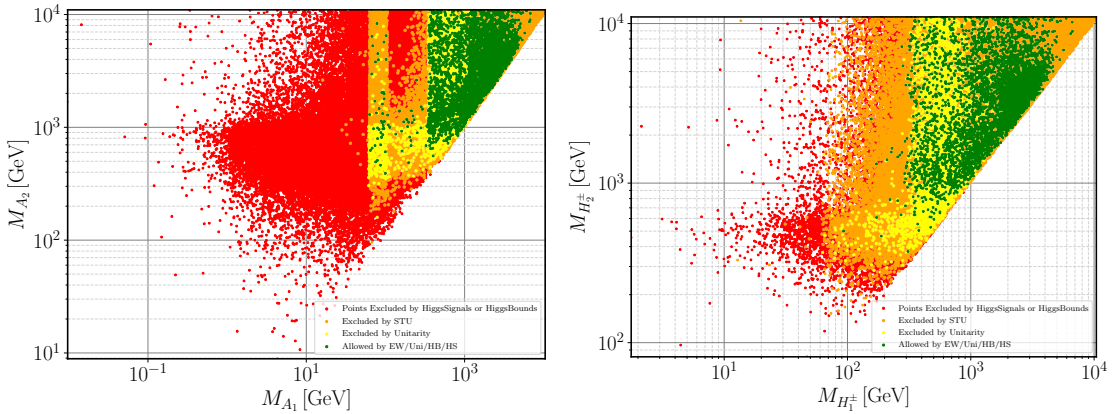


Figure 4.4: Scatter plots of parameter space allowed under several cuts imposed on the BGL-like 3HDM. On the upper right side we have the plot showing the masses of the two heavier CP-even scalars H_2 and H_1 while in the right we show the relation between the lightest (non SM Higgs) of the CP-even and pseudoscalar particles. As for the bottom plots see the remaining CP-odd scalars and how they are excluded under several cuts. Right we have the pseudoscalar masses A_1 and A_2 while in the left side we have the CP- odd charged Higgs states H_1^\pm and H_2^\pm . Red points failed HS and HB tests; yellow points violate unitarity constraints; orange points only fail electroweak precision constraints, and green ones satisfy all restrictions.

We can observe that direct searches tightly constrain the pseudoscalar and scalar masses. These direct search exclusions are directly tied to the red zones where HiggsBounds and HiggsSignals do not allow scalars to exist. Further examination of these areas shows, firstly the lighter values for the pseudoscalar masses are all excluded by direct Higgs. However there is space for pseudoscalars in case they are "masked" by the observed SM-like Higgs boson signal. As for all other scalars there does not seem to be a way to reproduce the same effect.

Furthermore, observing the top right figure in Fig 4.4, direct searches are not responsible for the exclusion of lighter charged Higgs, but our model can not respect STU limits and unitarity constraints for lighter charged Higgs.

We can then argue that our model should predict the existence of masses as low as a few hundred GeVs motivating the continuation of direct searches at the LHC. The precise values for benchmark points will be presented after the Quark flavour observables are performed.

A feature of HiggsBounds is it also enables us to see the most stringent channel for a given parameter point. From this we can see the most stringent channels that constrict our model are di-photon production and gluon fusion into light scalars (Limits taken from Refs. [103, 104, 105]).

Flavour Cuts

Let us now look at the QFV observable results, first by constraining all the most stringent QFV to be within 2σ bounds as discussed previously,

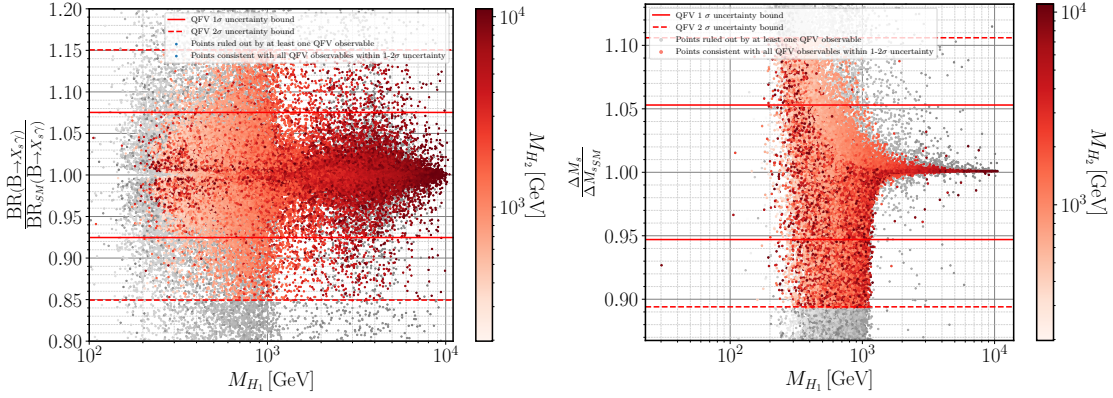


Figure 4.5: Scatter plot of the estimated QFV observables normalized to the SM values versus the lightest scalar Higgs. The grey points in all plots represent a point that would be outside the 2 σ bound for one of the observables while in a red color scale we see the second CP-even neutral scalar mass for the remaining points.

Note the available zone for $\varepsilon_K/\varepsilon_{K_{SM}}$ and some other decays seems quite small, this is due to $\text{BR}(\text{B} \rightarrow X_s \gamma)/\text{BR}_{SM}(\text{B} \rightarrow X_s \gamma)$ and $\Delta M_s/\Delta M_{s,SM}$ being very tightly constraint and the most sensitive in our model.

When combined with the EW and scalar analysis these exclusions yield,

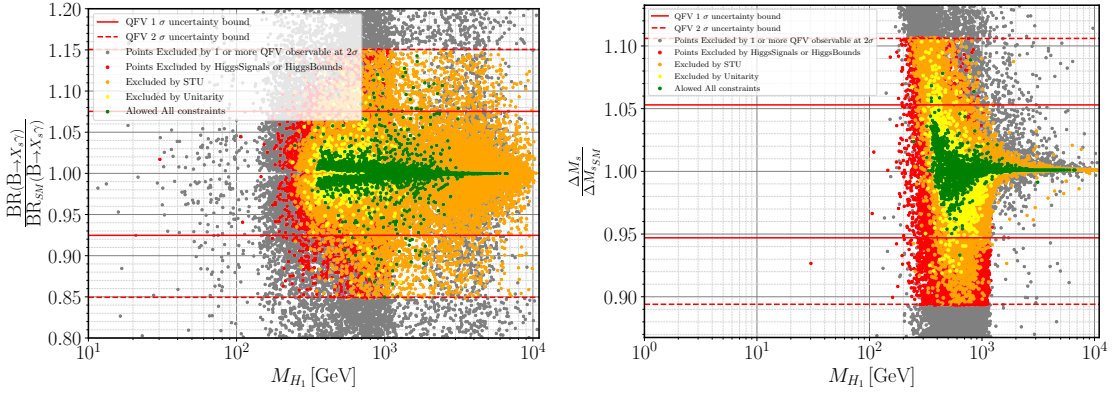


Figure 4.6: Scatter plot of the estimated QFV observables normalized to SM values overlaid with EW and Higgs sector just as in previous figures.

Here you can clearly see that there is a central region where the points that verify all EW and scalar constraints are all also consistent with QFV observables. This is a very important conclusion we take from our model. Through the stabilization of the 3HDM by the flavour symmetry all QFV observables are kept under significant deviation for all the viable mass spectrum.

We can now extract possible benchmark points, these are written in Tab. ??.

	m_{H_1}	m_{H_2}	m_{A_1}	m_{A_2}	$m_{H_1^\pm}$	$m_{H_2^\pm}$
Lightest H_1	251	2488	247	2616	157	2510
	327	1528	359	1616	229	1561
Lightest A_1	386	452	87	467	189	466
	337	446	100	395	311	374
Lightest H_1^\pm	251	2488	247	2616	157	2510
	398	1314	282	1525	173	1314

Table 4.2: A selection of four benchmark points. All written masses are given in GeV. These correspond to the lightest scalars found that respect all QFV and scalar sector constraints.

We discussed that some NHDMs use deliberate fine-tuning in their model as to have NP contributions balance out and artificially control flavour changing effects in their models. In this model we do not follow this process, our scans were purely randomly generated. However, randomness combined with the large amount of data collected could have found a synchronicity where flavour observables are fine-tuned by accident.

To check if this phenomena was present, all points were recalculated with slight a variation of masses trough a 1% variation of soft breaking terms, μ_{13} , μ_{23} and μ_{21} . Such a mass variation is expected to lead to variation of the flavour channel decay amplitude.

Through this exercise we expect to show that there is no abruptly high variation of masses or QFV observable as to show no fine-tuning is present. The results can be seen in,

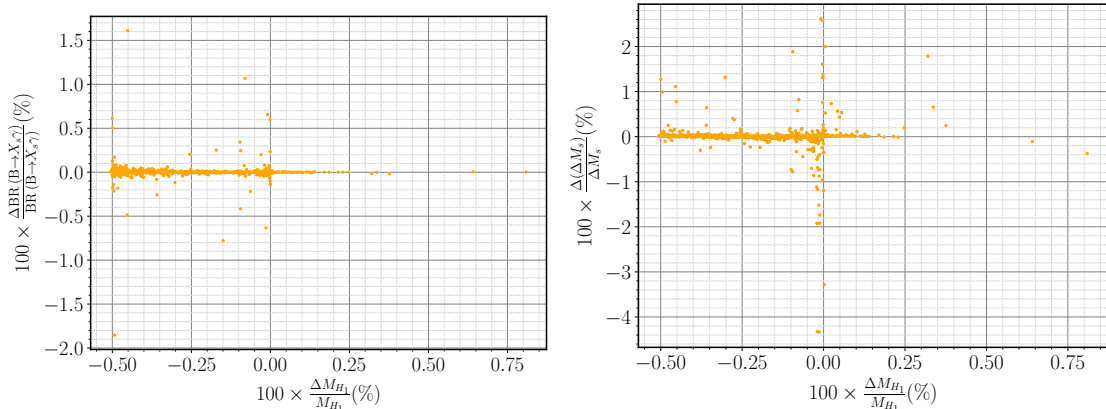


Figure 4.7: Relative mass and QFV observable changes with the increase of 1% in all softbreaking terms

Finally a complementary study was also implemented through Madgraph in this model. This study served a dual purpose to ensure that proper gluon fusion was being calculated by Higgs-Bounds and HiggsSignals and to show how close the model was to exclusion. The results are seen in,

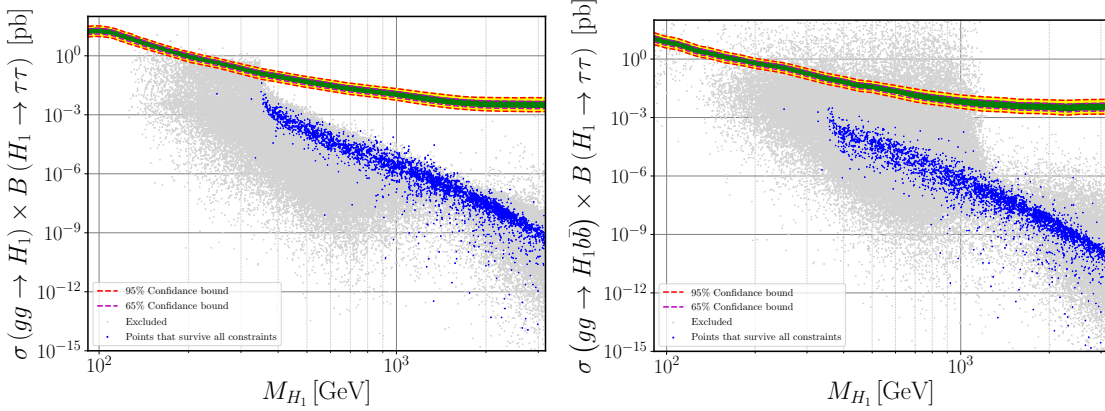


Figure 4.8

With these plots we can see that not only the region is clearly all below detection validating HiggsBounds, as we can also see there is space left to be probed at new collider experiments, both near and far from detection. This means we could be close to a new signature detection at the LHC through gluon fusion.

Chapter 5

Conclusions

To summarise, in this thesis we have performed a detailed phenomenological analysis of the minimal $U(1)_{B-L}$ extension of the Standard Model known as the B-L-SM and a BGL-like 3HDM with a $U(1) \times \mathbb{Z}_2$ symmetry. This phenomenological analysis was produced by a set of tools developed as to be easily adaptable to fit new models.

In the B-L-SM (chapter 3), we have confronted the model with the most recent experimental bounds from the direct Z' boson and next-to-lightest Higgs state searches at the LHC. Simultaneously, we have analysed the prospects of the B-L-SM for a consistent explanation of the observed anomaly in the muon anomalous magnetic moment $(g-2)_\mu$. Done by exploring the B-L-SM potential for the observed $(g-2)_\mu$ anomaly in the regions of the model parameter space that are consistent with direct searches and EW precision observables.

As one of the main results of our analysis, we have found phenomenologically consistent parameter space regions that simultaneously fit the exclusion limits from direct Z' searches and can explain the muon $(g-2)_\mu$ anomaly. We have distinguished four benchmark points for future phenomenological exploration at experiments, the first one with the lightest allowed Z' ($m_{Z'} > 3.1$ TeV), the second with the lightest additional scalar boson ($m_{h_2} > 400$ GeV), and the other two points that reproduce the muon $(g-2)_\mu$ anomaly within 1σ uncertainty range. Besides, we have studied the correlations of the Z' production cross section times the branching ratio into a pair of light leptons versus the physical parameters of the model. In particular, we have found that the muon $(g-2)_\mu$ observable dominated by Z' loop contributions lies within the phenomenologically viable parameter space domain. For completeness, we have also estimated the dominant

contribution from the Barr-Zee type two-loop corrections and found a relatively small effect.

As for the 3HDM portion of our work in this these seen in Chapter 4. We verified the phenomenological consistency of our model, we identified a region where both flavour and scalar sector physics are within experimental bounds including, like in the B-L-SM, EW precision observables and direct detection bounds. Narrowing down consistent the parameter space regions that simultaneously fit the exclusion limits from direct scalar searches and flavour constraints.

For this we determined the most sensitive flavour violation channels, and concluded that the stabilizing flavour symmetry is a mechanism that allows the model to be consist with current flavour observations. We also propose that further deviations in these flavour observables might be a pathway as to discover Higgs boson (or other exotic particle) mediating these phenomena. Being that the most appropriate channels to peer into this could be B meson oscillations and B meson decays for this type of 3HDM.

However a key take away from our results we show that the most stringent constraint on the model is not the flavour observables but the Higgs physics limits. A significant conclusion seeing that new upgrades at the LHCb, Belle and Atlas experiments could mean that despite the flavour sector being constraint the lightest possible Higgs might soon be in the TeV range.

We recognize these conclusions might not be sufficient to fully examine the model since there might be room for a wider paramater space if exact alignment is not performed or if loop order effects are allowed.

In our study of the 3HDM we have highlighted six benchmark points to illustrate how low masses are still within the range of future colider experiments.

Bibliography

- [1] M. Aaboud *et al.*, “Search for new high-mass phenomena in the dilepton final state using 36 fb^{-1} of proton-proton collision data at $\sqrt{s} = 13 \text{ TeV}$ with the ATLAS detector,” *JHEP*, vol. 10, p. 182, 2017.
- [2] e. a. Tanabashi, “Review of particle physics,” *Phys. Rev. D*, vol. 98, p. 030001, Aug 2018.
- [3] C. Collaborations *et al.*, “Measurements of the higgs boson production and decay rates and constraints on its couplings from a combined atlas and cms analysis of the lhc pp collision data at $\text{sqrt s} = 7$ and 8 tev,” *arXiv preprint arXiv:1606.02266*, 2016.
- [4] L. Bergström, “Non-baryonic dark matter: observational evidence and detection methods,” *Reports on Progress in Physics*, vol. 63, p. 793–841, Apr 2000.
- [5] U. Sarkar, *Particle and Astroparticle Physics*, vol. 1 of 1. The name of the publisher, 1 ed., 12 2007.
- [6] S. Mertens, “Direct neutrino mass experiments,” *Journal of Physics: Conference Series*, vol. 718, p. 022013, May 2016.
- [7] F. Capozzi, E. Lisi, and A. Marrone, “Neutrino mass hierarchy and electron neutrino oscillation parameters with one hundred thousand reactor events,” *Phys. Rev. D*, vol. 89, p. 013001, Jan 2014.
- [8] F. F. Freitas, J. Gonçalves, A. P. Morais, and R. Pasechnik, “Phenomenology of vector-like leptons with deep learning at the large hadron collider,” 2020.
- [9] M. Ilyushin, P. Mandrik, and S. Slabospitskii, “Constraints on the higgs boson anomalous fcnc interactions with light quarks,” *Nuclear Physics B*, vol. 952, p. 114921, 2020.
- [10] K. Huitu and N. Koivunen, “Suppression of scalar mediated FCNCs in a $SU(3)c \times SU(3)l \times u(1)x$ -model,” *Journal of High Energy Physics*, vol. 2019, Oct. 2019.
- [11] E. Noether, “Invariant variation problems,” *Transport Theory and Statistical Physics*, vol. 1, no. 3, pp. 186–207, 1971.
- [12] M. W. Grünwald, “6 experimental precision tests for the electroweak standard model,” *Landolt-Börnstein - Group I Elementary Particles, Nuclei and Atoms*, p. 166–224, 2008.
- [13] P. W. Higgs, “Broken symmetries and the masses of gauge bosons,” *Physical Review Letters*, vol. 13, no. 16, p. 508, 1964.
- [14] H. D. Politzer, “Reliable perturbative results for strong interactions?,” *Physical Review Letters*, vol. 30, no. 26, p. 1346, 1973.
- [15] C. Quigg, *GAUGE THEORIES OF THE STRONG, WEAK AND ELECTROMAGNETIC INTERACTIONS*, vol. 56. Princeton University Press, 1983.

- [16] J. H. Christenson, J. W. Cronin, V. L. Fitch, and R. Turlay, “Evidence for the 2π decay of the k_2^0 meson,” *Phys. Rev. Lett.*, vol. 13, pp. 138–140, Jul 1964.
- [17] N. Foundation, “The nobel prize in physics,” 1979.
- [18] M. T. et alii, “Review of particle physics,” *Physical Review D*, vol. 98, Aug. 2018.
- [19] S. L. Glashow, J. Iliopoulos, and L. Maiani, “Weak interactions with lepton-hadron symmetry,” *Physical review D*, vol. 2, no. 7, p. 1285, 1970.
- [20] G. Castelo-Branco and D. Emmanuel-Costa, “Flavour physics and CP violation in the standard model and beyond,” in *Springer Proceedings in Physics*, pp. 145–186, Springer International Publishing, Dec. 2014.
- [21] E. G. and, “Flavour anomalies: a review,” *Journal of Physics: Conference Series*, vol. 1137, p. 012025, Jan. 2019.
- [22] A. M. Sirunyan, A. Tumasyan, W. Adam, F. Ambrogi, E. Asilar, T. Bergauer, J. Brandstetter, E. Brondolin, M. Dragicevic, and et al., “Search for lepton flavour violating decays of the higgs boson to $\mu\tau$ and $e\tau$ in proton-proton collisions at $s=13 \sqrt{s} = 13$ tev,” *Journal of High Energy Physics*, vol. 2018, Jun 2018.
- [23] G. D’Amico, M. Nardecchia, P. Panci, F. Sannino, A. Strumia, R. Torre, and A. Urbano, “Flavour anomalies after the $r k *$ measurement,” *Journal of High Energy Physics*, vol. 2017, Sept. 2017.
- [24] Q.-Y. Hu, X.-Q. Li, and Y.-D. Yang, “ $\{b \rightarrow c\tau\bar{\nu}\}$ transitions in the standard model effective field theory,” *The European Physical Journal C*, vol. 79, Mar. 2019.
- [25] S. Fajfer, J. F. Kamenik, and I. Nišandžić, “ $B \rightarrow d^* \tau \nu^- \tau$ sensitivity to new physics,” *Physical Review D*, vol. 85, May 2012.
- [26] R. Alonso, B. Grinstein, and J. Martin Camalich, “Lifetime of bc - mesons constrains explanations for anomalies in $b \rightarrow d(*)\tau \nu$,” *Physical Review Letters*, vol. 118, Feb 2017.
- [27] J. T. Wei, P. Chang, I. Adachi, H. Aihara, V. Aulchenko, T. Aushev, A. M. Bakich, V. Balagura, E. Barberio, A. Bondar, and et al., “Measurement of the differential branching fraction and forward-backward asymmetry for $b \rightarrow k(*)l+l-$,” *Physical Review Letters*, vol. 103, Oct 2009.
- [28] R. N. Mohapatra and R. E. Marshak, “Local B-L Symmetry of Electroweak Interactions, Majorana Neutrinos and Neutron Oscillations,” *Phys. Rev. Lett.*, vol. 44, pp. 1316–1319, 1980. [Erratum: Phys. Rev. Lett. 44, 1643 (1980)].
- [29] L. Basso, S. Moretti, and G. M. Pruna, “Constraining the g'_1 coupling in the minimal $B - L$ Model,” *J. Phys.*, vol. G39, p. 025004, 2012.
- [30] L. Basso, S. Moretti, and G. M. Pruna, “Theoretical constraints on the couplings of non-exotic minimal Z' bosons,” *JHEP*, vol. 08, p. 122, 2011.
- [31] M. Tanabashi *et al.*, “Review of Particle Physics,” *Phys. Rev.*, vol. D98, no. 3, p. 030001, 2018.
- [32] G. Degrassi, S. Di Vita, J. Elias-Miro, J. R. Espinosa, G. F. Giudice, G. Isidori, and A. Strumia, “Higgs mass and vacuum stability in the Standard Model at NNLO,” *JHEP*, vol. 08, p. 098, 2012.
- [33] S. Alekhin, A. Djouadi, and S. Moch, “The top quark and Higgs boson masses and the stability of the electroweak vacuum,” *Phys. Lett.*, vol. B716, pp. 214–219, 2012.

- [34] D. Buttazzo, G. Degrassi, P. P. Giardino, G. F. Giudice, F. Sala, A. Salvio, and A. Strumia, “Investigating the near-criticality of the Higgs boson,” *JHEP*, vol. 12, p. 089, 2013.
- [35] M. S. Chanowitz, J. R. Ellis, and M. K. Gaillard, “The Price of Natural Flavor Conservation in Neutral Weak Interactions,” *Nucl. Phys.*, vol. B128, pp. 506–536, 1977.
- [36] H. Fritzsch and P. Minkowski, “Unified Interactions of Leptons and Hadrons,” *Annals Phys.*, vol. 93, pp. 193–266, 1975.
- [37] H. Georgi and D. V. Nanopoulos, “T Quark Mass in a Superunified Theory,” *Phys. Lett.*, vol. 82B, pp. 392–394, 1979.
- [38] H. Georgi and D. V. Nanopoulos, “Ordinary Predictions from Grand Principles: T Quark Mass in O(10),” *Nucl. Phys.*, vol. B155, pp. 52–74, 1979.
- [39] H. Georgi and D. V. Nanopoulos, “Masses and Mixing in Unified Theories,” *Nucl. Phys.*, vol. B159, pp. 16–28, 1979.
- [40] Y. Achiman and B. Stech, “Quark Lepton Symmetry and Mass Scales in an E6 Unified Gauge Model,” *Phys. Lett.*, vol. 77B, pp. 389–393, 1978.
- [41] F. Gursey, P. Ramond, and P. Sikivie, “A Universal Gauge Theory Model Based on E6,” *Phys. Lett.*, vol. 60B, pp. 177–180, 1976.
- [42] F. Gursey and M. Serdaroglu, “E6 GAUGE FIELD THEORY MODEL REVISITED,” *Nuovo Cim.*, vol. A65, p. 337, 1981. [,271(1981)].
- [43] V. Barger, P. Langacker, M. McCaskey, M. Ramsey-Musolf, and G. Shaughnessy, “Complex Singlet Extension of the Standard Model,” *Phys. Rev.*, vol. D79, p. 015018, 2009.
- [44] T. Yanagida, “Horizontal gauge symmetry and masses of neutrinos,” *Conf. Proc.*, vol. C7902131, pp. 95–99, 1979.
- [45] M. Gell-Mann, P. Ramond, and R. Slansky, “Complex Spinors and Unified Theories,” *Conf. Proc.*, vol. C790927, pp. 315–321, 1979.
- [46] R. N. Mohapatra and G. Senjanovic, “Neutrino Mass and Spontaneous Parity Nonconservation,” *Phys. Rev. Lett.*, vol. 44, p. 912, 1980. [,231(1979)].
- [47] K. Kaneta, Z. Kang, and H.-S. Lee, “Right-handed neutrino dark matter under the $B - L$ gauge interaction,” *JHEP*, vol. 02, p. 031, 2017.
- [48] N. Okada and O. Seto, “Higgs portal dark matter in the minimal gauged $U(1)_{B-L}$ model,” *Phys. Rev.*, vol. D82, p. 023507, 2010.
- [49] S. Okada, “Z’ Portal Dark Matter in the Minimal $B - L$ Model,” *Adv. High Energy Phys.*, vol. 2018, p. 5340935, 2018.
- [50] M. Fukugita and T. Yanagida, “Baryogenesis Without Grand Unification,” *Phys. Lett.*, vol. B174, pp. 45–47, 1986.
- [51] A. Pilaftsis, “CP violation and baryogenesis due to heavy Majorana neutrinos,” *Phys. Rev.*, vol. D56, pp. 5431–5451, 1997.
- [52] A. Pilaftsis and T. E. J. Underwood, “Resonant leptogenesis,” *Nucl. Phys.*, vol. B692, pp. 303–345, 2004.
- [53] T. Bandyopadhyay, G. Bhattacharyya, D. Das, and A. Raychaudhuri, “Reappraisal of constraints on z’ models from unitarity and direct searches at the lhc,” *Physical Review D*, vol. 98, Aug 2018.

- [54] S. Khalil, “TeV-scale gauged B-L symmetry with inverse seesaw mechanism,” *Phys. Rev.*, vol. D82, p. 077702, 2010.
- [55] F. F. Deppisch, S. Kulkarni, and W. Liu, “Searching for a light Z' through Higgs production at the LHC,” *Phys. Rev.*, vol. D100, no. 11, p. 115023, 2019.
- [56] A. Czarnecki and W. J. Marciano, “The Muon anomalous magnetic moment: A Harbinger for ‘new physics’,” *Phys. Rev.*, vol. D64, p. 013014, 2001.
- [57] S. Khalil and C. S. Un, “Muon Anomalous Magnetic Moment in SUSY B-L Model with Inverse Seesaw,” *Phys. Lett.*, vol. B763, pp. 164–168, 2016.
- [58] J.-L. Yang, T.-F. Feng, Y.-L. Yan, W. Li, S.-M. Zhao, and H.-B. Zhang, “Lepton-flavor violation and two loop electroweak corrections to $(g - 2)_\mu$ in the B-L symmetric SSM,” *Phys. Rev.*, vol. D99, no. 1, p. 015002, 2019.
- [59] W. Porod, “SPheno, a program for calculating supersymmetric spectra, SUSY particle decays and SUSY particle production at e+ e- colliders,” *Comput. Phys. Commun.*, vol. 153, pp. 275–315, 2003.
- [60] W. Porod and F. Staub, “SPheno 3.1: Extensions including flavour, CP-phases and models beyond the MSSM,” *Comput. Phys. Commun.*, vol. 183, pp. 2458–2469, 2012.
- [61] F. Staub, “SARAH,” 2008.
- [62] F. Staub, “SARAH 4 : A tool for (not only SUSY) model builders,” *Comput. Phys. Commun.*, vol. 185, pp. 1773–1790, 2014.
- [63] P. Bechtle, O. Brein, S. Heinemeyer, O. Stål, T. Stefaniak, G. Weiglein, and K. E. Williams, “HiggsBounds – 4: Improved Tests of Extended Higgs Sectors against Exclusion Bounds from LEP, the Tevatron and the LHC,” *Eur. Phys. J.*, vol. C74, no. 3, p. 2693, 2014.
- [64] P. Bechtle, S. Heinemeyer, O. Stål, T. Stefaniak, and G. Weiglein, “*HiggsSignals*: Confronting arbitrary Higgs sectors with measurements at the Tevatron and the LHC,” *Eur. Phys. J.*, vol. C74, no. 2, p. 2711, 2014.
- [65] J. Alwall, R. Frederix, S. Frixione, V. Hirschi, F. Maltoni, O. Mattelaer, H. S. Shao, T. Stelzer, P. Torrielli, and M. Zaro, “The automated computation of tree-level and next-to-leading order differential cross sections, and their matching to parton shower simulations,” *JHEP*, vol. 07, p. 079, 2014.
- [66] M. E. Peskin and T. Takeuchi, “Estimation of oblique electroweak corrections,” *Physical Review D*, vol. 46, pp. 381–409, July 1992.
- [67] R. Costa, A. P. Morais, M. O. P. Sampaio, and R. Santos, “Two-loop stability of a complex singlet extended Standard Model,” *Phys. Rev.*, vol. D92, p. 025024, 2015.
- [68] M. Baak, M. Goebel, J. Haller, A. Hoecker, D. Kennedy, K. Mönig, M. Schott, and J. Stelzer, “Updated status of the global electroweak fit and constraints on new physics,” *The European Physical Journal C*, vol. 72, May 2012.
- [69] P. Z. Skands *et al.*, “SUSY Les Houches accord: Interfacing SUSY spectrum calculators, decay packages, and event generators,” *JHEP*, vol. 07, p. 036, 2004.
- [70] A. Freitas, J. Lykken, S. Kell, and S. Westhoff, “Testing the Muon g-2 Anomaly at the LHC,” *JHEP*, vol. 05, p. 145, 2014. [Erratum: JHEP09,155(2014)].
- [71] S. M. Barr and A. Zee, “Electric Dipole Moment of the Electron and of the Neutron,” *Phys. Rev. Lett.*, vol. 65, pp. 21–24, 1990. [Erratum: Phys. Rev. Lett. 65, 2920(1990)].

- [72] V. Ilisie, “New Barr-Zee contributions to $(g - 2)$ - in two-Higgs-doublet models,” *JHEP*, vol. 04, p. 077, 2015.
- [73] T.-F. Feng and X.-Y. Yang, “Renormalization and two loop electroweak corrections to lepton anomalous dipole moments in the standard model and beyond (I): Heavy fermion contributions,” *Nucl. Phys.*, vol. B814, pp. 101–141, 2009.
- [74] L. Siwe, “Using neural networks to probe the parameter space of a 3hdm with a $U(1) \times \mathbb{Z}_2$ flavor symmetry,” 7 2020.
- [75] I. Padilla, “Phenomenology of a three higgs doublet model with a $U(1) \times \mathbb{Z}_2$ flavour symmetry,” 2019. Student Paper.
- [76] D. M. Straub, “flavio: a python package for flavour and precision phenomenology in the standard model and beyond,” 2018.
- [77] T. D. Lee, “A theory of SpontaneousTViolation,” *Physical Review D*, vol. 8, pp. 1226–1239, Aug. 1973.
- [78] S. Weinberg, “Gauge theory of CPNonconservation,” *Physical Review Letters*, vol. 37, pp. 657–661, Sept. 1976.
- [79] G. Branco, P. Ferreira, L. Lavoura, M. Rebelo, M. Sher, and J. P. Silva, “Theory and phenomenology of two-higgs-doublet models,” *Physics Reports*, vol. 516, p. 1–102, Jul 2012.
- [80] P. Ferreira, R. Santos, and A. Barroso, “Stability of the tree-level vacuum in two higgs doublet models against charge or cp spontaneous violation,” *Physics Letters B*, vol. 603, p. 219–229, Dec 2004.
- [81] A. Barroso, P. Ferreira, and R. Santos, “Neutral minima in two-higgs doublet models,” *Physics Letters B*, vol. 652, p. 181–193, Aug 2007.
- [82] A. Barroso, P. M. Ferreira, R. Santos, and J. P. Silva, “Stability of the normal vacuum in multi-higgs-doublet models,” *Physical Review D*, vol. 74, Oct 2006.
- [83] I. P. Ivanov, “Minkowski space structure of the higgs potential in the two-higgs-doublet model. ii. minima, symmetries, and topology,” *Physical Review D*, vol. 77, Jan 2008.
- [84] I. P. Ivanov, “Minkowski space structure of the higgs potential in the two-higgs-doublet model,” *Physical Review D*, vol. 75, Feb. 2007.
- [85] I. P. Ivanov, V. Keus, and E. Vdovin, “Abelian symmetries in multi-higgs-doublet models,” *Journal of Physics A: Mathematical and Theoretical*, vol. 45, p. 215201, May 2012.
- [86] I. P. Ivanov and C. C. Nishi, “Symmetry breaking patterns in 3hdm,” *Journal of High Energy Physics*, vol. 2015, Jan 2015.
- [87] I. F. Ginzburg and I. P. Ivanov, “Tree-level unitarity constraints in the most general two higgs doublet model,” *Physical Review D*, vol. 72, Dec 2005.
- [88] G. C. Branco, L. Lavoura, and J. P. Silva, *CP Violation*, vol. 103. Clarendon Press, 1999.
- [89] P. Ferreira, L. Lavoura, and J. P. Silva, “A soft origin for ckm-type cp violation,” *Physics Letters B*, vol. 704, p. 179–188, Oct 2011.
- [90] M. Nebot and J. P. Silva, “Self-cancellation of a scalar in neutral meson mixing and implications for the lhc,” *Physical Review D*, vol. 92, Oct 2015.
- [91] P. M. Ferreira and L. Lavoura, “No strong cp violation up to the one-loop level in a two-higgs-doublet model,” 2019.